Stony Brook University

OFFICIAL COPY

The official electronic file of this thesis or dissertation is maintained by the University Libraries on behalf of The Graduate School at Stony Brook University.

© All Rights Reserved by Author.

Novel single photon sensors for highly sensitive fluorescence detection systems

A Dissertation Presented

by

Lu Cheng

to

The Graduate School

in Partial Fulfillment of the

Requirements

for the Degree of

Doctor of Philosophy

in

Electrical Engineering

Stony Brook University

May 2009

Stony Brook University

The Graduate School

Lu Cheng

We, the dissertation committee for the above candidate for the

Doctor of Philosophy degree, hereby recommend

acceptance of this dissertation.

Vera Gorfinkel – Dissertation Advisor
Associate Professor, Department of Electrical and Computer Engineering

Hang-Sheng Tuan – Chairperson of Defense
Professor, Department of Electrical and Computer Engineering

Dmitri Donetski
Assistant Professor, Department of Electrical and Computer Engineering

Alexander Kastalsky
Ph.D, Copytele Inc.

This dissertation is accepted by the Graduate School

Lawrence Martin
Dean of the Graduate School

Abstract of the Dissertation

Novel single photon sensors for highly sensitive fluorescence detection systems

by

Lu Cheng

Doctor of Philosophy

in

Electrical Engineering

Stony Brook University

2009

This dissertation is focused on studies of two types of low cost solid-state photodiodes working as single photon detectors and their applications for highly sensitive fluorescence detection systems.

An operation of the commercial linear avalanche photodiode (Hamamatsu Si APD S9073) has been studied in conjunction with a novel, unique quenching circuit. The operation of the diode in Geiger-mode has been experimentally demonstrated with dead time of ~50ns. Studies of the dark count of the un-cooled diode showed a very significant enhancement of the dark count with increase of the over-voltage. It has been found that at the over-voltages needed for sensitive photon detection, the dark count reaches 10^7/sec that puts the diode in the saturation region due to a relatively long quenching delay. The conclusion has been made that for an efficient single photon counting, one needs to cool the diode and to decrease the quenching delay. The schematic of quenching circuit that

makes the dead time smaller and less area consuming has been designed in standard 0.6um CMOS technology and simulated using Cadence tools.

A novel type of single photon diode, Silicon Photomultiplier (SiPM), has been studied in single photon counting mode. For the first time, the application of SiPM with external amplifiers for single photon detection to DNA sequencing has been demonstrated. A novel SiPM design, which requires neither external quenching nor amplification for photon counting has been proposed utilizing the unique performance of SiPM, optical cross-talk. A simulator has been developed based on the model of SiPM in Python. The output pulse distribution with different cross-talk probabilities and afterpulsing probabilities has been simulated. Experiments on SiPMs from two manufactures have been done and presented in the dissertation.

Table of Contents

List of Figures

List of Tables

1. Introduction

1.1. Overview

Our group has been devoted to the development of high-throughput DNA sequencing based on highly sensitive fluorescence detection systems. DNA sequencing instruments use fluorescence detection systems for detecting the fluorescence emitted by the DNA molecule. These fluorescence detection systems determine the sensitivity and the cost of DNA sequencing.

The most important component of the fluorescence detection system, which decides the sensitivity, the cost, and other performances of DNA sequencing, is the photodetector for detecting the ultra-weak fluorescence signals. In this dissertation, two types of semiconductor photon detector, avalanche photodiode (APD) and Silicon photomultiplier (SiPM) worked as the single photon detector (SPD) in fluorescence detection systems have been proposed and demonstrated.

Chapter 1 is an introduction to the concept of fluorescence detection (FD) based DNA sequencing. The requirements of single photon detectors for FD are studied. The choices of SPD: PMT, APD/SPAD, and SiPM are discussed briefly.

Chapter 2 explains two working modes of APD and quenching principle for Geiger-mode APD, so called SPAD. Physics and features of SPAD are discussed in details. Three types of quenching circuits are reviewed. And a novel and unique quenching circuit developed by our group is demonstrated.

Chapter 3 proposes two research directions on SPAD based single photon counting implementation. An operation of the commercial linear APD (Hamamatsu Si APD S9073) has been studied in conjunction with our unique quenching circuit. The experimental results of the diode working in Geiger-mode have been demonstrated for the first time. The ASIC design of quenching circuit, which makes the dead time smaller, and less area consuming has been presented in standard 0.6um CMOS technology and simulated using Cadence tools.

Chapter 4 introduces a promising semiconductor device, SiPM, which we are trying to operate in photon counting mode. Its evolution, operating principles, and features are discussed.

Chapter 5 shows the feasibility of using SiPM for DNA sequencing application. A novel design of SiPM optimized for photon counting mode is proposed. Two simulators are developed based on SiPM circuit model. Simulations of SiPM output pulse distribution and noise analysis under different conditions are presented.

Chapter 6 describes the dark count rate (DCR) measurements, noise measurements, and photo count measurements under different bias conditions for two types of SiPM. Compare the experimental results with simulations. Low temperature experiments using liquid nitrogen are done on SiPMs to obtain the optimum operating condition.

Conclusions and future works are presented in Chapter 7.

1.2. DNA sequencing based on Fluorescence Detection

In the fluorescence detection (FD) based DNA sequencing the FD system excites fluorescence markers using a laser source and then captures fluorescence with a photodetector. Usually either photomultiplier tube (PMT) or charged couple device (CCD) was used as photodetector for detection of weak fluorescence signal. This signal was then digitized, transferred to a computer, and analyzed to determine the sequence. Due to the relatively low detection sensitivity and the relatively narrow dynamic range limited by the analog-to-digital conversion circuitry, many efforts are needed to substantially reduce the sequencing cost and improve the data quality.

A number of extremely sensitive fluorescence detection techniques are available based on registering single photons. Commonly, they are referred to as the photon correlation techniques. Until recently single photon counting techniques were mostly used for specialized scientific applications, such as the detection of single fluorescent molecules [54–58]. Though very sensitive, these techniques are not widely used in commercial DNA sequencing for their complexity and the high cost per channel.

Figure 1.1A shows the photo of a single-lane DNA sequencer that utilized single photon counting techniques and Figure 1.1B shows a typical scenario in which a DNA sample is passing through a capillary (50-150μm diameter) and is irradiated by a laser. A labeled DNA sample undergoes separation in a single-capillary fiberized separation/reading module. The separated zones arriving at the detection window in the

capillary are excited by a laser source. The fluorescence from labeled DNA fragments is collected by a fiber receiver and delivered to the optical system (5 in Figure 1.1A). After appropriate filtering the fluorescence is focused on the photodetector that produces an output pulse corresponding to each detected photon. These pulses are then transferred to a computer for recording, processing, and graphical presentation. During the separation sequencing traces are displayed in real time on the computer screen. For detailed description and analysis of the DNA sequencers based on single photon detection techniques please refer to [53].

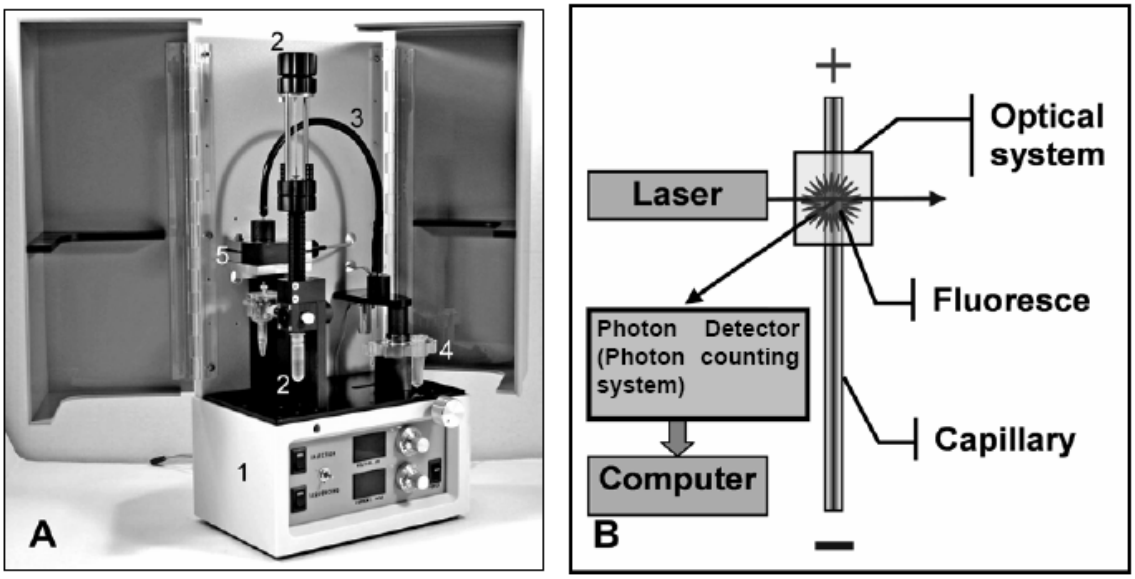

Figure 1.1 Single-lane DNA-sequencer (A) General view (1 - High voltage supply with a built-in voltmeter and current-meter; 2 - polymer replacement system; 3 - temperature control system; 4 - tube-changer carousel; 5 - fiberized precision optical system) (B) Schematics showing principle of operation

1.3. Requirements of single photon detector for FD

The typical laser excitation power is in the range of milliwatt, whereas the typical fluorescence in DNA sequencing is only femtowatt ~ picowatt. No linear photodetector is able to detect weak signals in such range.

The power of one picowatt is equal to a photon flux of ~10^7 photons per second. So if the response time of the photon detector to each incoming photon is much less than 10^{-7} second, the detector will see the photon flux as discrete particles. Responding to each single photon, the detector gives an output pulse with amplitude that depends on the internal gain of the detector. And the pulse should be in the window of less than 100ns.

The optimum photodetector is the one with largest signal noise ratio (S/N). How to get the minimum noise is the goal for many detection systems. Minimum noise of photon detection systems is defined by the Poissonian fluctuation due to the stochastic process of avalanche multiplication. Only single photon detectors can approach this lower limit. Other detectors can't avoid additional noises from electronics.

Under this situation we can summarize the major requirements of the single photon detectors for the highly sensitive FD as follows:

1. **Low dark noise:**

   The dark count noise should be as low as possible. The dark count rate (DCR) may vary from 1 to 10^6 counts/second. If the DCR is close to or higher than 10^7 counts/sec, the detector will be operated in the saturation region; the useful signals will be inundated in the dark noise. Noise of the system varies a square root of the sum of all the noise components. For example, the fluorescence signal is 10^7 photons/sec, using a detector with the DCR of 10^6 counts/second to detect

this signal; S/N of this system is 10^7 / 10^3 = 10^4, assuming DCR follows Possoinian distribution.

2. **Fast response time**

   In order to detect the photon flux as discrete particles using single photon counting techniques, the response time must be less than 100ns and even in the range of sub-nano second. And response pulse width is also ~ns.

3. **High gain**

   With adequate internal gain, detectable pulse can be generated for even single photon.

4. **High sensitivity**

   Sensitivity of a detector can be defined as the ability to detect the incident optical photons, which mostly depends on the quantum efficiency (QE). As we know the QE of PMT is 5~20%, QE of semiconductor photodiode could be up to 70%.

5. **Wide linearity range**

   The linearity range is very important if the variety of signal amplitude is expected. And this is a typical case for biomedical applications. The detector is required to have wide dynamic range such that it can measure the highest and the lowest of peaks with high accuracy.

6. **Spectral range**

   The desired spectral range is from ultraviolet to infrared.

Some additional requirements should be considered for the specific high-throughput DNA sequencing application:

7. **Large active area**

For very weak fluorescence detection, the large active area is preferred to obtain relatively high collection efficiency. However the small area diode is chosen sometimes for its low dark noise.

8. **Low cost**

   Low cost is always preferred, especially when the multi-channel is desired for the high throughput design.

9. **Multi-channel operation**

   The possibility of multi-channel operation is a consideration for many applications. The detection array or detection matrix would improve many applications dramatically.

Finally, new applications are still being realized that require detection of ultra-weak fluorescent signals in the order of femtowatts. Hence, there is an increasing need for highly sensitive photon detection systems.

1.4. Choice of single photon detector

Although PMTs can detect low levels of light, they suffer from low photon detection efficiency (PDE) (7-10% for a typical PMT), high noise, and the requirement of power supply in KV range. Recently, highly sensitive solid-state detectors namely Single Photon Avalanche Diodes (SPADs) (in the late 90's) and Silicon Photomultipliers (SiPM) (in early 2007) became commercially available.

It is known that DNA sequencing can be performed with a SPAD, but it is still not used widely due to the complexity of the involved optics and electronics. To perform high-speed photon counting, SPADs need to be used in conjunction with a special circuit called quenching circuit (QC). SPAD is a digital detector suitable for photon counting applications such as DNA sequencing whereas SiPM is an analog detector primarily designed for resolving photon numbers. Both the detectors have numerous advantages as compared to PMT. As we know so far, use of SiPM in photon counting applications has not yet been investigated. The brief comparison of these three devices is shown in Table1.1.

Table 1.1 Comparisons: PMT, SPAD, and SiPM

Performance parameter	**PMT**	**SPAD**	**SiPM**
Spectral response range	200~900 nm	200~1000 nm	300 ~1000 nm
Photosensitive diameter	large	0.1~0.5mm	0.1~3mm
Gain	10^6	10^6	10^6
Power supply	~KV	~200V	~50V
Price	~$500	~$1000	~$100
Dynamic range	1M	~10M	10~100M
Temperature coefficient	_	0.7V/ºC	0.05V/ºC
Processing technology	Vacuum tube	Dedicated	Standard CMOS
PDE	5~20%	20~70%	20~70%
Gain varies with magnetic field	yes	no	no

This dissertation is to investigate solid-state detectors (SPAD and SiPM) for highly sensitive fluorescence detection to achieve the goal of performing highly sensitive, high through-put DNA sequencing at low cost.

2. Single photon avalanche diode and quenching circuit

For many applications where very low levels of light are to be detected, it is desirable to use a detector with large sensitivity, that is, high optical gain. Avalanche Photodiode has been developed for this purpose. This device is essentially a PIN diode with high gain.

Until late1990s, solid-state avalanche detectors of single photon became available for experiments. However, in the 1960s, thanks to the work of R. H. Haitz's group, a basic insight into the avalanche phenomenon in p-n junctions biased above the breakdown voltage was gained. And a correct model of this device was presented [2]. In the 1970s, during the early development of Si APD, fundamental contributions to the understanding of the avalanche phenomenon and its statistical properties were given by R. J. Mcintyre and P. P. Webb. And the single photon generated pulses were observed in their APDs biased above breakdown voltage [3].

In an APD, if photogenerated carriers in the depletion region can acquire enough energy from the electric field during transit, an ionizing collision with the lattice will occur. The field necessary to start such an ionizing collision is usually in the range of 10^4~10^5 V/cm, depending on the material. Secondary electron-hole pairs are produced, which also drift in opposite directions; together with the primary carrier, and all or some

of them may produce new carriers. The process is known as *impact ionization* (shown in Figure 2.1), which leads to avalanche multiplication and gain.

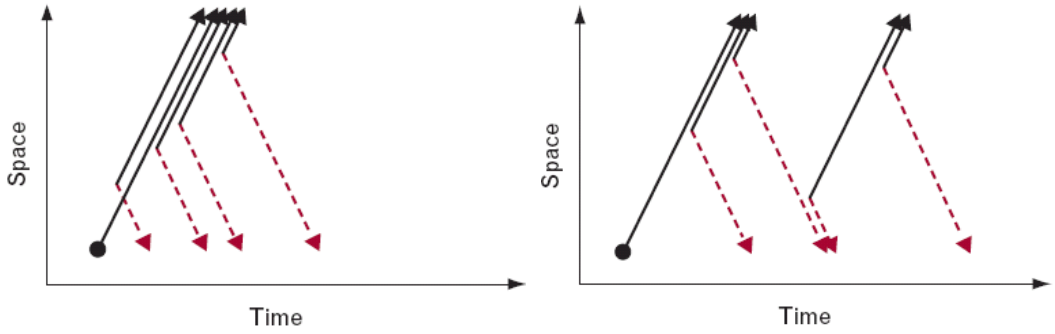

Figure 2.1 Avalanche multiplication process. On the left, only electrons can initiate impact ionization. On the right, electrons and holes are equally likely to initiate impact ionization.

The avalanche process is itself asymmetric. The probability for initiating an avalanche is usually different for electrons and for holes. This asymmetry is characterized by the ratio k = αh/αe, where αh and αe are the impact ionization coefficients for holes and electrons respectively. As it may seem obvious from Figure 2.1, the value of αh/αe should be as large or as small as possible. In these cases the recycling of carriers through the depletion region is minimized. Consequently the noise is reduced for less fluctuation in the ionization process compared to the case when both carriers participate. Meanwhile, the response of the device is faster. The Slik^{TM} device produced by PerkinElmer Optoelectronics, which is applied to the highly successful single photon counting module SPCM [6] represents a remarkable evolution of the reach-through avalanche diode structure. Slik^{TM} stands 'super low k', where k is the ratio of impact ionization coefficients for holes and electrons.

Due to impact ionization process that leads to avalanche multiplication in an APD, it can be sensitive enough for single photon detection. These kinds of APD which can be

biased above breakdown voltage and generate macroscopic current pulse in response to single photons are referred as single photon avalanche diode (SPAD). Their operation is radically different from that of normal APDs that are biased near but below the breakdown voltage.

2.1. Linear-mode and Geiger-mode

A diode working in the region near the breakdown voltage can be operated in two different ways: 1. the reverse bias is below the breakdown point (APD); 2. the reverse bias is above the breakdown point (SPAD). These two operation regions are shown in Figure 2.2.

In the case 1, the device is called APD. Each absorbed photon creates in average a finite number M of electron-hole pairs exploiting the impact ionization process. This mode is called *linea- mode* because a linear amplification of the primary photogenerated electrical signal is produced. But due to the avalanche process there is an intrinsic positive feedback in the amplification. This positive feedback loop strongly enhances the statistical fluctuations of the multiplication process, which increases much more than proportionally to the gain. Hence, whereas Photomultiplier Tube provides a gain with a mean value around 10^6 and moderate fluctuations, the mean value of the gain obtainable in APD with acceptable fluctuations is lower than 1000 in the best cases.

So APDs operated in linear mode can detect single photons only in the most favorable cases and their performance as single photon detectors is not very satisfactory.

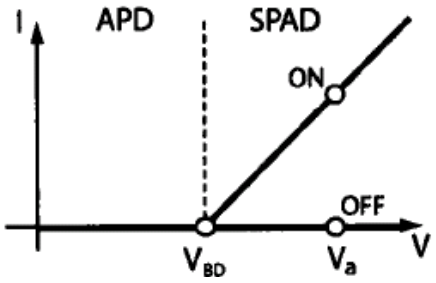

Figure 2.2 Regions of APD operation and SPAD operation in the reverse I-V characteristics of a p-n junction

In the case 2, the device is usually referred to as SPAD or *Geiger-mode* APD. Under this bias condition, the electric field is so high that a single carrier injected into the depletion region can start a self-sustaining avalanche. So the drawback of intrinsic positive feedback for APDs is exploited in SPADs to obtain a different operating mode, unlike an amplifier, but like a bistable circuit.

In the quiescent state the SPAD device is biased at voltage *Va* above the breakdown voltage V_{BD} and no current flows (OFF-state): in the junction depletion layer the electric field is very high but no free carriers existing. When a single charge carrier is injected into the high-field region, it is strongly accelerated and can impact and generate a secondary electron-hole pair, to trigger a self-sustaining avalanche multiplication process. The current then swiftly grows until the space charge effect limits its value to a constant level. This level is proportional to the over-voltage $V_{ov} = Va - V_{BD}$**,** hence an avalanche resistance can be defined. The SPAD device is thus switched to the ON-state, where a constant macroscopic avalanche current flows (in the milliampere range). The fast onset of the current marks the time of arrival of the photon that generated the initial charge carrier. The device remains in this ON-state until the avalanche is quenched by an

external circuit, which drives the applied voltage down to breakdown or lower. The circuit then completes the operating cycle by resetting the voltage to the quiescent level. An avalanche current pulse with standard amplitude is thus generated. The detector is insensitive to any subsequent photon arriving in the time interval from the avalanche onset to the voltage reset, which is the dead time. So in this case, SPAD is a digital device.

2.2. SPAD Structures

What structure of the p-n junction can be worked as a SPAD? The factors to make local field concentration are necessary to be avoided to attain Geiger-mode operation, such as edge effects or local defects of the material [2]. The higher electric field lowers the breakdown voltage in this restricted area. Then the device may work as a SPAD only in the restricted area with a correspondingly a low current or it may not work as a SPAD at all, going into steady breakdown as soon as biased.

There are two types of structure designed for photon counting [7]:

(1) Planar structure with a thin junction depletion layer (1~5um) and a low breakdown voltage (15~50V), a deep diffused guard ring defined a small sensitive area (diameter 10~50um), see Figure 2.3 (this APD is developed in S. Cova's lab).

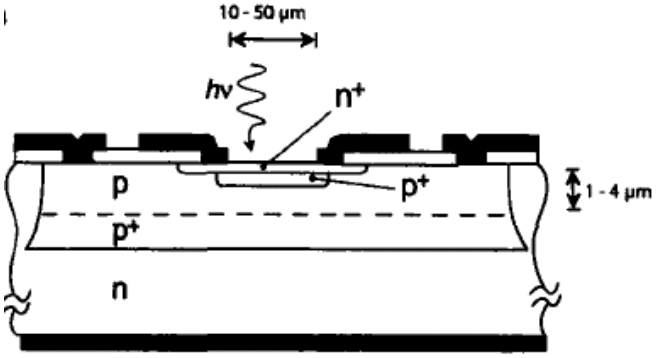

Figure 2.3 Schematic cross-section of planar epitaxial silicon APD

(2) Reach-through structure with a thick junction depletion layer (20~100um) and a high breakdown voltage (100~500V), a p+ implanted enrichment to avoid edge effects defined the active area (diameter 50~500um).

The first reach-through structure is patented by [15]. The structure in Figure 2.4 is a very successful evolution of the structure from PKI. This reach-through thick layer SPAD requires an ultra-pure high resistance Si substrate and a dedicated fabrication process incompatible with CMOS technology. So it is almost impossible to produce chips that integrate detectors and the associated circuitry. And there is no perspective on arrays.

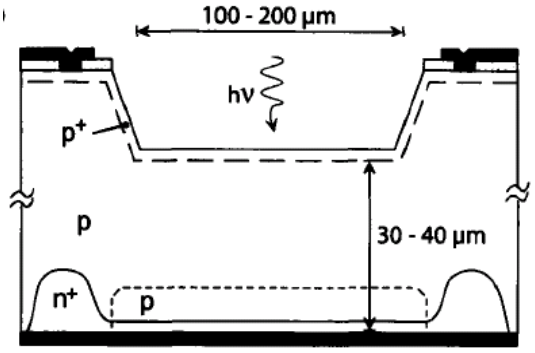

Figure 2.4 Schematic cross-section of reach-through Slik ™ device

Figure 2.5 shows a simplified reach-through structure along with the field profile, where intrinsic layer "i" is the absorption region and "p" is the multiplication region designed to sustain very high electric fields. Photon enters the device through the p^+ side as shown in the figure and drifts to the "i" region. The electric field in the "i" region separates the photo-generated electrons and holes and sweeps electrons towards the multiplication region. The multiplication region provides internal photocurrent gain by the process of impact ionization and is called the gain region. The length of this region determines the value of gain and hence must be selected large enough to provide sufficient gain.

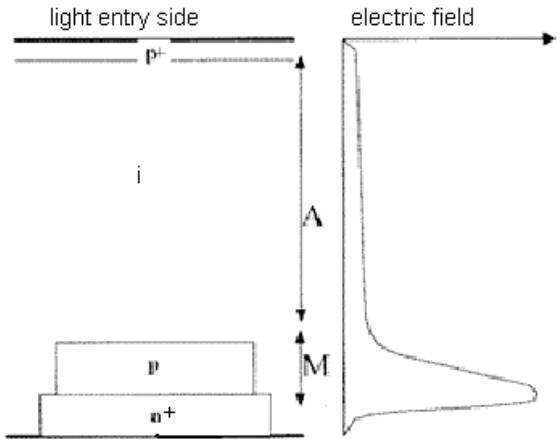

Figure 2.5 A simplified reach-through structure along with the field profile

The thick junction APD model C30902S-DTC from PerkinElmer Photoelectronics designed with reach-through structure had been tested and applied to our multi-channel single photon counting system [8]. The advantages of this device are thick depletion layer (20~90μm) and large active area (diameter up to 500 μm). The disadvantage is an expensive dedicated fabrication process, with low yield and high voltages (200-500V). To reduce the cost of our system is the motive for me to do the experiments on the

Hamamatsu Silicon APD. The experimental results and discussions will be presented in the chapter 3.

2.3. SPAD physics and features

2.3.1. Detection efficiency

The detection efficiency of a SPAD is the product of two factors: the quantum efficiency (QE) and the turn-on probability (triggering probability, Pt).

The quantum efficiency (QE) represents the probability for a photon to be absorbed and generate a primary carrier (an electron-hole pair) in the active thickness of the device. If the incident light energy is higher than the band gap, electron-hole pairs are generated. So the light energy E (eV) and the wavelength λ (nm) have a relation: $\lambda = 1240/E$ (nm). For the silicon with a band gap 1.12 eV at room temperatures, it is sensitive to light wavelengths shorter than 1100 nm.

Actually, there is a finite probability for the primary carrier to trigger an avalanche when it is generated and passing through the high field region. The avalanche triggering probability increases with the over-voltage V_{ov}, because it is enhanced by a higher electric field. For moderate values of over-voltage above breakdown, the triggering probability can be approximated by,

$$Pt = 1 - \exp(-V_{ov}/Vc)$$

Where characteristic voltage Vc, depends on the depletion layer thickness and on keff [10], which is a weighted average of the ratio of the ionization coefficient of holes to that

of electrons. For example, the Slik structure from PKI with keff = 0.002 to 0.004 (depending on wavelength) has a Vc 8-9 V.

Detection efficiency of thin SPAD and thick SPAD has been studied in [9]. Figure2.6 is the relationship between photon detection efficiency and the light wavelength with the over-voltage V_E for the PKI Slik thick SPAD (25um junction width, V_B = 420V, active area diameter 250um).

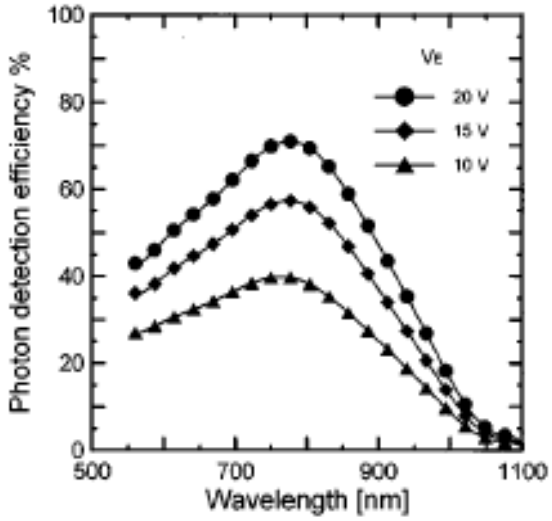

Figure 2.6 Detection efficiency versus wavelength for different over-voltages

For the thin depletion layer diode (typically 1um thick) devised in S. Cova's lab, the corresponding photon detection efficiency is high in the visible and declines in the red and near infrared (NIR) spectral range: typical values are over 40% at 500nm, 30% at 630nm, 15% at 730nm, 10% at 830nm and a few 0.1% at 1064nm [11]. For the thick depletion layer diode (Slik^{TM} from PKI), the photon detection efficiency is very high in the visible region and fairly good in the NIR up to about 1um wavelength. The typical value is remarkably higher than 50% over all the range from 540 to 850nm wavelength and is still about 3% at 1064nm [6].

2.3.2. Dark count rate

Even in the absence of illumination, free carriers are generated thermally. The dark count rate in SPAD has the same role as the dark current in ordinary photodiodes. Its Poissonian fluctuations are the internal noise source of the detector.

Dark count rate includes primary pulses and secondary pulses. Primary dark counts are due to thermally generated carriers in the SPAD junction. So the dark count increases with the temperature. And this rate also increases with over-voltage V_E for two reasons: field-assisted enhancement of the emission rate from generation centers and an increase of the avalanche triggering probability.

Secondary dark counts are due to afterpulsing effects. Impurities and crystal defects causes not only GR centers at mid-gap, but also local levels at intermediate energy between mid-gap and band edge, called deep levels. During avalanche some carriers are captured by deep levels in the junction depletion layer and subsequently released with a statistically fluctuating delay. The number of carriers captured depends on the total number of carriers crossing the junction, which depends on the total charge of the avalanche pulse generated. The after-pulsing depends on the time required to quench the avalanche since it was initiated and the current intensity which is proportional to over-voltage V_E, both of which are a feature of the associated quenching circuitry. Therefore, a trade-off has to be established between acceptable after-pulsing, the desired photon-detection efficiency and acceptable dead time. Figure 2.7 is a result tested by [9] on a thick SPAD at room temperature with 40 ns hold time.

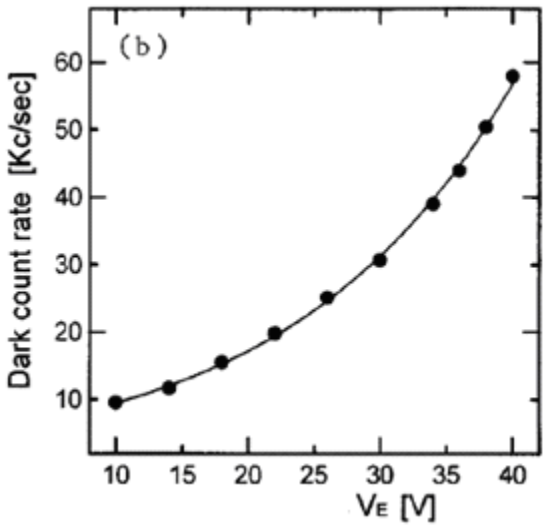

Figure 2.7 Dependence of the dark count rate on over-voltage V_E

2.3.3. Thermal effects

Breakdown voltage V_{BD} strongly depends on the junction temperature. The thermal coefficient value depends on the SPAD device structure and is fairly high, typically around 0.3%/K. At constant supply voltage Va, the increase of V_{BD} causes a decrease of over-voltage V_E. The resulting percent variation of V_E is very strong at a low V_E level, about 30%/K. And the resulting percent variation is fairly high at a high V_E level, could be 3%/K. The decrease lowers the photon detection efficiency, causing non-linear distortion in photon counting. The effects on device performance are significant.

2.4. Quenching Circuits

2.4.1. Principle of quenching

As I mentioned in the chapter 2.1, the APD operated in Geiger-mode (called SPAD)

behaves like a bistable-type switching circuit. When avalanche occurs, macroscopic current (milliamps range) flows through the device, switching to ON-state. The device remains in this ON-state until the avalanche is quenched by an external circuit, which drives the applied voltage down to breakdown or lower. The circuit then completes the operating cycle by resetting the voltage to the quiescent level (OFF-state). Figure 2.8 illustrates the principle of quenching in the diode reverse I-V characteristics.

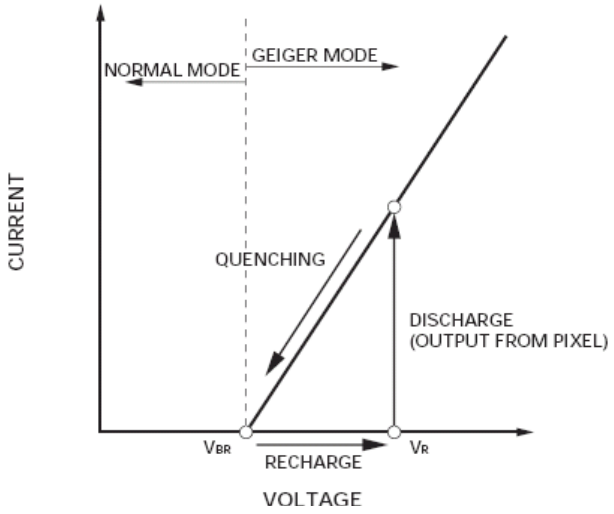

Figure 2.8 Principle of quenching

There are two basic types of external circuit to shut off the avalanche in the junction: passive quenching and active quenching.

2.4.2. Passive quenching

Let's have a look to the circuit model describing the APD behavior during passive quenching. It has been studied by several groups [12, 13, 9].

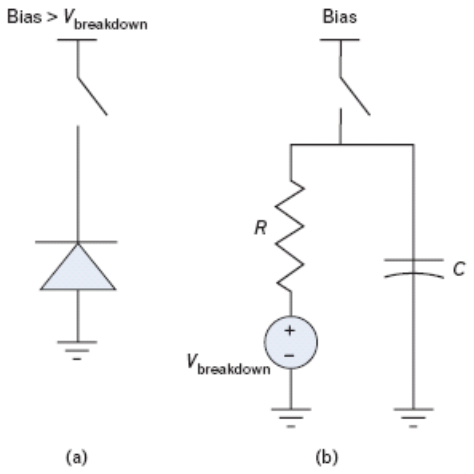

Figure 2.9 Circuit model of SPAD in Geiger-mode

The SPAD is charged up to a bias above breakdown, and then left it open (in Figure 2.9a). Once the SPAD is turned on by the incident photons, it discharges its own capacitance until it is no longer above breakdown voltage, at which point the avalanche dies out (in Figure 2.9b). The corresponding model is a voltage source equal to the breakdown voltage in series with the internal resistance *R* of the SPAD. The model predicts exponential decay of the current to zero and voltage to the breakdown with a time constant RC.

Now put the SPAD reverse biased through a high ballast resistor R_L of 100K Ohms or more, as shown in Figure 2.10, where C_d is the internal capacitance of the diode, it depends on the active area of the diode and varies proportionally with it; R_d is the internal resistance of the diode, generally in the range of ~ 500 Ohms for large area SPADs; R_s is a small value series resistor in order to get the output pulse; C_s is the stray capacitance or the wiring capacitance due to the circuit design and layout.

Then the avalanche current will quench itself by developing a voltage drop on the high impedance load. When the load resistor is much larger than the internal resistor of SPAD, the load resistor is working as a virtual open circuit during the discharge.

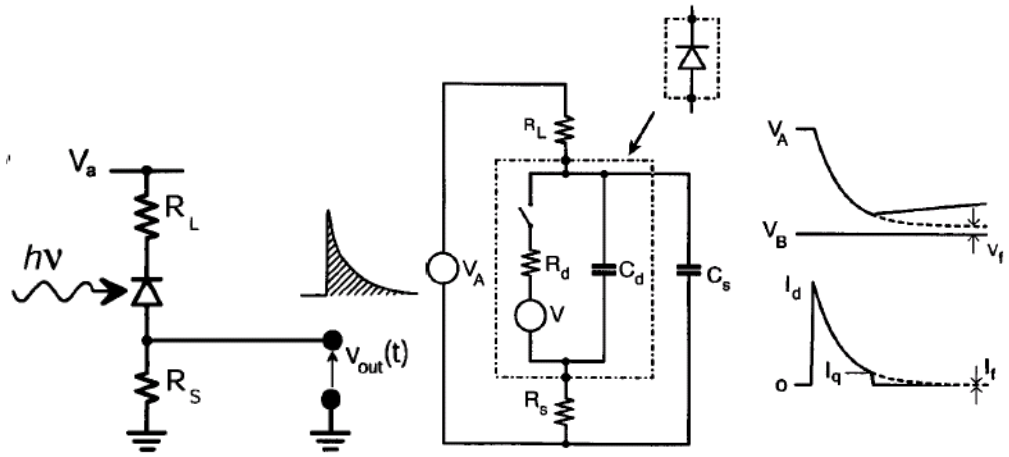

Figure 2.10 Equivalent circuit of passive quenching

Once the avalanche has been quenched, corresponding to opening the switch in the diode equivalent circuit (Figure 2.9), Cd and Cs are recharged slowly by the small current in the load resistor RL. The diode voltage recovers toward the bias voltage exponentially to get the correct over-voltage. A photon that arrives during the recovery time is almost certainly lost, because the avalanche triggering probability is very low during that time interval.

For the slow recovery transient, passive quenching circuit (PQC) is not a good choice for high counting rate applications though it is very simple.

2.4.3. Active quenching

Though the drawbacks of passive quenching mentioned above can be overcome by circuit technology to reduce the stray capacitance Cs and so as to make the recovery time shorter. Cs could be a few picoFarads and the recovery time well below 1us. For high counting rates of million of counts per second, the passive quenching is still not applicable.

In 1975, the active quenching circuit (AQC) was devised to completely avoid the

drawbacks of passive quenching circuit firstly by S. Cova's group [14].

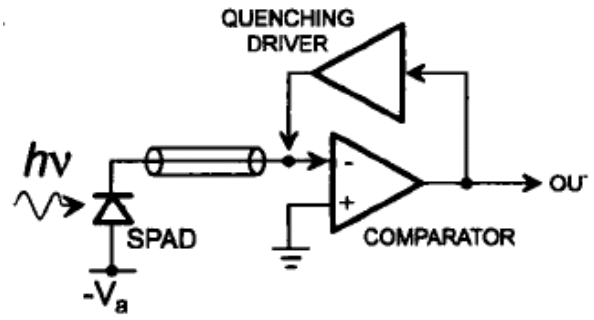

Figure 2.11 Principle of active quenching

Figure 2.11 illustrates a basic active quenching circuit. The circuit is composed of a comparator and a voltage driver circuit. The comparator is used to detect the avalanche rise for photon counting or timing. The output pulse from comparator must be shaped to be processed by signal processing circuitry. Generally, a line driver is used to boost the amplitude of this pulse before sending it to appropriate circuitry for registering the photon. The comparator also sends a command to the voltage driver, which will lower the bias across the SPAD to a voltage below breakdown. And, after a precisely controlled hold-off time, the bias voltage is restored back to the bias voltage Va which is above breakdown and the SPAD is ready to detect the next photon. At this point, one quenching cycle is completed. The time when the avalanche happens to the moment it is again restored back to the quiescent state is defined as dead time for this circuit and during the dead time the diode is insensitive to detect incoming photons. The dead time feature leads to the non-linearity of the circuit.

Since S. Cova's group introduced the AQC, several configurations of AQC design are contributed by various laboratories. [16~23]

2.4.4. Mixed passive-active quenching

The quenching and reset transitions do not necessarily have to be both passive or to be both active. And even a single transition can be implemented partly in active and partly in passive ways. As the name indicated, there are active quenching with passive reset, passive quenching with active reset, mixed passive-active quenching, and mixed active-passive reset. These mixed solutions can be chosen to satisfy specific application requirements.

Here, we discuss the mixed passive-active quenching circuit [18, 19] only.

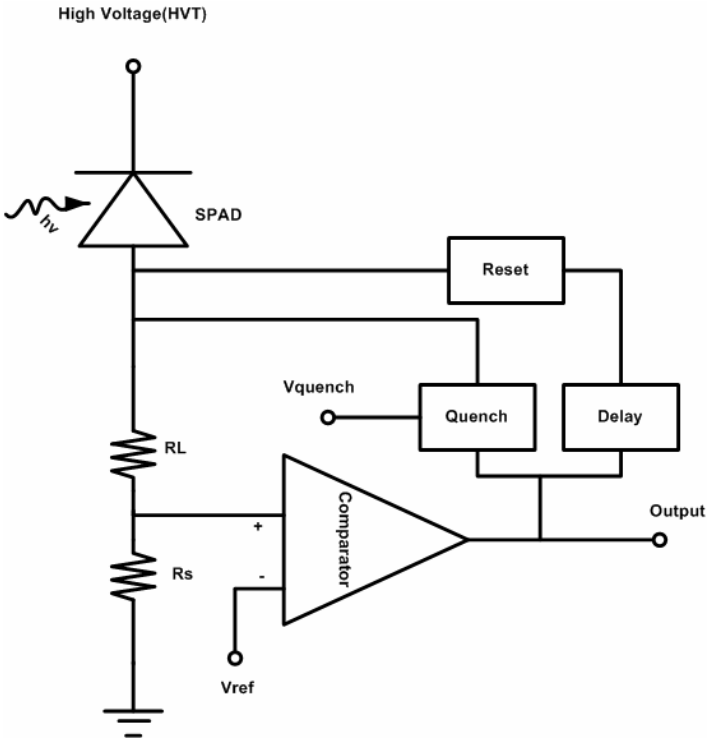

Figure 2.12 Mixed passive-active quenching

Mixed passive–active quenching is convenient for minimizing the charge in the avalanche pulse, particularly for SPAD's having small diode resistance and small stray capacitance. A passive load R_L can provide a prompt drastic reduction of the avalanche current. An active loop can complete the task after loop delay by forcing the SPAD

voltage well below the nominal V_B, with sufficient margin to ensure final quenching and avoid resignation that is due to non-uniformity of V_B over the SPAD active area. The active loop also forces a fast reset transition and makes it possible to introduce a controlled hold-off time. By minimizing the pulse charge, trapping and SPAD power dissipation can be minimized.

Furthermore, this mixed approach appears particularly suitable for developing compact circuits. It is worth stressing that it gives flexibility in the choice of the passive load. Since a quasi-quenching action is sufficient, load resistance R_L can be smaller than the minimum value required for passive quenching. An inductive load can also be employed to enhance the reduction of the avalanche current for a short time, covering the delay of the active feedback loop. However, to obtain satisfactory results and avoid overshoots and ringing that are due to the unavoidable combination of inductance and capacitances, such a circuit must be accurately analyzed and carefully implemented.

2.5 Unique quenching circuit designed in our lab

A successful single photon counting module (SPCM) is developed and implemented in our lab. Please refer to **"***Single Photon Counting Module Based on large area APD and novel logic circuit for quench and reset pulse generation***"** IEEE Journal of Selected Topics in Quantum Electronics. The system block diagram is shown in Figure 2.13.

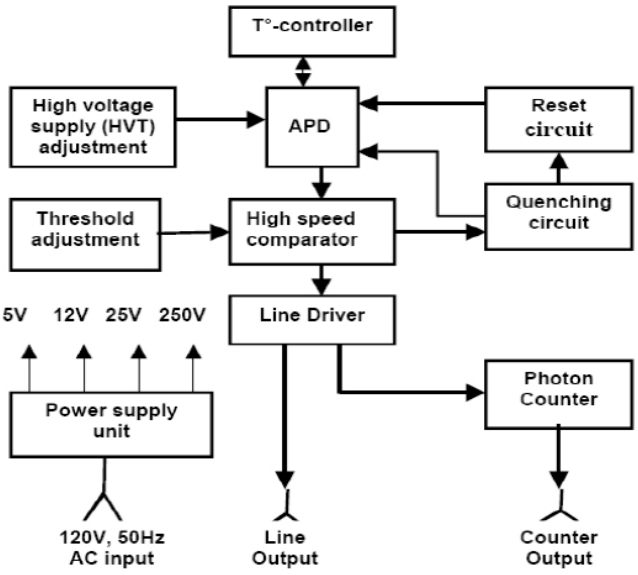

Figure 2.13 Block diagram of the single photon counting system developed in our lab

This system was designed for universal purpose at the start point so that different devices can be plugged in and tested with a few modifications. The system has been implemented by using the large area APD (C30902S-DTC model) from PerkinElmer Optoelectronics as the single photon detector. Satisfactory results have been obtained for DNA sequencing tests. We can divide the system into five parts: power supply, temperature controller, APD, quenching and reset circuit, and counter. The Single Photon Counting Model (SPCM) includes three parts: temperature controller, APD, quenching and reset circuit. The connectors going to the power supply and temperature controller are mounted on the module. The part which needs most complicated and creative design is the quenching and reset circuit. The schematic of this part is illustrated in Figure 2.14.

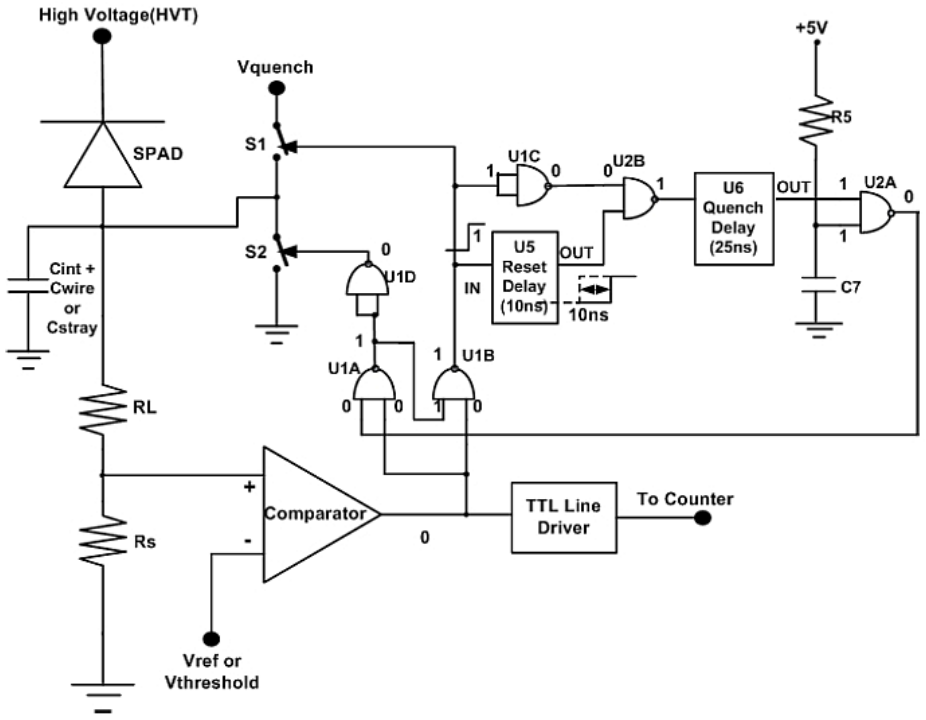

Figure 2.14 Quenching and reset circuit with NAND gates

To explain how the circuit work, we assume that S1 (quench switch) is a P-channel device that turns on when a 0 is applied; and S2 (reset switch) is an N-channel device that turns on when a 1 is applied.

Case 1: No photon is detected

When no photon is detected, the comparator output remains zero, the outputs of U1A, U1B and U1D are 1, 1 & 0 respectively, and hence S1 and S2 both are off. The output states of all other gates and devices are shown in Figure 2.14. The circuit continues to remain in this state until a photon is absorbed in the active region of the device and initiates an avalanche.

Case 2: Photon is detected and avalanche is initiated

When a photon is detected and an avalanche is initiated, large current flows through the SPAD. This current is partially quenched to a very low value due to the voltage drop

across the large resistor R_L. When the voltage at the positive input of comparator crosses Vref (threshold of comparator), the comparator's output goes to a high level. Output of U1A and hence U1D remains same, hence S2 continues to remain off. U1B output goes low, hence S1 is turned on and Vquench is applied to the anode of the SPAD, quenching the avalanche. The output of U1B is also applied to U1C and the reset delay IC U5. The output from U1C propagates further through U2B, quench delay IC U6, U2A, U1A and finally generating a '1' at the output of U1D, thus turning on switch S2, initiating the reset action. At the same time, output from U1A goes to U1B, which generates a '1' to turn off switch S1. The reset action is terminated after about the time determined by the reset delay IC U5 when the '0' at the input of reset delay IC U5 propagates through the same loop and turns off S2 and so the SPAD is ready to detect another photon. Therefore, the quench delay is generated by U6 and reset delay is generated by U5 and they are adjustable. This loop action takes place each time the SPAD fires and the current is large enough to trigger the comparator.

Figure 2.15 is the picture of final PCB module design composed of SPAD, quenching circuit, and temperature controller. The power supply and the counter are mounted on a separate board respectively.

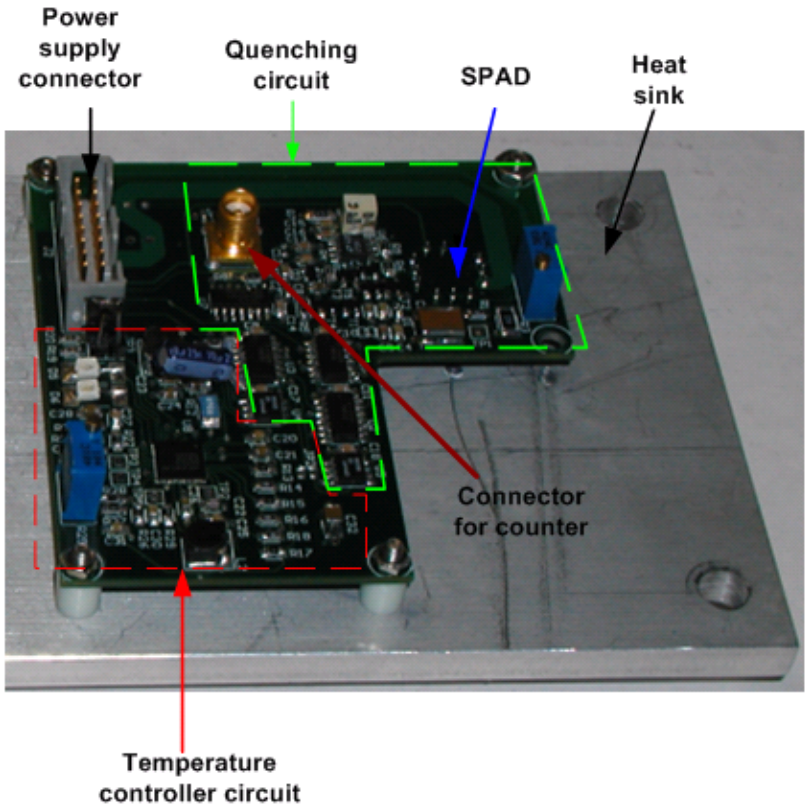

Figure 2.15 Final PCB mounted on heat sink

Testing results of the PCB single photon counting module (SPCM)

Dark Count Rate

Figure 2.16 shows the measured dark count rate of the PKI C30902S-DTC model at two different temperatures, viz. -20°C and +22°C. DCR has a linear dependence on the V_{OV} at both temperatures. When the temperature was changed from +22°C to -20°C, the DCR decreased by ~42 times and this difference is consistent at almost all V_{OV}, which clearly showed that DCR can be significantly reduced by operating the device at lower temperatures. For -20°C, the DCR does not increase much with V_{OV} and even at V_{OV} = 15V the DCR is just 500 Hz, which can be negligible for DNA-sequencing.

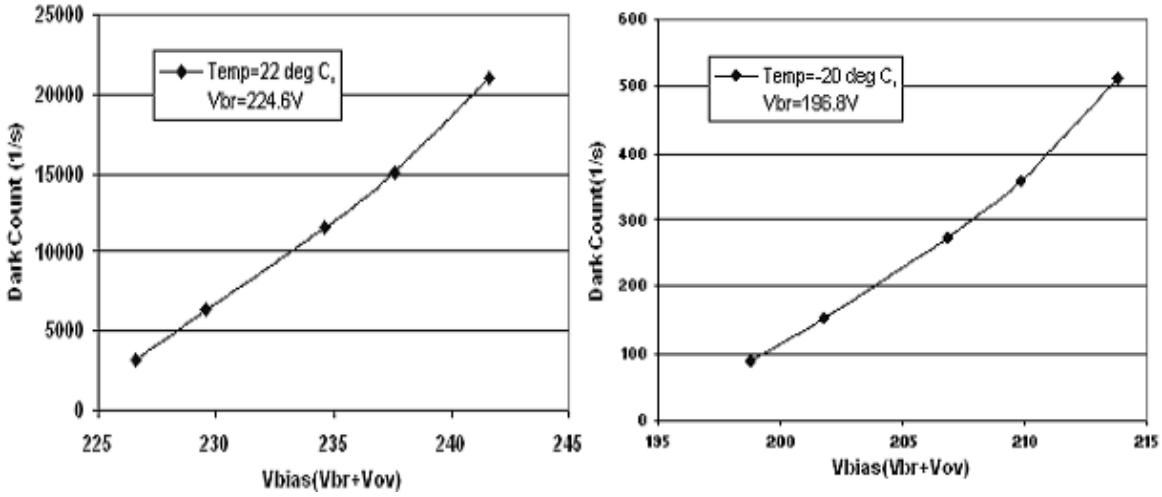

Figure 2.16 PKI C30902S-DTC: dependence of dark count rate on over-voltage

Dead Time

The dead time is the time for which the detector is insensitive to incoming photons. Beginning of the dead time can be considered to be the time when the detector starts generating an avalanche and the ending time can be considered when the bias voltage is restored above the breakdown. Therefore for our quenching and reset circuit the dead time is approximately equal to the sum of three times: time to quench, quench delay time, and reset delay time. Based on the component delay and the selected delay time, the dead time of our SPCM is 50~60ns. This means that theoretically a maximum saturation count rate of 16-20 MHz is possible.

Sensitivity and linearity

The optical attenuation versus photo count rate (PCR) curve for each V_{OV} is plotted in Figure 2.17. And the attenuation versus PCR curve of PKI SPCM plotted as a benchmark is also shown in Figure 2.17. The PKI SPCM is known as the best commercial photon counting module on the market. The experiments are taken under the

same condition for both our SPCM and PKI SPCM. Our SPCM is approved comparable with the PKI SPCM in sensitivity and linearity.

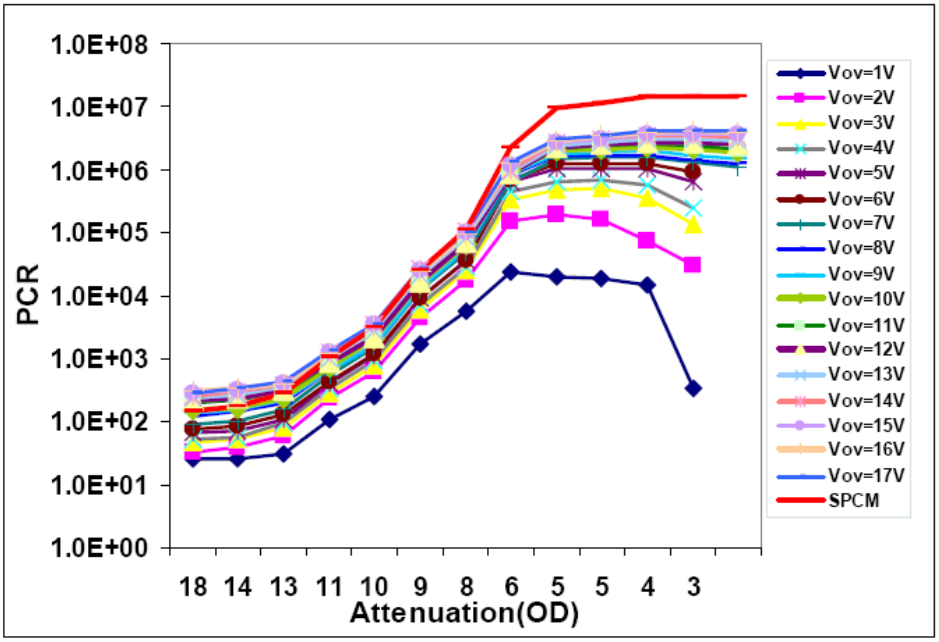

Figure 2.17 Our SPCM: Attenuation versus PCR at different over-voltages

Sensitivity of a SPAD can be increased by increasing the V_{OV} since the avalanche triggering probability increases with V_{OV}. But since increasing V_{OV} also has the effect of increasing the DCR and after-pulsing, operating at high V_{OV} is not feasible in many applications. And the maximum count rate was found to be ~4.3 MHz at V_{OV} = 17V. Comparing to the theoretical maximum saturation count rate of 16-20 MHz, this means that either the SPAD was not capable of operating at such a high frequency or the quenching circuit was not capable of working at high speed.

To solve the existing problems and to improve the performance of the current SPCM was the research which I have worked on.

3. Research on new SPAD selection and ASIC quenching circuit design

Though the single photon counting system has been implemented in our lab, there are still chances to optimize it in many aspects: circuit complexity, dead time, sensitivity and linearity, area, portability, and cost.

There are two research directions to do the improvements. One is to find a cheaper and smaller photon detector to replace the expensive and bulky PKI C30902S-DTC model, so as to make upgrading the single channel module to multi-channel module much easier. The other is to implement the quenching and reset circuit with ASIC design to make the dead time smaller and to make the detector array possible.

3.1. Experiments on Hamamatsu Si APD S9073

3.1.1. Motives to select Hamamatsu Si APD S9073

Our existing SPC module uses the C30902S-DTC model from PerkinElmer Photoelectronics as the single phone detector. It has a good performance on dark count rate and sensitivity, but it is built with cooler and it is very expensive (~$2000). The

cooler with heat sink and temperature controller covers almost half area of the PCB (see Figure 2.15). So the high price for a single device and the large area covered is an obstacle for us to upgrade the single channel to multi-channel system or to upgrade to a detector array. This encouraged me to test Hamamatsu Si APD on our quenching circuit.

There are not so many available SPADs in the market. Hamamatsu Si APD S9073 series interests us for its cost (~$10) and performance. It is without cooler, and much smaller than the C30902S-DTC model. But it is designed for linear mode application. Actually, the C30902S-DTC model is also designed for linear mode applications at the beginning. But we approved that it is working well for Geiger-mode applications in our lab for DNA sequencing if it can be quenched well.

For above reasons, to test the Hamamatsu Si APD S9073 with our successfully designed quenching circuit is a meaningful experiment.

3.1.2. Experimental results

Table 3.1 Specifications of Hamamatsu Si APD S9073

Effective active area	0.2 mm diameter
Spectral range	200~1000 nm
Quantum efficiency	80%
Breakdown voltage	150~200 V
Dark current	0.2~5 nA
Gain	50
Cutoff frequency at Rl=50	900M

In Table 3.1 are the specifications of this APD taken from the data sheet [24]. Under 50 gain, 0.2~5 nA dark current is equivalent to 25~600MHz DCR. It is a huge DCR. Cutoff frequency of 900M means that this APD can be used in very high speed applications potentially. It is the fastest detector which I have known so far. The Hamamatsu APD has been characterized as follows:

Output pulse

The breakdown voltage of this series is ranged from 150V to 200V which is specified in the datasheet. Breakdown voltage is different for individual APD. It is marked in the passport which comes with each APD. As I mentioned in chapter 2, the breakdown voltage depends on temperature due to the thermal effects. The temperature coefficient is also specified in the datasheet. So the breakdown voltage in our room temperature can be measured or calculated.

The temperature coefficient of the model is 0.14V/C. The breakdown voltage on the passport Vb = 160V at 25C. The natural room temperature in which experiments are undertaken is 20C. So the calculated breakdown voltage is 159.3V.

This Hamamatsu Si APD is without cooler, so the temperature controller on our PCB is jumped. The first step is to measure the breakdown voltage in the room temperature. And a metal heat sink is also attached to the surface of APD to avoid the temperature rising from circuit heating. A three pin connector is used to plug the APD into our quenching circuit board. The high voltage bias should be increased slowly starting from a voltage much below breakdown, just to make sure the diode will not be damaged by a suddenly applied very high voltage. Until the bias voltage adjusted to 159.2V, the output pulse (see Figure 3.1) can be observed. So we can determine that 159.2V is the breakdown voltage at which the avalanche process can be observed.

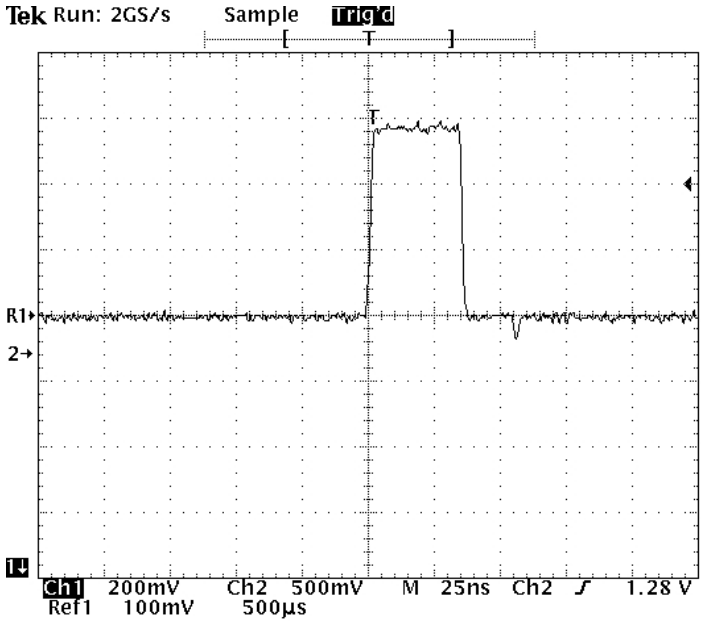

Figure 3.1 Output pulse from the line driver

The breakdown voltage 159.2V is much lower than the breakdown voltage of the C30902S-DTC model (224V at 20C). It is an advantage for reducing power dissipation.

The standard output pulse can be observed from this small Si APD as seen in Figure 3.1. So we can conclude that it is able to be operated as a single photon detector potentially.

Dark count rate

Dark count rate is one of the most important parameters, usually the first measurement to take on any APD. For the details about dark count rate, please refer to chapter 2. Hamamatsu Si APDs are designed for linear applications, so in the datasheet there is no dark count rate but only the dark current. Nobody had quenched it and used it for photon counting so far.

The Stanford counter SR200 was used to record the count number per second. Before testing, it is important to make sure if all the connections are correct and if the diode is

properly biased. The dependence of dark count on the over-voltage with different reference voltage of comparator (Vcomp) is illustrated in Figure 3.2.

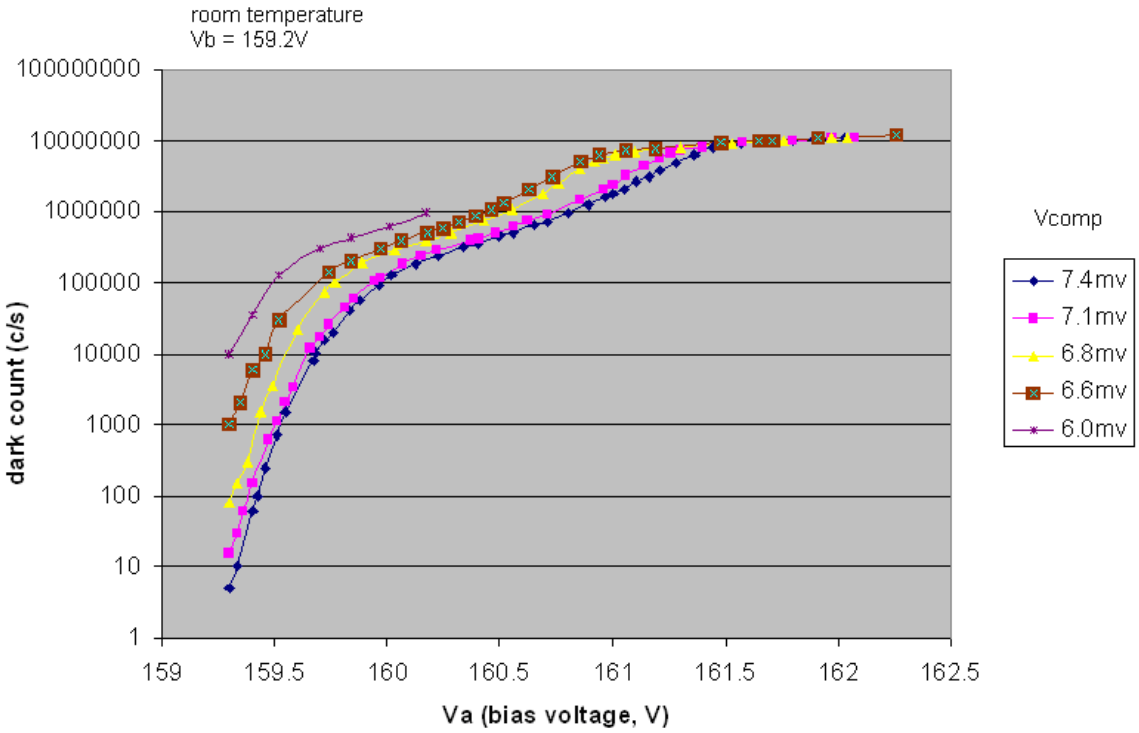

Figure 3.2 Dependence of dark count on bias voltage of Hamamatsu Si APD S9073

In the range of 159.3~160.5V, the dark count depends on the bias voltage linearly with a large slope. In the range of from 160.5~161.5V, the dependence is linearly with a small slope. When the bias voltage is higher than 161.5V, the dark count saturates to 10 million counts per second. The expected DCR is 25~600MHz as described before. It means that the traps in the APD have never been exhausted. More over-voltage is required to obtain enough gain.

As described in the chapter 2.5., even in the temperature 22C and over-voltage 10V, the dark count of the PKI C30902S-DTC model is just about 10,000 counts per second. But for the Hamamatsu Si APD S9073, in the temperature 20C and over-voltage 1V, the dark count is 100,000 counts per second.

Testing with light source

Though the dark count is high, I still expect the Hamamatsu APD could "see" the light. The experiment is setup according to the block diagram shown in the Figure 3.3.

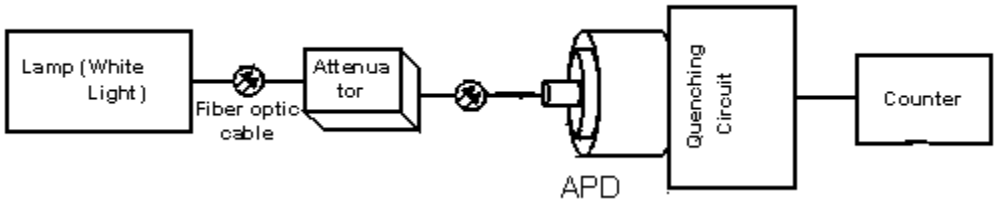

Figure 3.3 Block diagram of experiments with light source

The optical fibers used are standard fibers with a core of 62.5μm. The attenuator box consists of 2 adjustable neutral density filter wheels for selecting filters with different optical density (OD) from 0 to 5 OD.

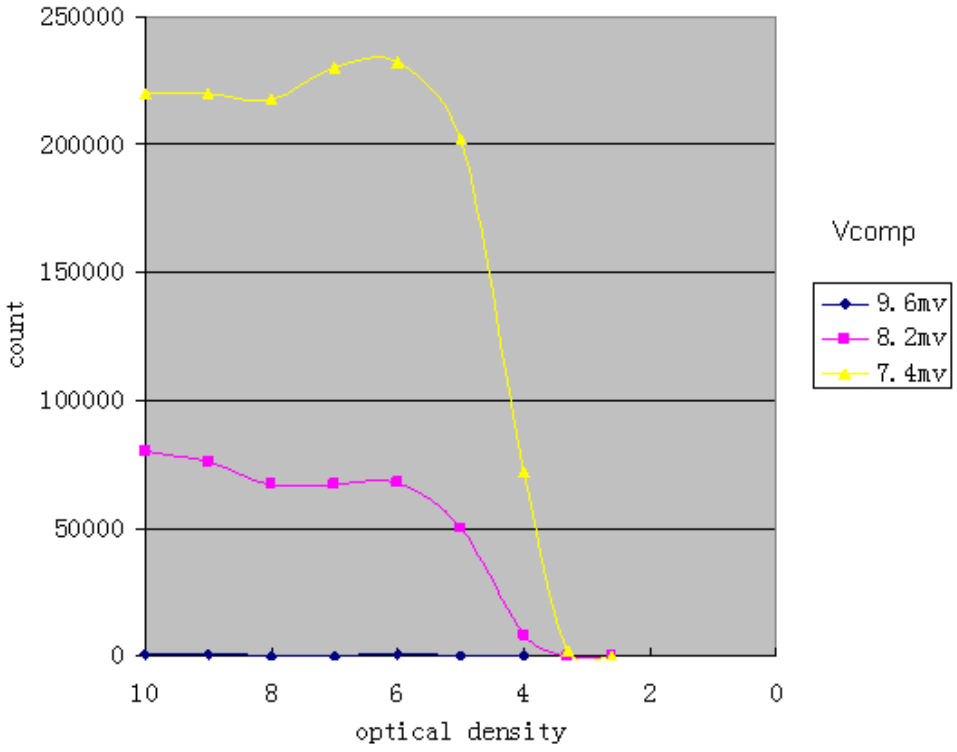

Figure 3.4 Photo-count versus attenuation with different thresholds of comparator

Unfortunately, the Hamamatsu Si APD is almost “blind” to our light source. See the results in Figure 3.4. At OD = 10, the photo-count is the dark count. When the OD is decreasing, the intensity of the light increasing, the photo-count is decreasing instead of increasing. After OD = 5, the photo-count drops to zero, saturation point is hit.

Actually for each over-voltage, the photo-count should saturate at a point and then the count drops fast when more light is applied. After the saturation point, the APD goes to “blind”. There is supposed to be a linear increasing region of the photo-count according to the increase of light intensity. But in Figure 3.4, for the Hamamatsu APD which is operated in reverse biased 1V above the breakdown voltage, there is no such a linear increasing region. Hamamatsu APD keeps counting the dark count until hitting the saturation point at OD=5.

Operating region

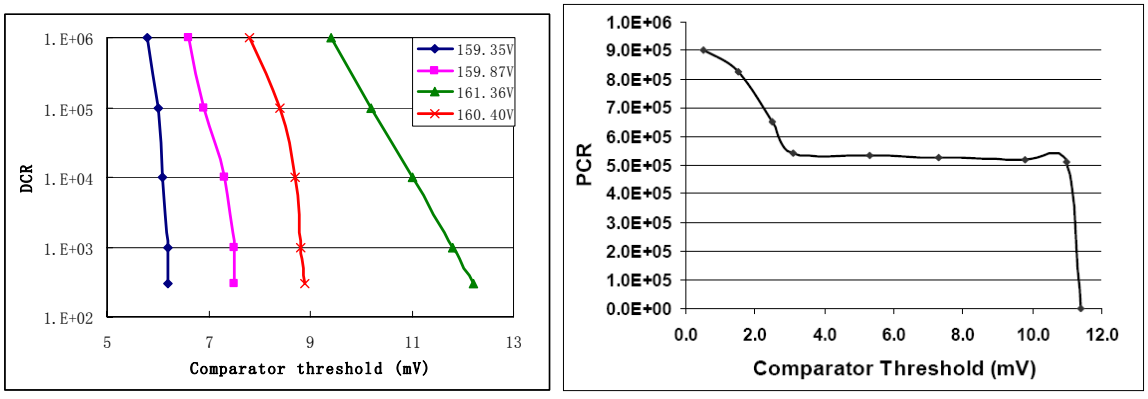

(a) (b)

Figure 3.5 DCR vs. Comparator threshold (a) Hamamatsu APD (b) PKI C30902S-DTC model

For PKI C30902S-DTC model, in the curve of PCR vs. Comparator threshold there is a flat region can be found. The PCR doesn’t change with the readout comparator threshold. It means that all the traps are exhausted and the device is able to count photons. This is the operating region which we need to find out. But for Hamamatsu APD, we

can't find this region. DCR of this APD keeps changing with comparator threshold. So under the current condition, Hamamatsu APD is not able to count single photons. What we observed on oscilloscope could be the pulse of more than 1 photon electron.

3.1.3. Discussion

Let me analyze the situation using Poisson distribution. During the 50ns deadtime, there are more than 1 release from the traps happened. And we count all the release as one pulse. Using Poisson probability mass function, we can get the distribution of DCR.

$$f(k;\lambda) = \frac{\lambda^k e^{-\lambda}}{k!}$$

Assume total count is 10MHz; K = 0~15 events happen in 50ns, average occurrence during 50ns is $\lambda = 5$. Now calculate the distribution as shown in Figure 3.6.

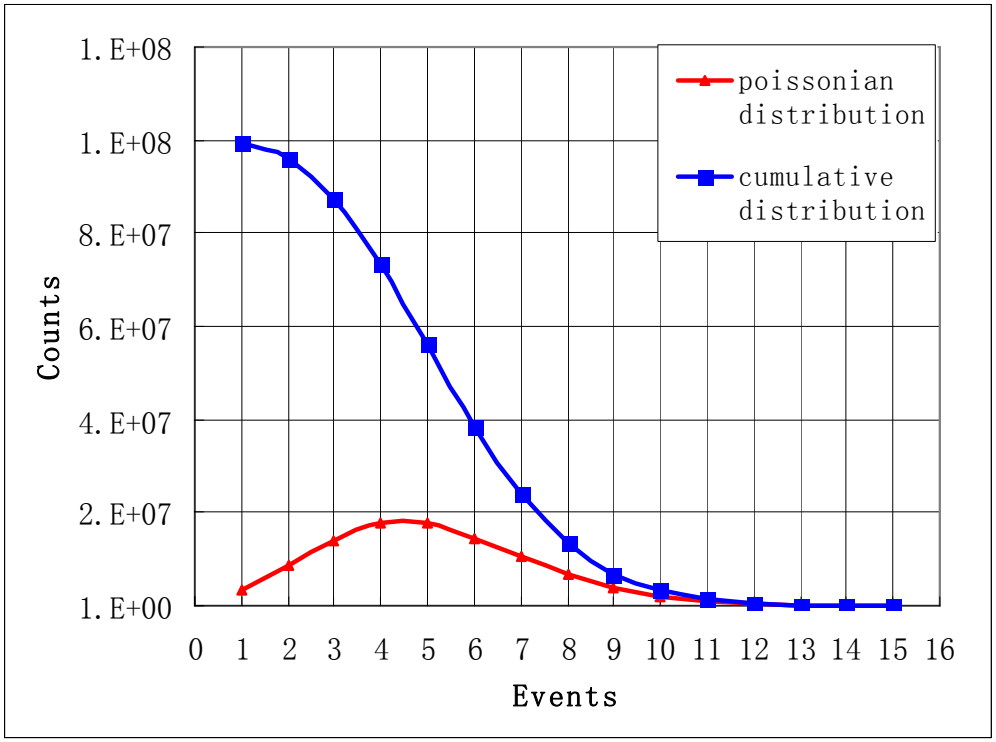

Figure 3.6 Poisson distribution of DCR

So at 10MHz, what we count is 8 photon electrons, not single photons. At least 8 times of gain is required for this APD to count single photons. The higher over-voltage can be applied to obtain enough gain for counting single photons. But our quenching circuit (50ns deadtime) is not fast enough for Hamamatsu APD.

Hamamatsu Si APD S9073 is a linear-mode device. It is not supposed to work in a very high reverse bias voltage. But for Geiger-mode APD, the very high electric field in the avalanche multiplication region is necessary to accelerate carriers. If the over-voltage is not enough for a high field in this region, some carriers are captured by deep levels. Subsequently released carriers can trigger the avalanche, generating afterpulses correlated with previous avalanche pulse. These afterpulses increase the thermally generated dark count as a positive feedback. So we can say that Hamamatsu APD still need to be fined to remove all generation-recombination centers so that the after-pulsing introduced dark count can be reduced.

3.2. ASIC Design of Quenching Circuits

3.2.1. Motives

The PCB design of single photon counting module based on the PKI large area APD has been described in the chapter 2.5. The performance of this module, such as dark count rate, dead time, dynamic range, and linearity has been discussed. The 32-channel SPCM based on the single-channel PCB module is shown in Figure 3.7.

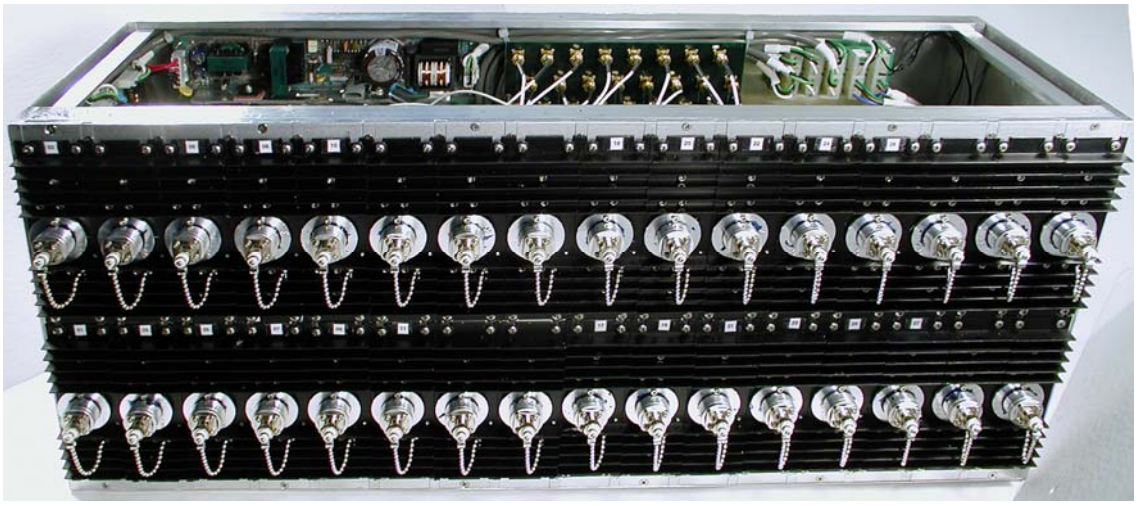

Figure 3.7 32-channel single photon counting module based on PCB design

You see from the above picture how bulky the module is. And it is not feasible to develop more than 100 channels based on the PCB design. To implement the quenching and reset circuit in ASIC design is an idea to make the module more compact. And it is also a very good approach to make the dead time smaller if a high-speed circuit can be designed.

3.2.2. ASIC design specifications

Firstly we need to decide what component will be in the ASIC design and what processing technology we are going to use. The block diagram of the single-channel module is seen as Figure 3.8.

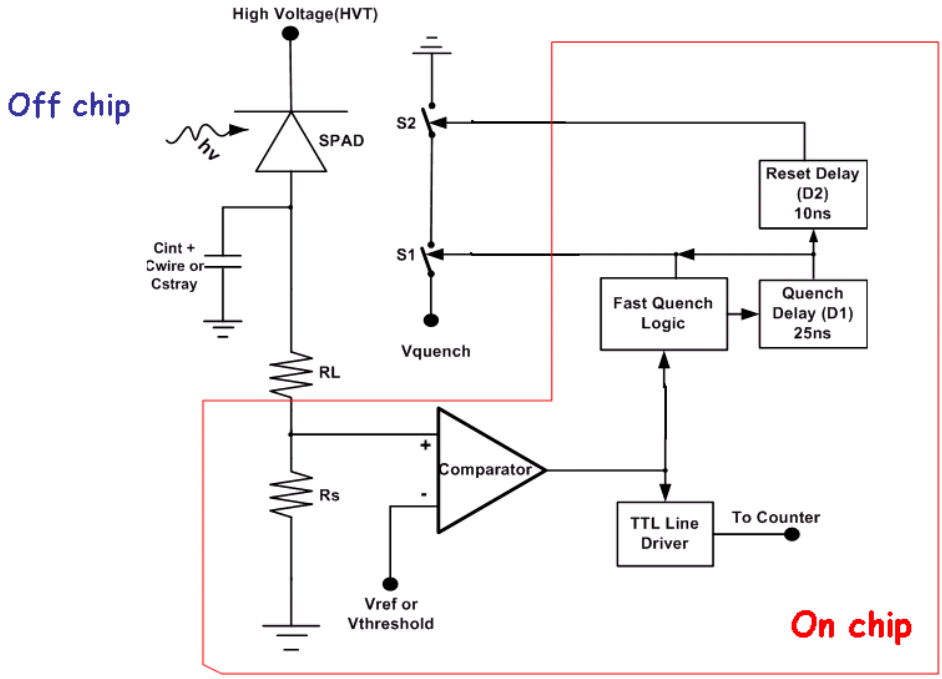

Figure 3.8 Block diagram of the single-channel module

The bias voltage for SPAD is usually 100~200V. The drain source voltage of transistor can be up to 100V for some high voltage CMOS process. So to implement the photodetector and the switch S1 and S2 in CMOS technology is not practical. I prefer to leave them off chip. Then only the comparator and the timing logic part will be on chip. The standard 0.6um CMOS technology is enough to implement the design. The quenching logic, reset delay, and quenching delay can be designed using the logic gates from the standard digital library. The critical part is the comparator design.

There are two approaches to sense the avalanche: one is to sense the voltage drop on the load resistor; the other is to sense the current change. To sense the current change is more sensitive and high speed. I am going to design a charge comparator other than a voltage comparator, so low input impedance is necessary.

The specifications of the charge comparator are as follows:

- High speed

Propagation delay should be less than 10ns

- High sensitivity (small offset)

  Minimum detectable current is ~10uA

- Low input impedance
- Moderate gain amplifier with low input noise
- Large bandwidth

3.2.3. Schematic design and simulations

The schematic of the comparator has been designed in 0.6um CMOS technology and simulated using Cadence tools. Three main parts are in the comparator design: input stage, feedback OPAMP, and the output stage. Please see the schematic in Figure 3.9.

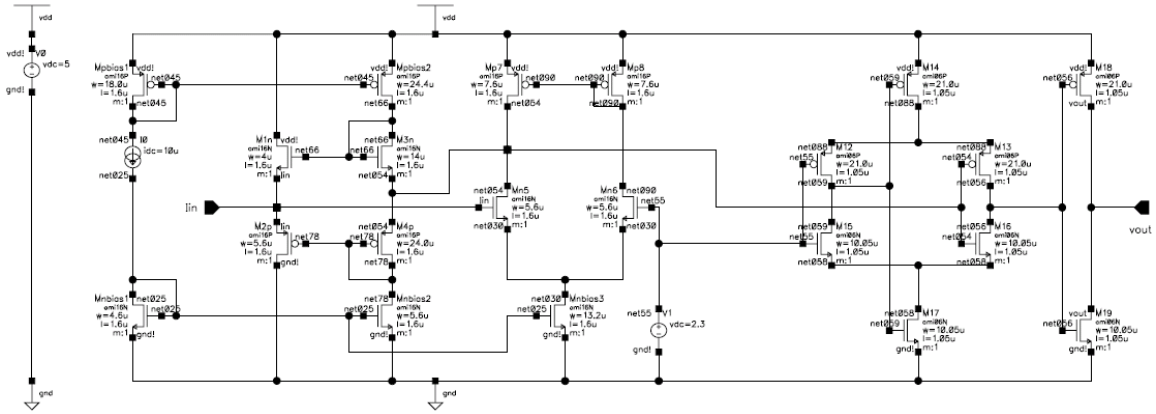

Figure 3.9 Schematic of comparator

- Input stage

  Two common gate transistors are designed to sense the input current of both polarities and to have low input impedance;

- Feedback OPAMP

  To amplify the voltage change due to input current, and is also a negative

feedback to reduce the input impedance and enlarge the bandwidth;

- Output stage

  A latch is designed to speed up the output and make the output a square wave from ground level to power rail according to the input current change, then going to the external counter.

The transient simulation with a 10uA input current pulse is done in Cadence Spectra simulator, and the results are shown in Figure 3.10. A standard output pulse which can be registered by external counter is observed from the simulation. The simulated propagation delay is around 6ns.

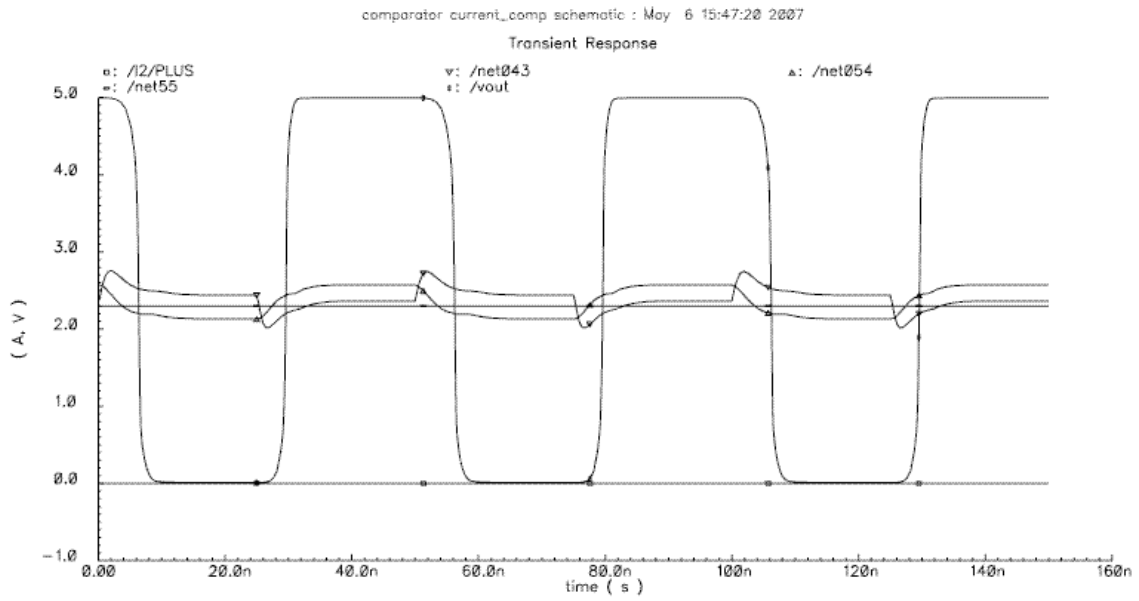

Figure 3.10 Simulation results of comparator in Cadence

3.3. Summary

To improve the existing design of single photon counting module, we put effort on two research directions. One is to replace the expensive and cooled large area PKI C30902S-DTC model by a more compact and cheaper SPAD; the other is to implement the quenching and reset circuits in ASIC design.

For the first time, Hamamatsu Si APD S9073 has been studied thoroughly. A detectable output pulse has been obtained from this small diode by working with our unique quenching circuit. So we can conclude that this linear photodiode is potentially can be used as a SPD (single photon detector) if quenched well. More gain is required to detect single photon by increasing over-voltage or by adding micro-circuit for amplification. Being cooled to -60C, it is believed to reduce DCR by at least 100 folded. Then with moderate DCR and detectable output pulse, Hamamatsu Si APD S9073 will be a very good candidate for many single photon detection systems.

For the second direction, a high speed charge comparator and the timing logic have been designed in the standard 0.6um CMOS technology. The simulations have been done in Cadence. The results are presented and meet the specifications. Due to the high voltage issue the quench and reset switches can not be implemented on chip. And the detector itself can not be fabricated in CMOS technology either. So we believe the ASIC design is more suitable for another promising device, SiPM. The details about this device are presented in the following chapters.

4. Introduction to Silicon Photomultiplier (SiPM)

4.1. Need for novel single photon detectors

In the recent decade, an emerging attention has been devoted to a solid-state version of photomultiplier, usually referred to as Silicon photomultiplier. This semiconductor photo sensitive device is built from an avalanche photodiode matrix on common substrate. The dimension of each single APD microcell can vary from 20 to 100 micrometers depending on the mask used, and their density can be up to 1000 per millimeter square. Every microcell operates in Geiger mode and is decoupled from the others by a polysillicon quenching resistor. Even if the microcell works in a digital mode, the SiPM is an analog device because all the microcells are read in parallel making possible to generate signals with a dynamic range from single photon to 1000 photons per millimeter square. The operating voltage supplied on SiPM depends on junction type and vary from a minimum of about 30V up to 70V, much less than that of the one needed for a PMT or APD.

SiPM has been developed for ten years and there is still room for improvement. It is a very promising device for many applications. Many parameters can be tailored and optimized for special needs. The operating principles, evolution, applications and

characteristics parameters of SiPM will be discussed later.

4.2. Structure and technology

A standard CMOS technology fabricated APD can be operated in Geiger-mode to work as a single photon detector. But the dark count, the dead time and recovery time after avalanche limit the area to ~100 square micrometers. When large areas are needed, a brilliant solution came up, which is to subdivide the large area into many micro-pixels and connect them all in parallel via individual quenching resistors. Every micro-pixel is an APD working in Geiger-mode which is passively quenched by the individual resistor. This kind of APD has properties similar to PMTs, therefore they are called *Silicon Photomultiplier (SiPM)*, sometimes referred to avalanche micro pixel diode (AMPD), metal-resistor-semiconductor (MRS), and limited Geiger mode photodiode (LGM). Its equivalent circuit can be seen in Figure 4.1.

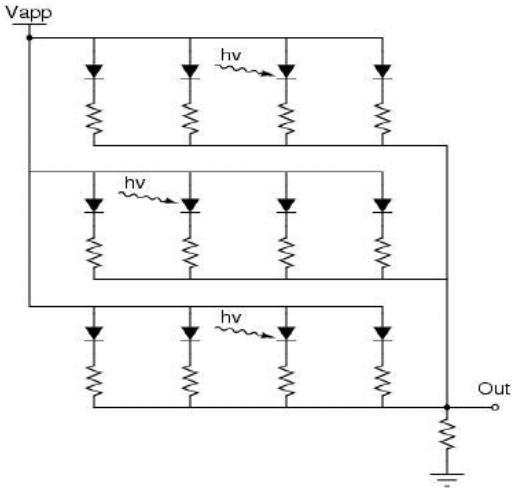

Figure 4.1 Equivalent circuit of SiPM

The first devices of this type were developed in the late 1990s in Russia and since then several more institutes and companies involved in SiPM production.[37,38] Figure 4.2 illustrates the most well-known MRS structure SiPM from CPTA (Center of Perspective Technology and Apparatus), Moscow. In the MRS structure of this SiPM, the resistive load is a special technology layer deposited on the diode surface. By using the high-resistivity material SiC, the resistor element can be made small whilst providing adequate quenching. A semi-transparent metal contact layer on top of the quenching resistance forms the electrode.

The MRS SiPM structure divides the silicon-diode surface area into a large number of regions called microcells, each of which acts like an independent and identical Geiger-mode APD. Thus, the avalanche region is localized to individual cells. If the outputs of all these microcells are summed together then the output signal is proportional to the number of microcells activated.

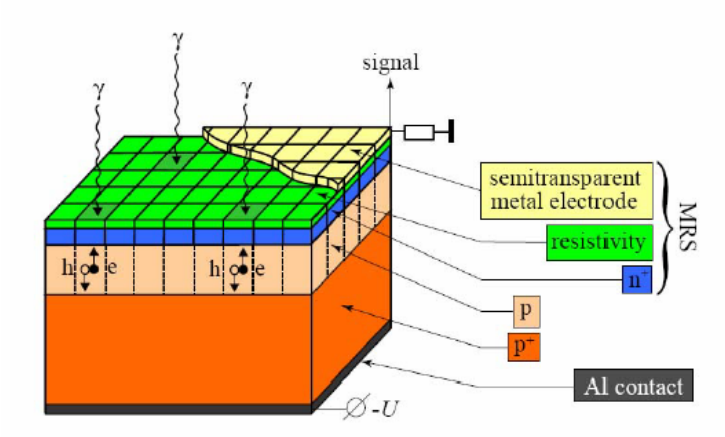

Figure 4.2 MRS SiPM structure from CPTA, Moscow

The MRS SiPM is pioneered by Obninsk State University/CPTA, Moscow and JINR, Dubna. The other type of SiPM, the polysilicon resistor structure SiPM is pioneered by MIPHI/PULSAR, Moscow [5]. The structure of this type of SiPM is illustrated in

Figure4.3. The example of SiPM has pixel size 42x42 um^2, and a total pixel number *m*=576 on the area of 1 mm^2. The SiPM topology is shown in Figure 4.3b. A few micron epitaxy layers on low resistive p substrate forms the drift region with low built-in electric field (see Figure 4.3c). The thin depletion region (0.7~0.8 um) between the p+ and n+ layers with very high electric field (~10^5 V/cm) is created, where the conditions for Geiger mode discharge take place (*Vbias* > *Vbreakdown*). The electrical decoupling between the adjacent pixels is provided by polysilicon resistive strips and uniformity of the electric field within a pixel by the n- guard rings around each pixel. All 576 pixels are connected by common Al strips, in order to readout the SiPM signal. The results of SiPM from MEPhI with 1000 pixels on the 1mm^2 sensitive area have been also reported [43]. And the SiPM of 3*3mm^2 active area is carried out by the two competitors, CPTA and MEPhI & PULSAR. 5*5 mm^2 is available and 10*10mm^2 is planned.

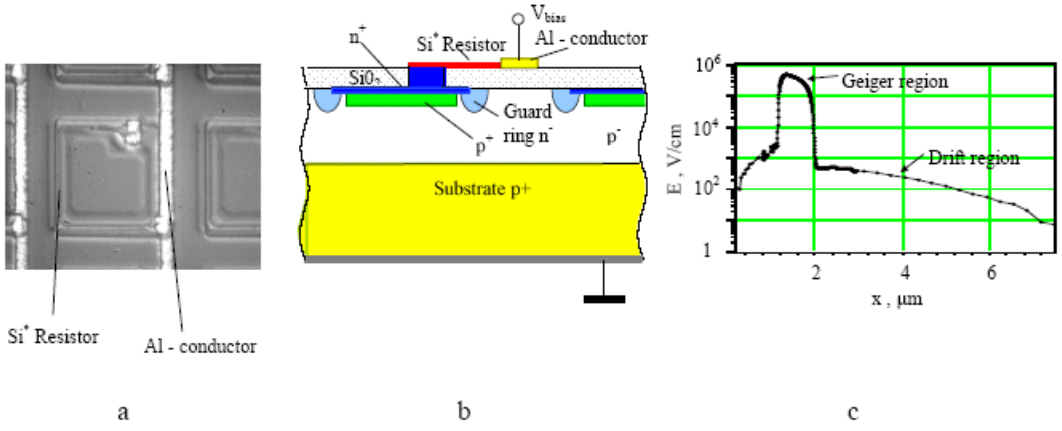

Figure 4.3 Polysilicon resistor SiPM from MEPhI & PULSAR®
(a) SiPM microphotograph, (b) topology and (c) electric field distribution in epitaxial layer

Since 2005, Paul Scherrer Institute (PSI) and Hamamatsu Photonics worked together for the development of a radiation-hard APD for CMS ECAL and had very good success. The development continued based on a similar design for a multi-cell avalanche

photodiode operated in Geiger-mode. Hamamatsu produced several prototypes of SiPM with an area of 1mm^2. Some of them are made with different masks on the same wafer. They have different cell areas and different quenching resistors, but all other parameters like the doping profiles and the thickness of the various silicon layers are identical. Some of the properties of the devices have been measured and reported by D.Renker et al [44].

On July, 2007, Hamamatsu Photonics released MPPC and its datasheet. The size is more compact, the number of pixel is available at 100, 400, and 1600, which is much more than the old version of 100 pixels. Figure 4.4 shows the picture of Hamamatsu MPPC.

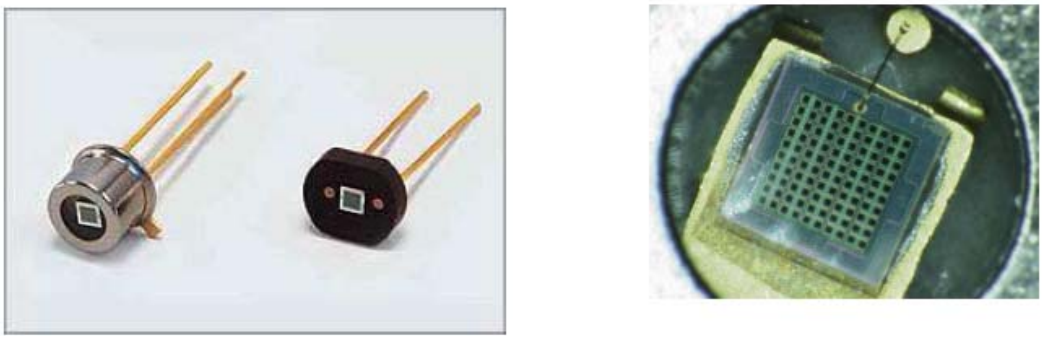

Figure 4.4 Photograph of MPPC (left) and the close-up view of the active area (right)

We ordered a SiPM with cooler, which is the only SiPM with cooler as knowm so far, from Voxtel, Inc. Its parameters can be obtained from http://www.voxtel-inc.com/.

At the beginning of 2005, within the collaboration between the Italian National Institute for Nuclear Physics (INFN) and the Center for Scientific and Technological Research of Trento (ITC-irst), a 3-year project aimed at the development and application of silicon photomultipliers was launched. The structure as seen in Figure 4.5, which can be fabricated in CMOS technology, is presented by ITC-irst in [49].

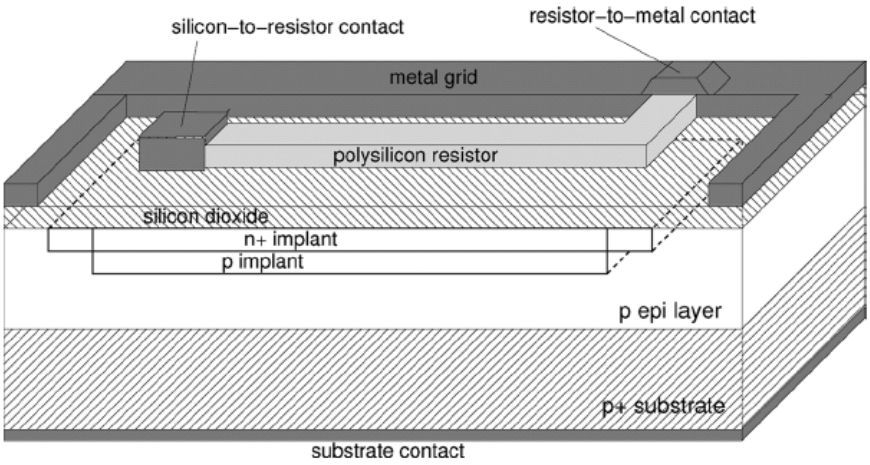

Figure 4.5 Sketch of a microcell composing the SiPM fabricated in ITC-irst

Unlike normal SPAD which has to be produced in a dedicated processing technology, such as the reach-through Slik APD from PerkinElmer mentioned before, SiPM can be produced in standard CMOS processing technology. That means its price is much cheaper, and more available. It is a great advantage for integrating the photodiode with the readout electronics, especially for multi-channel readout applications.

4.3. SiPM characteristics

4.3.1. Gain

SiPM produces a standard signal when the avalanche takes place in any micro-cell. The amplitude Ai is proportional to the capacitance of one cell times the over-voltage

$Ai \sim C (Va - Vbr)$,

where Va is the bias voltage, Vbr is breakdown voltage. The bias voltage is usually 10~20% higher than the breakdown. Therefore, the over-voltage for ~45 Volts

breakdown is of the order of a few volts, the capacitance is typically 50fF, the charge of one pixel is ~200fC, or 10^6 electrons. So the gain is usually in the range of $10^5 \sim 10^7$. When more than one cell are fired at the same time, the output is the sum of the standard pulses

$A = \sum Ai.$

The gain depends on the reverse bias almost linearly. And it also depends on temperature. As the temperature rises, the gain at a fixed reverse bias drops.

Gain measurement

Figure 4.6 below shows a typical connection for gain measurement (taken from Hamamatsu Photonics). Pulsed light is reduced in intensity by the optical attenuator and is irradiated onto the SiPM. The output of SiPM then processed by the PC to obtain a frequency distribution for that output charge. Examples of the frequency distribution are shown in Figure 4.7.

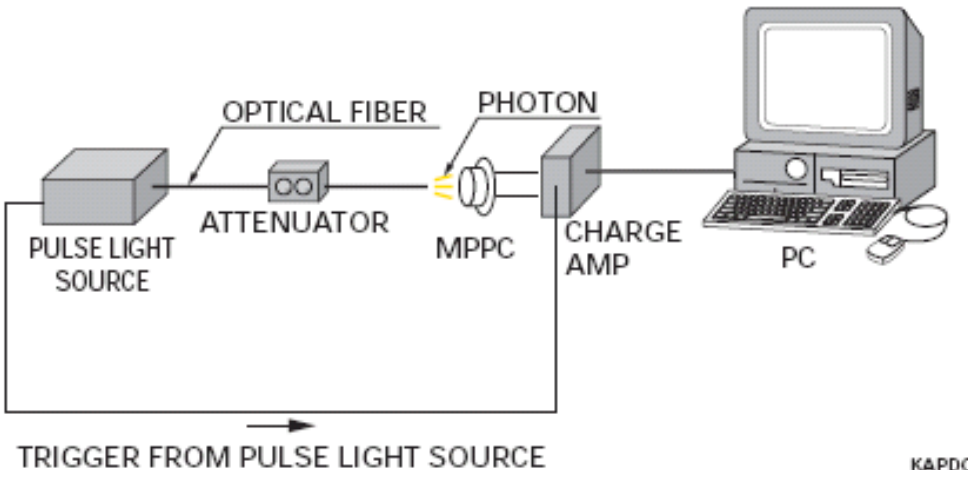

Figure 4.6 Block diagram for gain measurement setup

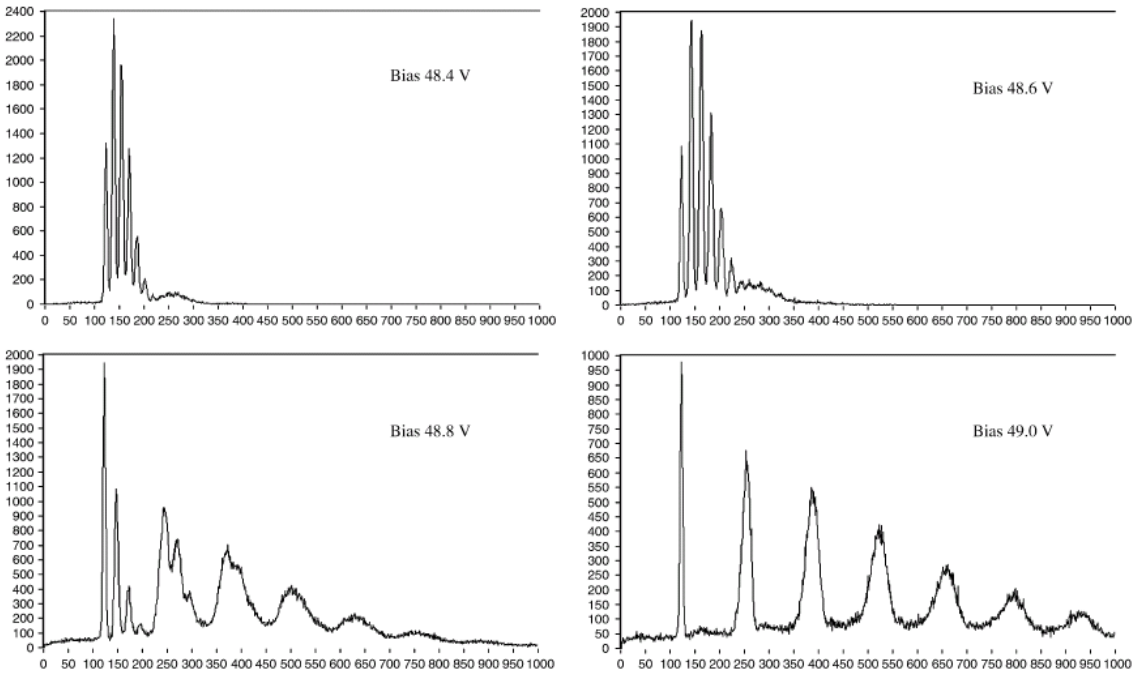

Figure 4.7 Pulse height spectra for four different bias voltages (taken from [44])

In Figure 4.7, the horizontal axis is the ADC channels that represent the amount of digitized output charge from the SiPM. The vertical axis is the frequency (count of events) at each channel (output charge). The distance between adjacent peaks exactly equals the output charge of one detected photon. The gain therefore can be expressed by the following equation:

Gain = Number of channels between 2 peaks * ADC conversion rate / one electron charge.

You also can see the dependence of gain on the bias voltage from Figure 4.7. Figure 4.8 shows the linear relationship with different temperatures and different wavelengths more obviously. This result is reported by MEPhI & PULSAR in [46].

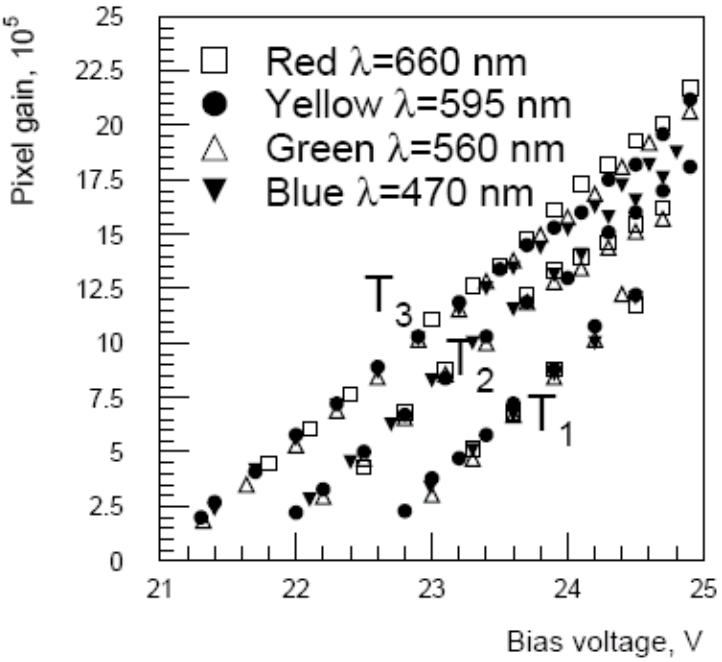

Figure 4.8 SiPM single pixel gain for different temperatures: T1=+22*o*C, T2=-22*o*C, T3=-61*o*C

The amplitude of output signal (depends on the gain of SiPM) versus the bias voltages is also tested on the MRS from CPTA with a ~150Hz green LED and reported by D. Beznosko in [45]. From Figure 4.9, you can see that after some value of bias voltage, a further increase in the bias doesn't yield an increase in amplification, indicating that gain is limited.

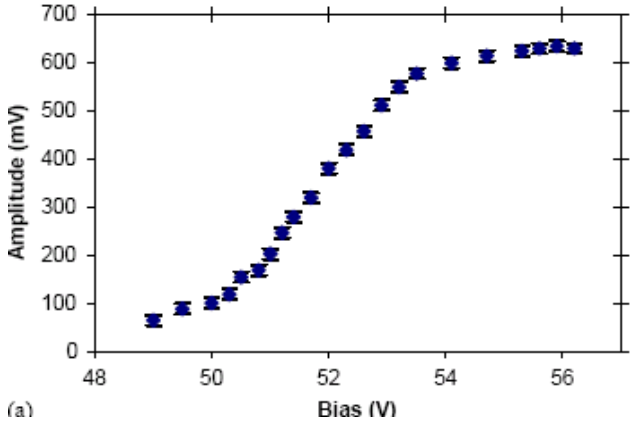

Figure 4.9 Signal amplitude as a function of the bias voltage for MRS excited with LED

4.3.2. Dark count rate

As a solid-state device, SiPM produces dark counts which are initiated by thermal generation or field assisted generation of free carriers. This dark count rate could exceed 1MHz/mm^2. The first effect can be reduced by cooling. The second effect can be reduced by a smaller field, a lower applied bias voltage. The dark counts can be reduced in SiPM production process by minimizing the number of generation-recombination centers, the impurities and crystal defects.

Dark count measurement

To measure dark count, the connection in Figure 4.6 can be used but no light source is needed. The dark count rate dependent on temperature for Hamamatsu SiPM with cell size 70*70um^2, pitch 100um, and pixel number of 100 has been tested by [44]. The gain of the device was kept at a constant value by an adjustment of the bias voltage. The one photon peak in the pulse height spectra was kept at the same position. The measurement is shown in Figure 4.10. It is good to know that the dark count is weakly dependent on the temperature. That means there are only a few impurities and lattice defects where carriers can be generated thermally. Most of the dark counts are probably due to field-assisted generation.

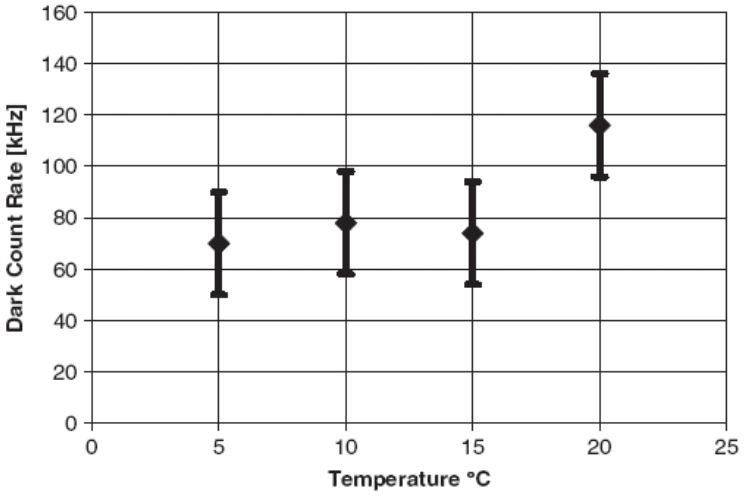

Figure 4.10 Dark count of Hamamatsu SiPM 0-100-1.5 at different temperatures

Figure 4.11 shows the linear dependence of the dark count rate on the bias voltage. And two threshold levels are tested: 0.5 and 1.5 photoelectrons. The measurement is for Hamamatsu MPPC series released by Hamamatsu Photonics on July, 2007.

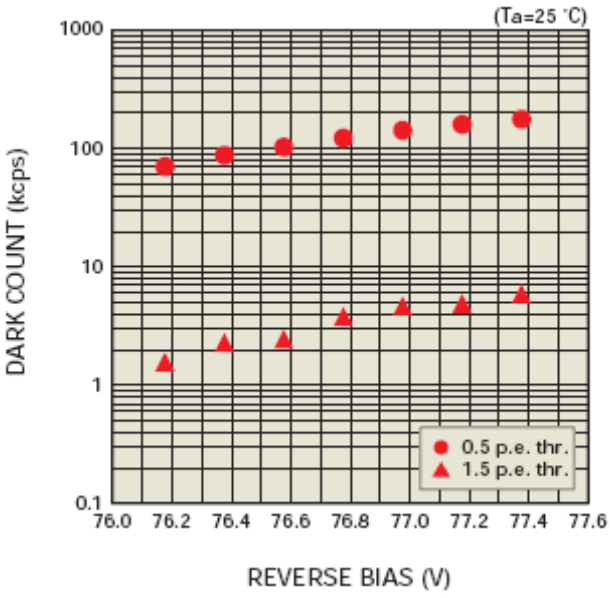

Figure 4.11 Dark count of Hamamatsu MPPC for different bias voltages

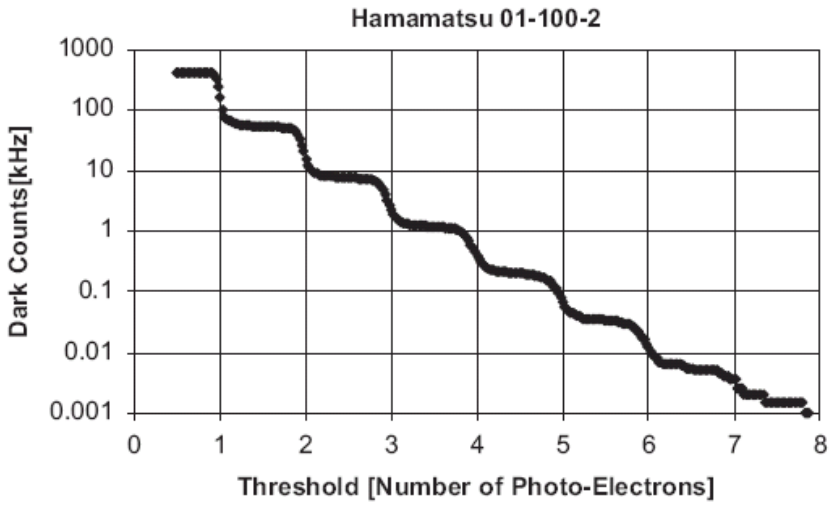

Figure 4.12 Dark count of Hamamatsu SiPM 01-100-2 for different threshold levels

Figure 4.12 is the dark count of another Hamamatsu SiPM with 70*70um2 and pitch 100um for different threshold levels taken from D. Renker's paper. The horizontal axis is the amplitude of different number of photoelectrons which can be obtained by the method mentioned in the gain measurement. The count rate falls dramatically with increasing of the readout threshold. For high energy applications, such as PET, threshold corresponding to 5 photoelectrons is still extremely low. Under such a threshold, the dark count rate is well below 100counts/second. But for our application, the high dark count rate is a concern.

The dark count signals correspond not always only to a single electron signal, but because of cell to cell crosstalk, quite large amplitudes can sometimes occur. About the crosstalk, we will discuss later.

4.3.3. Detection efficiency

As I mentioned in the chapter 2, for the SPAD, the photon detection efficiency (PDE) is the product of quantum efficiency (QE) and the avalanche triggering probability (Pt).

For SiPM, a matrix of SPAD, one more factor is added, which is called geometrical efficiency (Pgeo). Pgeo is the fraction of total SiPM area occupied by active cell areas, which is so-called fill factor sometimes. Then we have PDE = QE * Pgeo * Pt.

The QE is maximal 80~90% depending on the wavelength. The geometrical efficiency (fill factor) is limited by the dead area around each cell since some space is needed between cells for the individual resistors and to reduce the optical crosstalk. And the fill factor needs to be optimized for specific applications. Some needs large number of small cells, but some needs small number of big cells. So the fill factor can be in the range of 20~80%. The triggering probability Pt is probability that the primary carrier to trigger an avalanche when it is generated and passing through the high field region. (Please refer to section 2.3.1.)

Photon detection efficiency measurement

Figure 4.13 is the setup from Hamamatsu for the MPPC photon detection efficiency measurement. A monochromator is used.

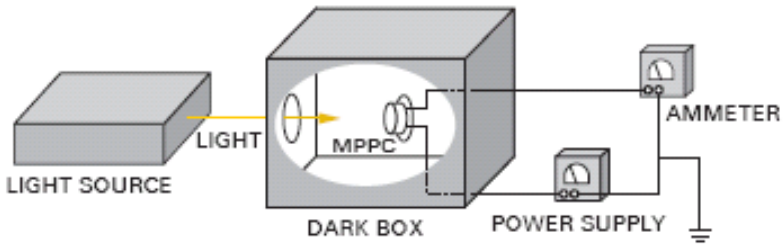

Figure 4.13 Measurement setup for MPPC photon detection efficiency

First, a well known photodiode is prepared. The ratio of its photocurrent to the incident light intensity is known. So the number of incident photons can be calculated from the output photocurrent. Next, the MPPC is installed at the same position. The gain

at the fixed bias voltage is already known. The number of photons detected by MPPC can be obtained by dividing the photocurrent by the electric charge of electron. So the MPPC photon detection efficiency is calculated by the following equation:

$$PDE = \frac{\text{Number of photons detected by MPPC}}{\text{Number of photons incident on photodiode}} \times \frac{\text{Photodiode active area}}{\text{MPPC active area}}$$

The measurement is shown in Figure 4.14.

Note: this measurement obtained by above method also take into account the effects from crosstalk and afterpulsing.

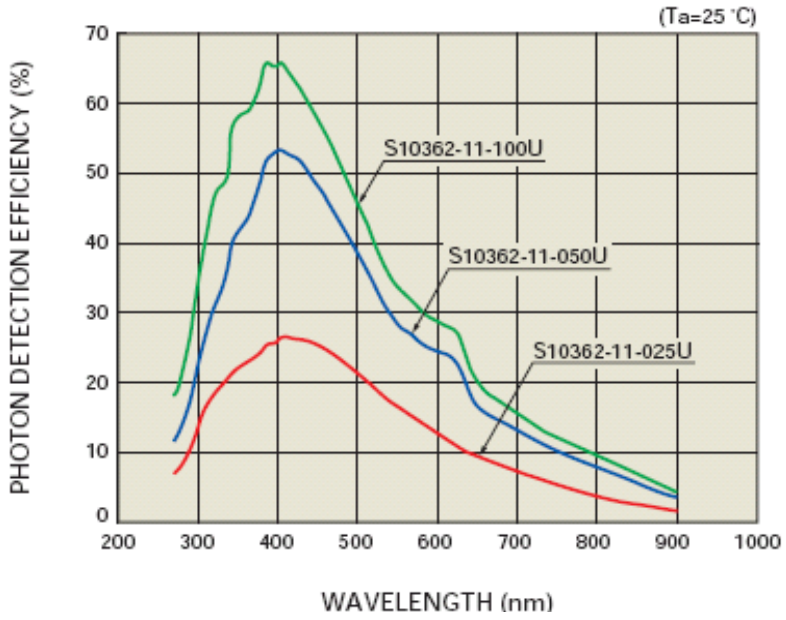

Figure 4.14 Photon detection efficiency versus wavelength for Hamamatsu MPPC

I doubt that the photon detection efficiency could reach ~70% at the peak.

Figure 4.15 is the photon detection efficiency of Hamamatsu type 0-100-1.5 tested by D.Renker's group.

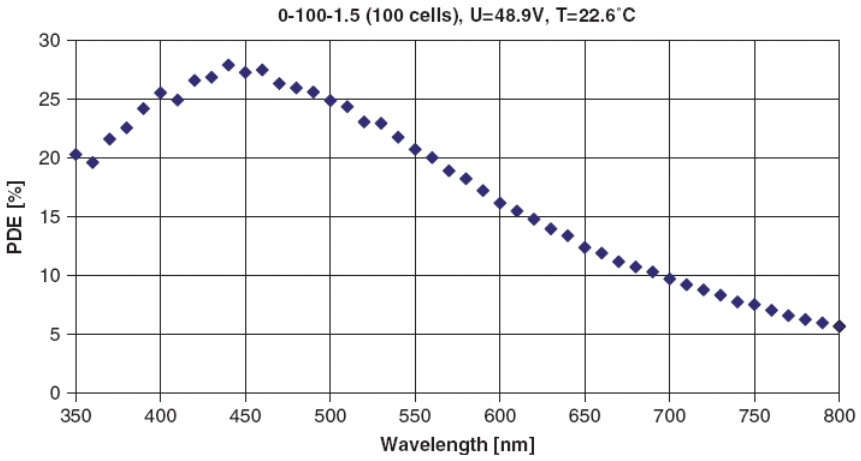

Figure 4.15 Photon detection efficiency vs. wavelength for Hamamatsu 0-100-1.5

They explained that Light with shorter wavelength is absorbed in the first layer of silicon, which has a high dopant concentration and is therefore not depleted. Carriers generated there have a high probability for recombination. Light with longer wavelength penetrates deeper and might generate carriers in or even behind the high field region. The avalanche probability is reduced because electrons have a higher chance to trigger an avalanche.

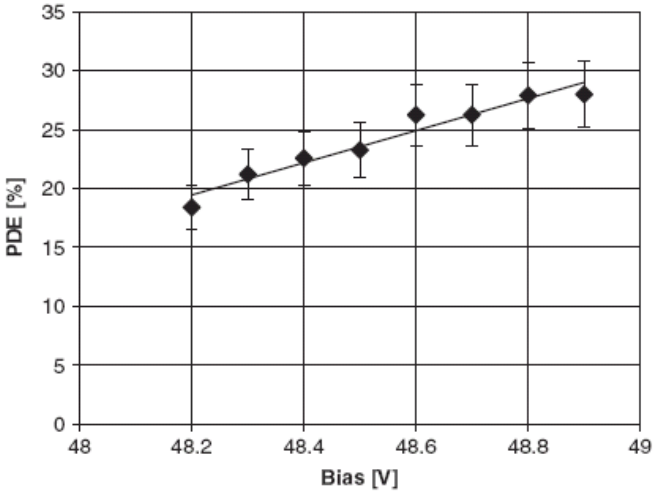

Figure 4.16 Photon detection efficiency versus bias voltage for Hamamatsu 0-100-1.5

Figure 4.16 shows the dependence of photon detection efficiency on bias voltage.

4.3.4. Linearity and dynamic range

The total number of pixels determines the dynamic range for the simultaneously incident photons.

$$Nfired = Ntotal \times \left[1 - \exp\left(\frac{-Nphoton \times PDE}{Ntotal}\right)\right]$$

Where, Nfired is the number of excited pixels; Ntotal is the total number of pixels; Nphoton is the number of the incident photons.

The photon detection linearity lowers if the number of incident photons becomes large relative to the total number of cells because two or more photons enter individual cell. The high density of cells (100–10 000/mm^2 are available) makes the response of a SiPM linear over a wide range of light intensities. The finite number of cells results in a deviation from linearity of the SiPM signals with increasing light intensity, as shown in Figure 4.17. The average number of photoelectrons per cell should be less than 50%.

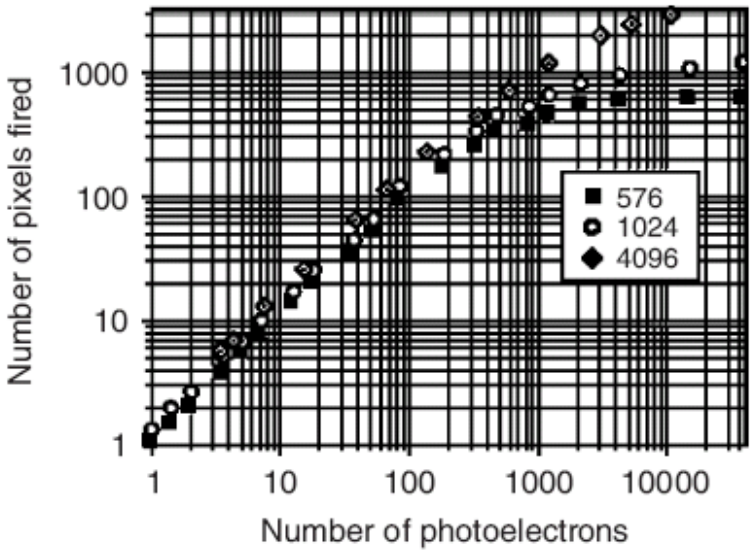

Figure 4.17 Nonlinear responses for SiPM with different number of cells. Taken from [39]

4.3.5. Optical cross-talk

In general, reverse biased silicon diodes emit light when they are operated in Geiger-mode. The photon emission rate is $2.9*10^{-5}$ photons with energy higher than 1.14eV per carrier crossing the p–n junction [40]. Photons emitted by a cell could travel to a neighboring cell and trigger an avalanche there. This effect leads to photon-assisted crosstalk between the cells and has a small but not negligible contribution to the SiPM output signals. This is a stochastic process.

Photons could be emitted towards an attached crystal and reflected there and trigger an avalanche in additional cells. This effect has been seen but it is small and can be neglected in most applications.

Cross-talk measurement

Method 1:

During the avalanche, photons generated due to microplasma could travel inside the silicon (or even retransmitting and reflecting materials, such as the case of small crystals), where they may be reflected and may trigger the avalanche of additional cells. In [47] this was tested by mounting directly in front of a SiPM a diffuse Teflon block acting as an additional reflector for photons escaping towards the front side. Figure 4.18 shows the pulse height spectrum of dark counts.

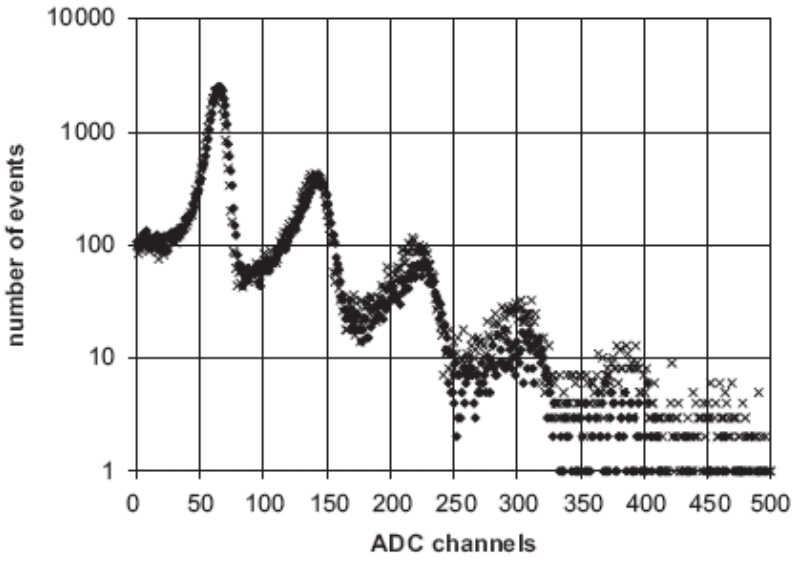

Figure 4.18 Crosstalk of the SiPM from Photonique without (■) and with a Teflon reflector (×).

With the particular SiPM used in this test the probability that cells fired was 19% without the reflector and the probability went up to 24% when the reflector was mounted. The difference of 5% was caused by photons generated in the avalanched pixels which were reflected and have triggered an additional avalanche in another cell.

Method 2:

Because cross-talk only occurs when an avalanche happens in a certain pixel, the fraction of pedestal events is independent of cross-talk. Therefore the fraction of 1 p.e. events estimated from the fraction of pedestal events is the value when there is no cross-talk. If there is cross-talk, the observed fraction of 1 p.e. events must be smaller than the estimated fraction of 1 p.e. events. This difference is attributed to cross-talk. The cross-talk rate estimated by the above method is written as:

Cross-talk rate = 1 – Fobserved / Festimated,

where Fobserved is the observed fraction of 1 p.e. events and Festimated is the estimated

fraction of 1 p.e. events. Fraction of pedestal events is calculated from the ADC distribution. Fraction of 1 p.e. events is estimated from the fraction of the pedestal events assuming a Poisson distribution.

This method is described in [48] and the results will be used for the datasheets of Hamamatsu MPPC. Figure 4.19 is one of results for Hamamatsu SiPM series with 100 pixels and 400 pixels respectively.

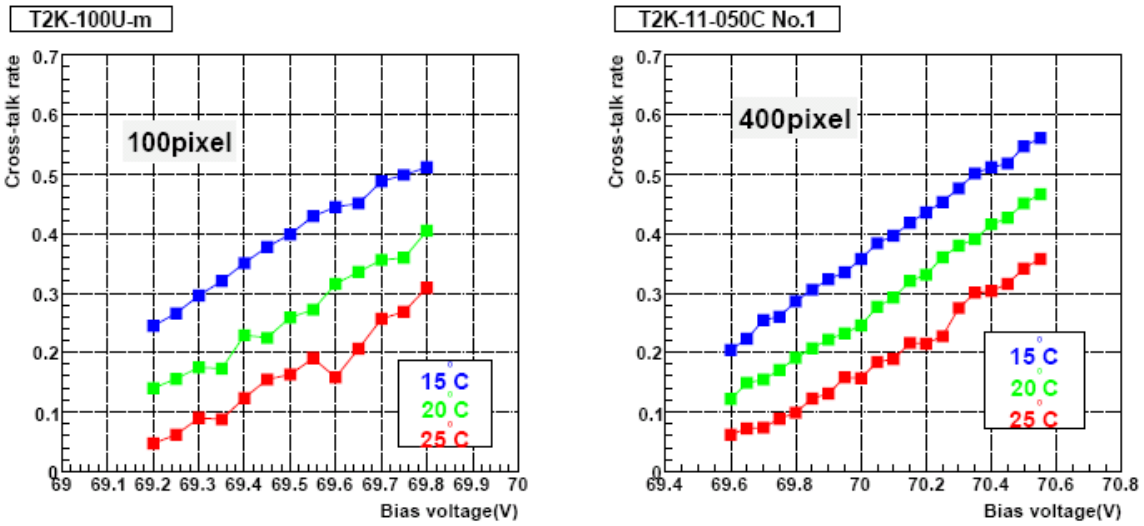

Figure 4.19 Crosstalk rates of 100 (left) and 400 (right) pixel devices as a function of the applied voltage.

4.3.6. Recovery time

The rise time for all types of SiPM is less than 2ns. The time to recharge a cell after avalanche clearly depends on the capacity and the individual resistor (RC). The capacity is proportional to the cell area. The fastest recovery time could be obtained by small cells and small resistors.

If polysilicon resistors are used, their resistance changes with temperature. Therefore there is a dependence of recovery time on the temperature. Afterpulses can prolong the recovery time because the recharging starts again.

Figure 4.20 is the output pulses from 4 types of Hamamatsu SiPM which were observed on 50Ohm input resistance oscilloscope.

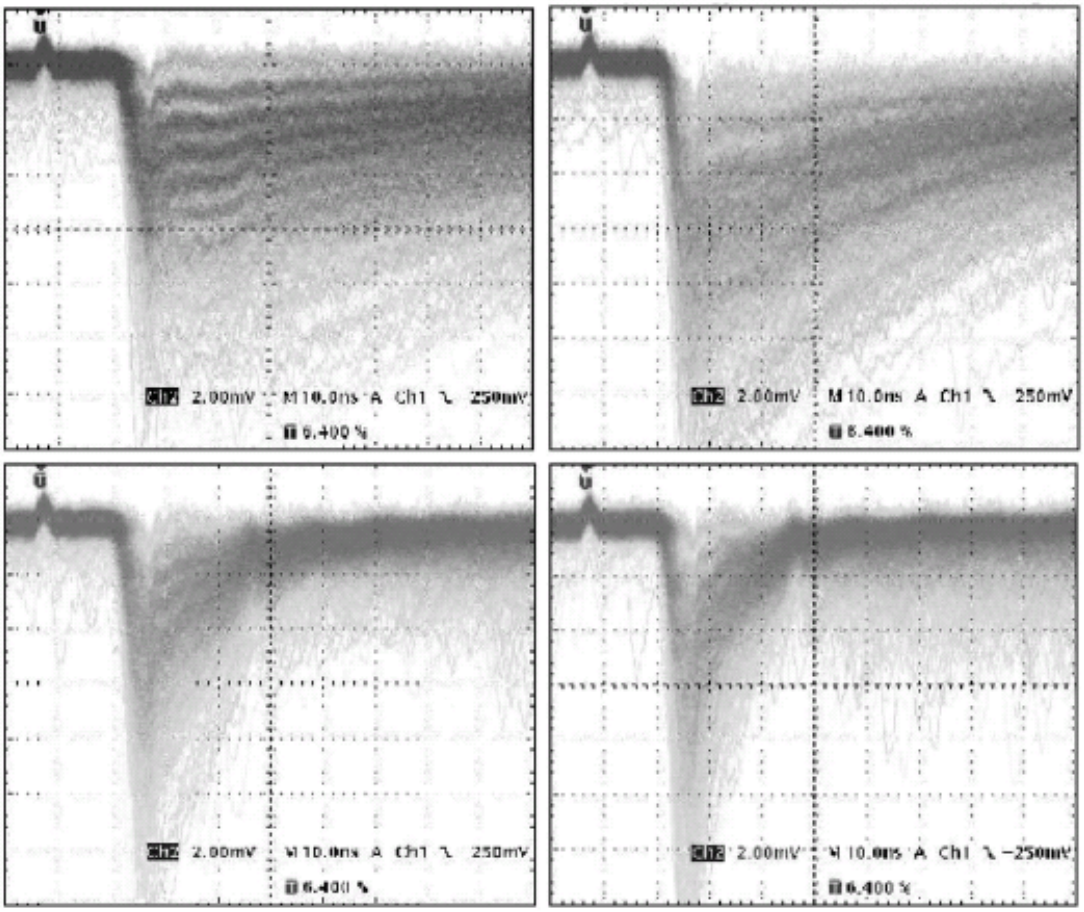

Figure 4.20 Signals from Hamamatsu 0-100-1.5 (70_70mm2, upper left) and Hmamatsu 0-50-1.5 (20_25mm2, upper right) and signals from types with smaller resistors (0-100-2, lower left and 0-50-2, lower right) directly fed into the 50O input of an oscilloscope. (Taken from [44])

As we can see that devices with smaller cells show shorter pulses. The last digit of the device name stands for the width of the polysilicon resistors. Devices with wider polysilicon, which makes the value of the resistors smaller, are faster.

4.4. Possible applications

For its high gain, insensitivity to magnetic fields, stability and durability, low bias, radiation hardness, compactness and much cheaper price, SiPM is a very promising candidate for replacing PMT and APD to be the detector of light in high energy physics experiments, medical instruments and astrophysical applications.

Experimental studies of SiPM based scintillator fiber detector, plastic scintillator plus wavelength shifter readout, and imagining Cherenkov counters have been illustrated in [41, 42], and the preliminary results are compared to other photodetectors. The conclusions show that after the tuning of some parameters (photon efficiency, gain, timing, dynamic range, etc.) the SiPM can be considered as a very promising photodetector for scintillator imaging applications. Such application is so called Photon Number Resolving application.

Up to now there is no reported result of SiPM for single photon counting applications though it is promised to have the ability for single photon detection. For the photon number resolving applications, a bunch of photons (more than 100 photons) go to the active area of SiPM. The readout threshold could even be set at some tens of photoelectrons to eliminate any contribution from dark counts altogether. But in our application we can not use high threshold to avoid large DCR because we are detecting discrete single photons.

4.5. Optimum choice of parameters

For SiPM, there are many different design possibilities for specific applications. In Table4.1, the design choices are listed with their consequences on some operating parameters.

Table 4.1 Design choices versus SiPM operating parameters

Design choices	**Operating parameters**
semiconductor material	PDE and the range of wavelengths
p-silicon on a n-substrate	highest PDE for blue light
n-silicon on a p-substrate	highest PDE for green light
thickness of the layers	range of wavelengths, optical crosstalk
doping concentrations	operating voltage
impurities and crystal defects	dark counts, afterpulses
area of the cells	gain, geometric factor, dynamic range, recovery time
number of cells	dynamic range, linearity, geometric factor
value of the resistors	recovery time, count rate/cell
type of resistors	temperature dependence
optical cell isolation (groove)	crosstalk

A circuit model of SiPM will be presented in the next chapter; the circuit parameters will be extracted. A novel design of SiPM which is desired for our specific application will be demonstrated and discussed.

5. SiPM modeling and simulation

It is known that high-speed photon counting is possible with a Geiger-mode APD which is so called SPAD. A successful single photon counting module (SPCM) has been implemented in our lab using the large area APD model C30902S-DTC from PKI. PKI C30902S-DTC is too expensive for its unique SLIK technology and bulky for the mounted cooler. So it is not a good choice to be used for upgrading to multi-channel photon counting system. It is also impossible to be made a detector array because the associated temperature controller and quenching circuit is complex. Another choice, Hamamatsu Si APD S9073, has been developed and tested with our unique quenching circuit. When it worked in the Geiger-mode, a standard output pulse was observed from this Si APD which was supposed to work in Linear-mode. Then the high dark count due to the impurity made our quenching circuit can not quench it very well. This diode reach saturation region with only dark count. So it was not sensitive to incoming photon. Summarily, the complexity of quenching and reset circuit, the unavoidable dead time, the difficulty to be made large area, and the required high bias voltage (~200V) limit the APD/SPAD working as a perfect photon detector. Recently SiPM attracted our attention for its passive quenching, high frequency, low bias voltage (30~70V), and the matrix structure which makes any active area possible.

SPAD is a digital device and hence can only resolve one photon at a time. This implies that SPAD can only be used in applications where it is expected that the probability of receiving two or more simultaneous photons is negligible. Being analog in nature, SiPMs have mainly been used in applications in which the signals are rare and where a bunch of photons are expected to be received simultaneously i.e. photon number resolving applications. Further SiPM is a matrix of small area microcells connected in parallel where each cell basically acts as an independent photon counter i.e. each cell is a small area SPAD. This implies that if a SiPM is used with the same source where the probability of receiving two or more photons is negligible it will essentially behave like a small area SPAD. In this case SiPM can be imagined as one large area SPAD and if the comparator threshold of the counter at the output of SiPM is set below the amplitude of the pulse due to 1p.e. then irrespective of whether one or more simultaneous photons are received at the input, only one photon will be registered at the output. So SiPM offers the combined advantages of both small-area and large-area SPADs.

5.1. Feasibility of using SiPMs for Single Photon Counting

The feasibility of using SiPM for single photon counting applications has been proved successfully in our lab. The commercial SiPMs, Hamamatsu MPPC series have been characterized and tested with our single lane DNA sequencer. The specifications of these two Hamamatsu devices are shown in Table 5.1. More information about

Hamamatsu MPPC series can be found in [51]. Two devices of different pixel sizes were studied in our lab: 100-pixel device and 1600-pixel device.

Table 5.1 Specifications of the characterized Hamamatsu MPPC

Specification	100-pixel	1600-pixel
Type/Model	S10362-11-100U	S10362-11-25U
Chip Size (mm)	1.5 x 1.5	1.5 x 1.5
Size of 1 pixel (μm)	100 x 100	25 x 25
Effective Active Area (mm)	1 x 1	1 x 1
Fill Factor* (%)	78.5	30.8
No of pixels/mm^2	100	1600
Operating Voltage, V_{OP} (V)	69.72	70.89
DCR **0.5 p.e. thr** **1.5. p.e. thr**	 716K 125K	 438K 12.5K
Gain (M)	2.4E+06	2.74E+05
Temp (ºC)	+25ºC	+25ºC

***** Ratio of active area of the pixel to the entire area of the pixel.

The sensitivity to the light source, dynamic range and the linearity are measured on both 100-pixel and 1600-pixel devices and compared to the PKI SPCM. The measured results are seen in Figure 5.1. It shows that the 1600-pixel device is more linear than the 100-pixel device. And its dynamic range is even better than PKI SPCM. The reason may be the small dead-time due to much smaller size of the microcell.

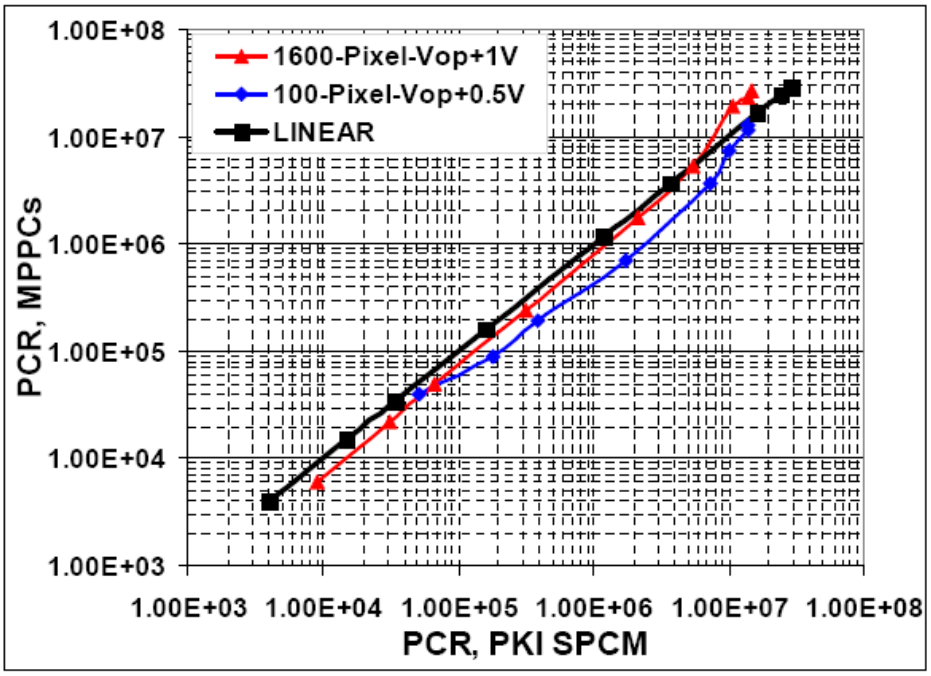

Figure 5.1 Comparison of sensitivity and linearity for 100-pixel and 1600-pixel device

The dark count rate, linearity, and dynamic range of SiPMs were proved to be good enough for DNA sequencing. High quality DNA traces (shown in Figure 5.4) have been obtained by SiPMs with the setup shown in Figure 5.2 and Figure 5.3.

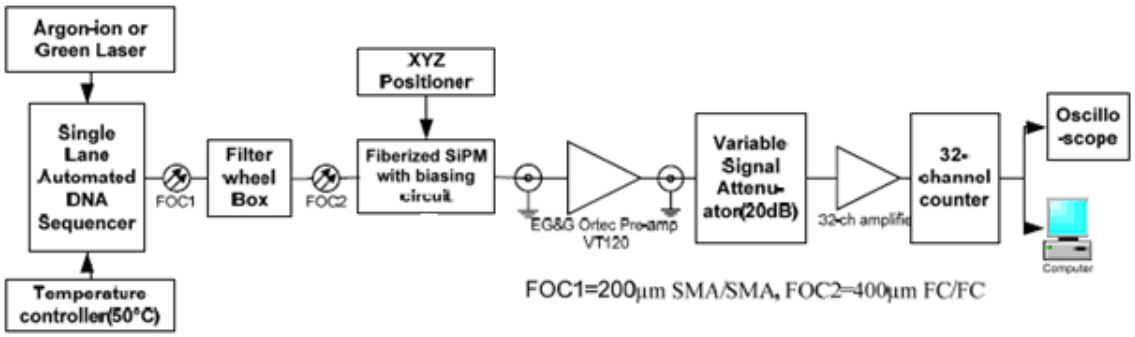

Figure 5.2 Block diagram of the complete DNA-sequencing set-up used for SiPMs.

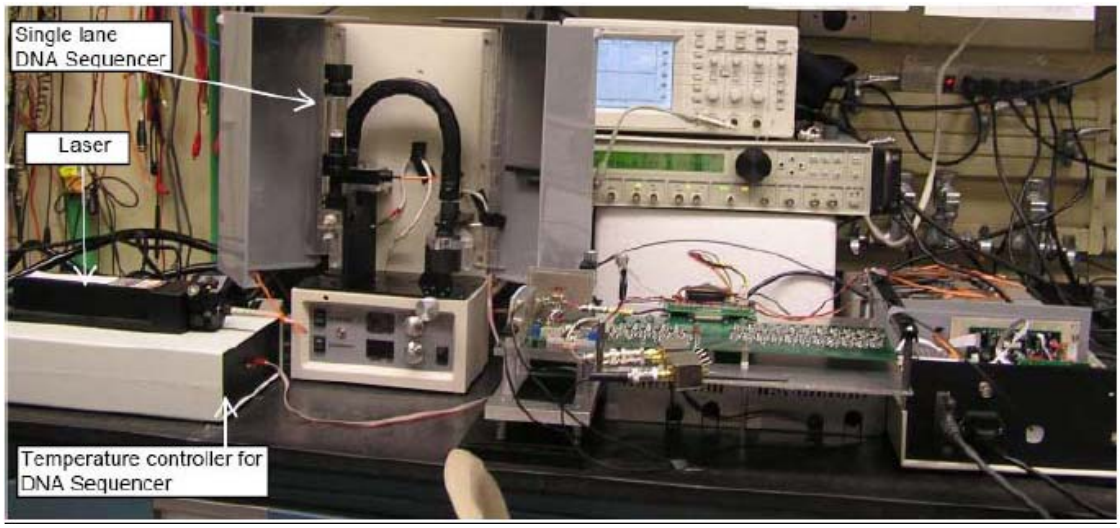

Figure 5.3 the complete DNA-sequencing set-up used for SiPMs

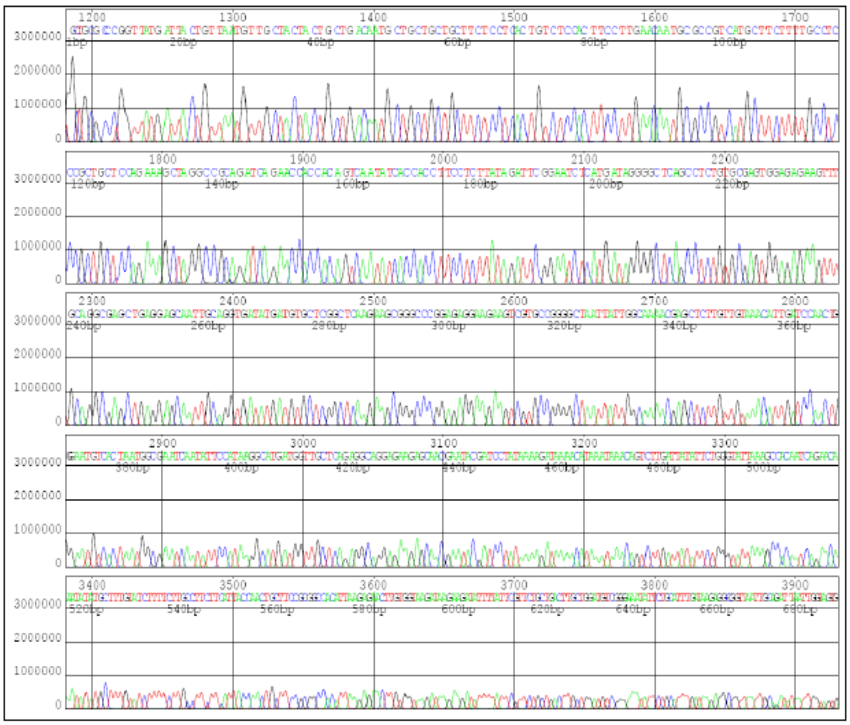

(a)

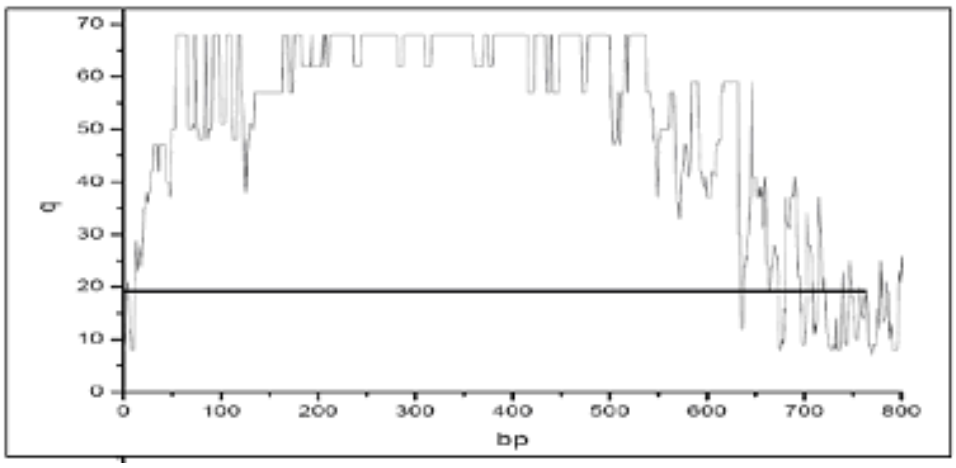

(b)

Figure 5.4 Hamamatsu MPPCs: (a) Typical sequencing traces (Laser power = 17mW) (b) Quality factor

So we were confident to continue the research on SiPMs based photon counting system development. Now what is the optimal SiPM required for our application is the first question we want to answer.

5.2. Novel SiPM design for photon counting mode

As we discussed in the previous section, high quality DNA sequencing traces can be obtained by SiPMs and even without any associate quenching and reset circuit. The SiPM is a good photon counter itself. Moreover, the operating voltage of SiPM is only around 70 Volts. Comparing to ~150 Volts bias voltage required for large area APD, SiPM is much easier to be utilized for multi-channel design or upgrading to detection array.

One thing is worthy to be noticed. For all the measurements which have been done so far, fast external amplifiers are necessary. Or the output pulse is too small to be caught by any digital counter. In our experiments, the ORTEC VT120C fast-timing preamplifier

is used. Its gain is 20 times; bandwidth is 350MHz. The rise time is promised to be less than 1ns. According to our experiments, the 1600-pixel device needs more external amplification to obtain the detectable output pulse. Because the pixel area is smaller, the internal gain is smaller. This is the same drawback as small area APDs. To design a high frequency, wide bandwidth, and low noise amplifier is an obstacle to develop the SiPM based photon counting system.

But for its matrix structure, SiPM has a unique performance which the APD doesn't have, optical cross-talk. As described in chapter 4, reverse biased silicon diodes emit photons at the rate of ~ 10^{-5} photons per electron crossing the p–n junction when they are operated in Geiger-mode [40]. The rate of ~ 10^{-5} photons per electron is really a huge number for an avalanche process which generates a considerate number of charging carriers. These photons may or may not initiate an avalanche in the neighboring microcells depending on where they are absorbed as shown in Figure 5.5. Since the travel time of these photons is much faster (speed of light) than the dead time (pulse width) of the already fired cells, even if they initiate a discharge, this discharge probably takes place in the same time frame as the original fired cell (pulse width 10-30ns). As a result, the cross-talk generated pulse is slightly shifted in time, but the time is so small that charge generated by both pulses is summed up in the same cycle, thus generating an output pulse with amplitude equal to the sum of all the fired cells.

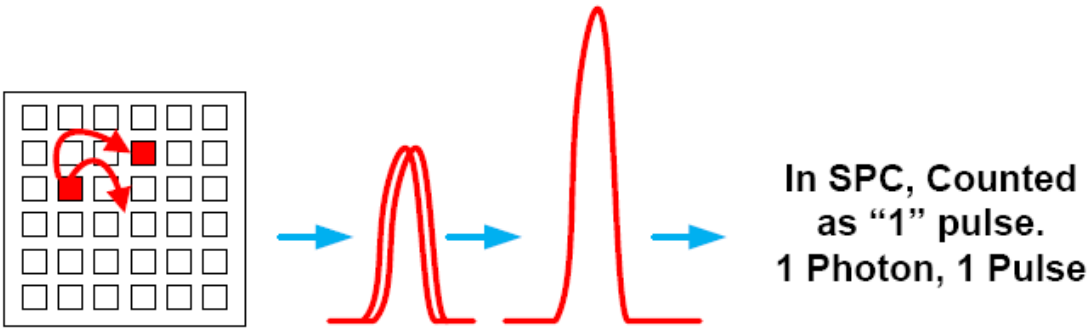

Figure 5.5 Effect of cross-talk on photon counting performance of SiPM

The cross-talk is usually not welcome because SiPM is usually used in photon number resolving applications. In photon number resolving, cross-talk is absolutely a noise resource, because the original photon is registered as two or more photons in this case. But in photon counting mode, only one pulse is registered for one originally fired cell as well as other cells fired due to cross-talk. Therefore no additional counts are generated due to cross-talk but a larger pulse is obtained.

Now, imagine that more than 10 microcells are fired simultaneously due to cross-talk for only one incoming photon. There is a possibility for this situation to happen. Then the output pulse is 10 times larger in amplitude than the original 1 p.e. output pulse. For example, if we can make all the cells in 100-pixel device to be fired simultaneously due to cross-talk, a 100 p.e. output pulse will be registered for the original incoming photon. With the extra 100 times internal gain, the external amplifiers will not be necessary any more.

The cross-talk mechanism has a counterpart in the Probability Theory: Randomized Broadcasting. Let G = (V, E) be a connected, undirected graph on N vertices. One vertex initially knows of a "rumor" that has to be conveyed to every other vertex in V. The rumor is propagated as follows: at each step, every vertex that knows of the rumor

chooses one of its neighbors in G uniformly at random, and informs it of the rumor. The number of steps elapse before every vertex knows the rumor is O(logN) steps.[52] The "rumor" is like the original photon which fires the first pixel. Each pixel is a vertex in the graph G. As said in this theory, to fire all the pixels in the SiPM needs O(logN) rounds. For example, a 1600-pixel device needs only 10 rounds of cross-talk to fire more than 1000 pixels simultaneously.

The optimal SiPM which we desired for the photon counting application is the SPAD matrix which doesn't need any quenching circuit or any external amplification circuit. If we can design a device like this, it will be a perfect photon detector for many photon counting applications. Then multi-channel and detection array will be implemented very easily. We really want to know if the perfect situation can really happen to SiPMs and how to implement it. The circuit modeling of SiPMs and its output signal simulation under many conditions will be presented in the following sections. The perfect situation will be simulated and discussed.

5.3. Circuit model of SiPM and parameters

The circuit model of a Geiger-mode operated APD and the equivalent circuit of passive quenching are described in the chapter 2.4. As introduced in the previous chapter, the SiPM is an APD matrix built on a common substrate. And each single microcell of SiPM is operated in Geiger-mode and quenched passively by an individual quenching resister. So the circuit model of SiPM can be illustrated in the Figure 5.6.

A cell consists of an APD and a quenching resistor Rq. The part inside the diode is the same as the circuit model of APD described in the chapter 2. During avalanche the junction is low ohmic with a varying conductivity and is behaving like a voltage source *Vbd* equal to breakdown voltage of the diode. For simplicity it is assumed that the conductivity 1/*Rd* and the output of the voltage source are constant during avalanche. The onset of the avalanche is described as a switch that is being closed, and then opened again at quenching. The condition for quenching is satisfied once the current that flows through the junction drops below a critical value of ~10 μA.

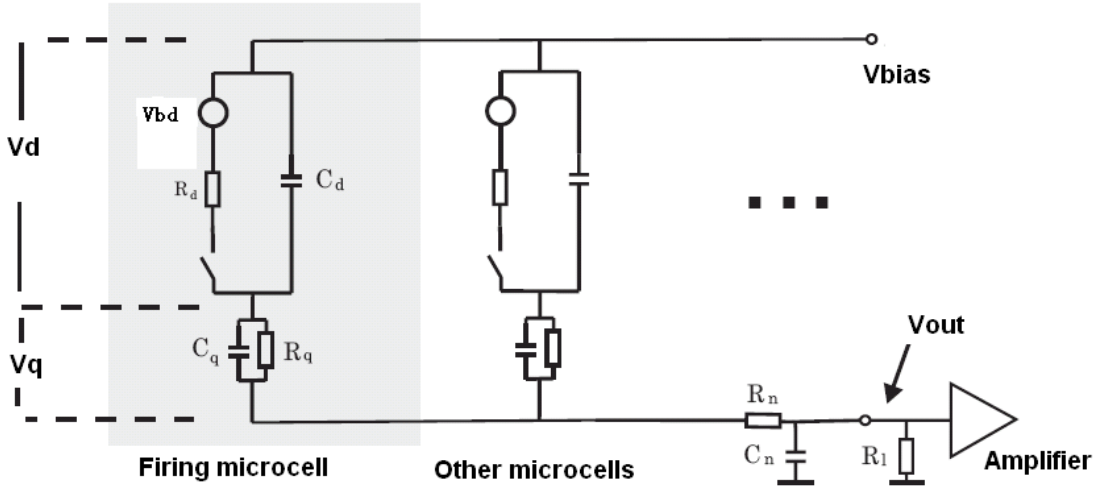

Figure 5.6 Circuit model of a SiPM

Parameters in the SiPM model:

Cd is the internal capacitance of the microcell, depending on the active area of the cell and varies proportionally with it;

Rd is the junction resistance of the microcell; typical value is 10K~100KOhm;

Rq is the quenching resistor, usually ~100KOhm;

Rn is a small series resistor and *Cn* is a parasitic parallel capacitance due to the routing of

the bias voltage to the N microcells, realized with a metal grid;

Rl is the load resistor, which is either the input resistance of the preamplifier or any other combination of parallel resistors, connected in series between the output of the SiPM and ground. Typically a value of 50Ω is chosen.

The measured output signal is the discharging current that flows during avalanche and after quenching through *Cq* and *Cd*. The avalanche current can be approximated as a short pulse containing the total amount of charge delivered by the firing microcell Q=dV(Cd+Cq), with dV=Vbias – Vbd.

There are two time constants in this circuit:

One is related to the sharp onset time of the avalanche current: Rl*Ctot, where Ctot is the total capacitance of Cn, Cd, and Cq;

The other is related to the slow recovery time: Rq*(Cd+Cq).

In this model the voltage across the load resister Vout, quenching resister Vq, and the diode Vd are related by three coupled differential equation according to the avalanche process:

$$dVd / dt = (Vbd – Vd) / Rd*Cd – (Vd + Vout + Vq – Vbias) / Rn*Cd \quad (1)$$

$$dVout / dt = -Vout / Rl*Cn – (Vd + Vout + Vq – Vbias) / Rn*Cn \quad (2)$$

$$dVq /dt = -Vq / Rq*Cq – (Vd + Vout + Vq – Vbias) / Rn*Cq \quad (3)$$

The above three differential equations can be solved numerically. One of the solutions of Vout for reasonable resistance and capacitance values looks like Figure 5.7.

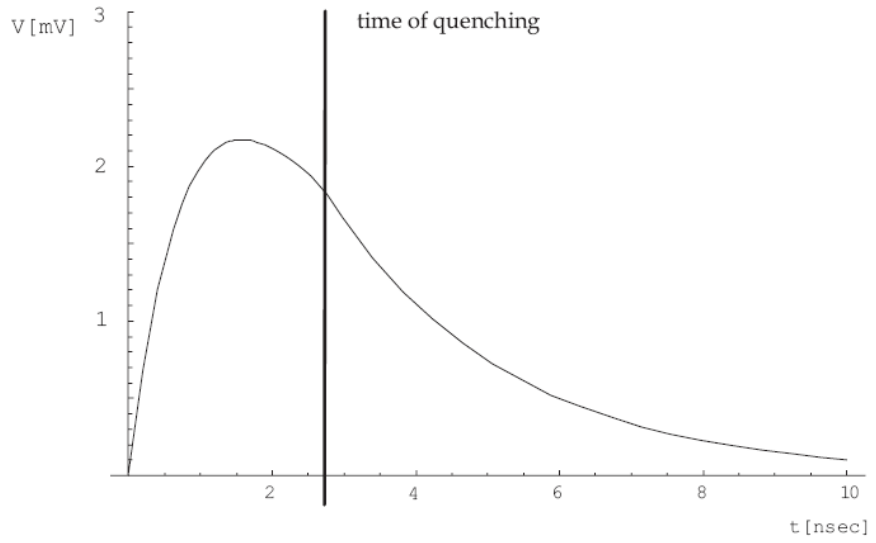

Figure 5.7 Simulated output pulse of a SiPM

The avalanche is quenched if the current flowing through Rd drops below ~10uA. The time of quenching is marked by the vertical line in the Figure 5.7.

5.4. Output signal simulation of SiPM with enhanced gain

To study the effect of optical cross-talk on the internal gain of SiPM a single-trial simulator and a multi-trial simulator have been developed in our lab. The simulators are programmed in the script language Python. The shell program of the single-trial simulator is shown as follows and the core program is not shown here:

```
import core
class settings:
   def __init__(self   ):
      pass

settings.number_of_photons=100 #The number of photons

#size of sensor, in Pixels
settings.x_size=40
```

```
settings.y_size=40

settings.DecayTau=10.0                          #in ns
settings.AfterPulseDelay=5.0                     #in ns
settings.CrossTalk_Maximum_Instigate_Time=0.3    #in ns
                                                #We can instigate
forever.
settings.Afterpulsing_Probability=0 #The afterpulsing probability.
settings.CrossTalk_Probability=0
settings.Comparator_Delay=3                  # in ns
settings.Comparator_Threshold_Start = 0.5
settings.Comparator_Threshold_Step = 0.2
settings.Comparator_Threshold_Stop = 6.0

#Run the simulation
core.run(settings)
```

In the shell program, parameters are provided to be set by users for simulating the output signals of SiPM under different conditions:

x_size and ***y_size*** in pixel

We assume the SiPM is a square matrix. Its geometry can be described by x_size pixels * y_size pixels. For example, x_size=40, y_size=40 is a 1600 pixel device.

DecayTau in ns

As we discussed in the previous section, there are two time constants in the avalanche process. One is related to the sharp onset time of the avalanche current; the other is related to the slow recovery time. In our simulator the very short onset time is ignored; the recovery is described by the exponential decay of a fixed DecayTau in 10ns.

CrossTalk_Maximum_Instigate_Time in ns

We assume that cross-talk happens only in the instigate time interval. Out of this interval a fired cell will not trigger its neighbor cells.

Afterpulsing_Probability and ***AfterPulseDelay*** in ns

As discussed in Chapter 2.3.2, during avalanche some carriers are captured by deep levels in the junction depletion layer and subsequently released with a statistically fluctuating delay. The number of carriers captured depends on the total number of carriers crossing the junction, which depends on the total charge of the avalanche pulse generated. We used these two variables to describe the probability and delay time in which afterpulsing happens.

CrossTalk_Probability

Please notice that the cross-talk probability here is a different concept from the cross-talk rate discussed in Chapter 4. This is the probability in which a fired cell generated photon triggers its neighbors to fire additional discharging. Each fired cell can trigger its direct neighbor cells only. Each cell has four direct neighbor cells around it.

Comparator_Delay

This is the triggering delay of the external comparator.

Comparator_Threshold_Start and ***Comparator_Threshold_Stop***

The threshold of comparator is set by the number of photoelectrons, such as 1p.e., 2p.e….. Usually start from 0.5 p.e. to count all the pulses which are generated.

number_of_photons

In this variable we can set the number of primary avalanche which is triggered by incoming photons or thermal effect. Both the incoming photons from illumination and the dark count due to thermal effect are Poissonian process.

Based on above parameters, simulations with enhanced cross-talk and enhanced afterpulsing have been done. The effect of cross-talk and afterpulsing on the output signals will be presented in the next two sections.

5.4.1. Single-trial simulations of enhanced cross-talk

To study the effect of cross-talk on the internal gain of SiPM, the simulations of different values for cross-talk possibility and zero afterpulsing probability have been done as follows. The graphic result of single-trial simulations has four windows: top left window is the simulated output pulse, x-axis is time in ns, y-axis is the count in p.e.; bottom left window is the list of variables to be set; top right window is the curve of pulse count versus comparator threshold; bottom right is the histogram which shows the pulse count distribution on different amplitude.

In this section, the afterpulsing probability is set to zero for all simulations. It means that no afterpulsing happens at all. However this is impossible in the real world, I want to study the only effect of cross-talk on output pulses. It is an ideal situation to enhance the internal gain utilizing this unique characteristic of SiPMs.

And the size of SiPM is set to be 40 pixels * 40 pixels = 1600 pixels. To make the computer running time reasonable ***number_of_photons*** is set to be 100 though SiPM can count to million counts per second, even the dark count rate can be up to MHz. ***number_of_photons = 100*** is enough to obtain the information of output pulse distribution.

As shown in Figure 5.8 when the crosstalk probability is very small, such as 0.004 in (a), most of output pulses are 1 p.e. pulse. As shown in (b) (c) (d) when the crosstalk probability increases from 0.01 to 0.05, more and more 2 p.e., 3 p.e., and 4 p.e. pulses can be seen. The curve of pulse count versus comparator threshold in (d) is very similar to the measured curve of dark count rate shown in the Figure 4.12. Both are step-like and 7

steps. From (e) to (h) when the crosstalk probability continues to increase, the steps disappear. Until crosstalk probability is up to 0.4, almost all the output pulses have amplitude of 1200. It means that the device has an extra internal gain of 60dB, 1000 times. The perfect situation we desired happened in the simulation.

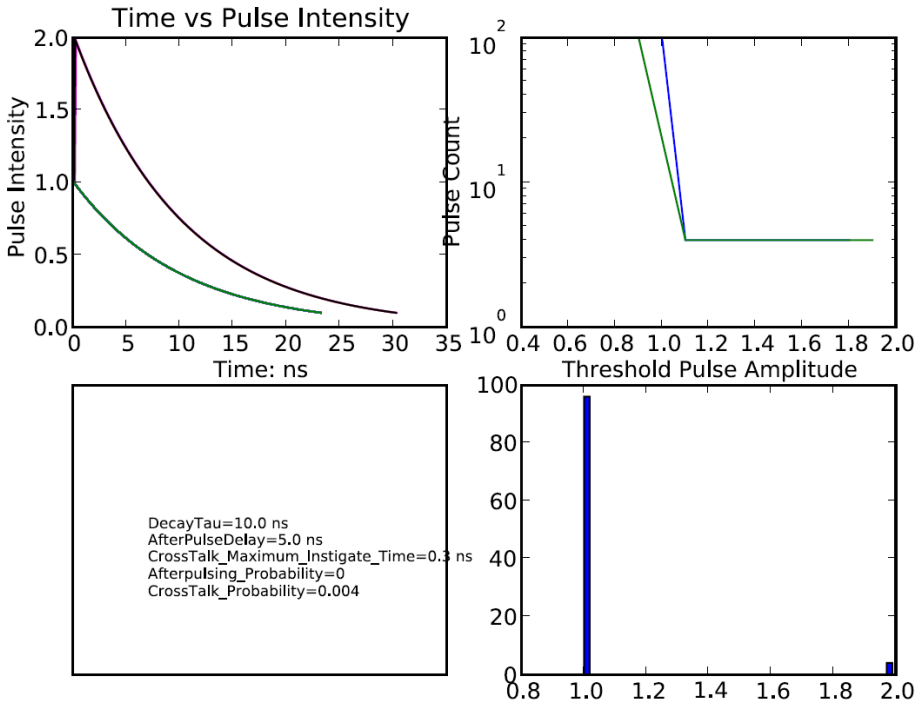

(a) crosstalk probability = 0.004

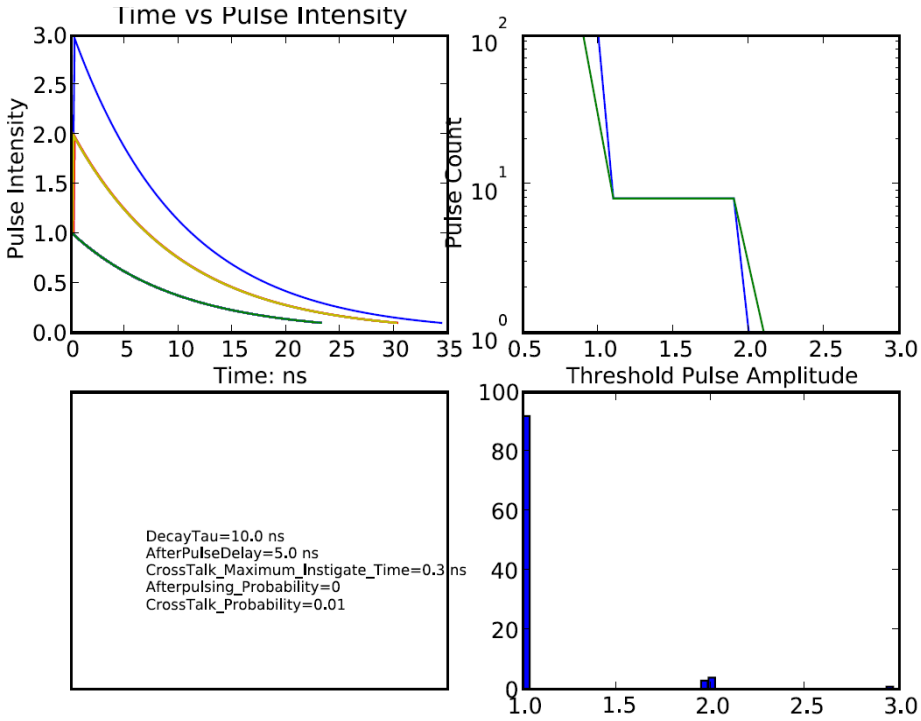

(b) crosstalk probability = 0.01

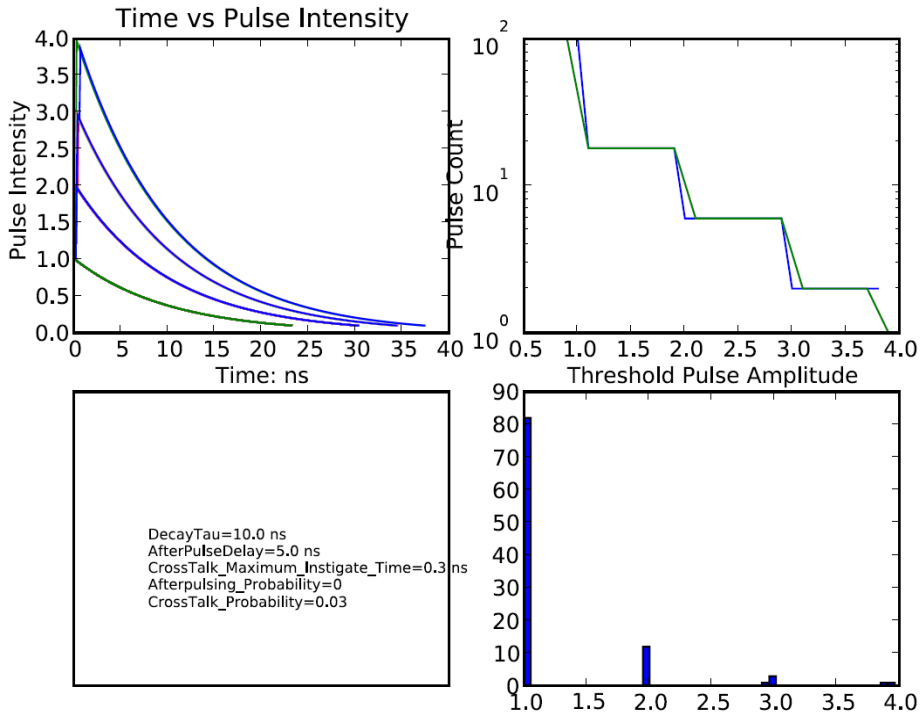

(c) crosstalk probability = 0.03

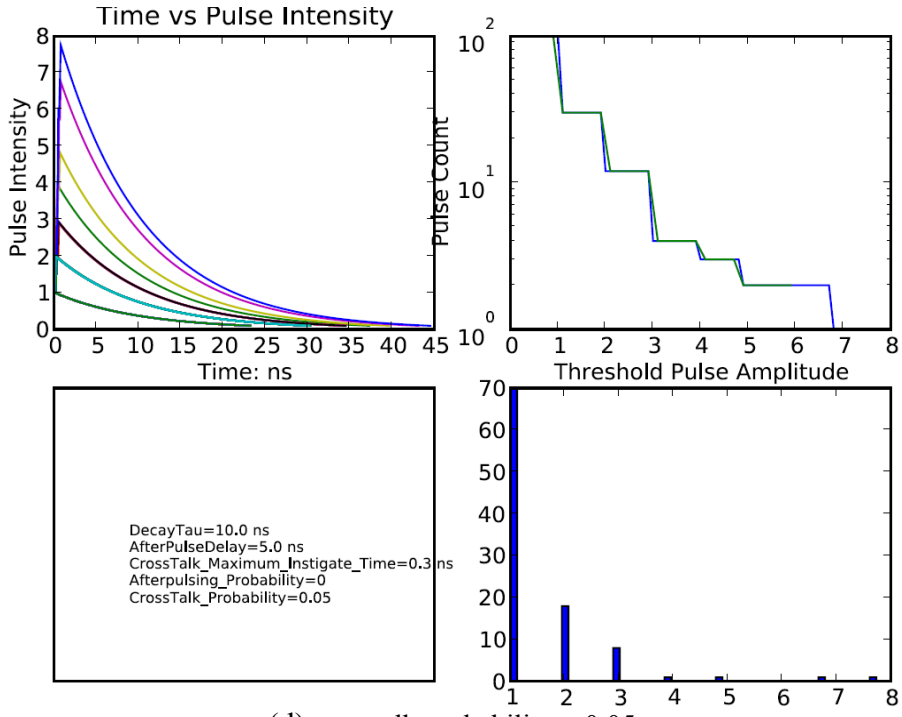

(d) crosstalk probability = 0.05

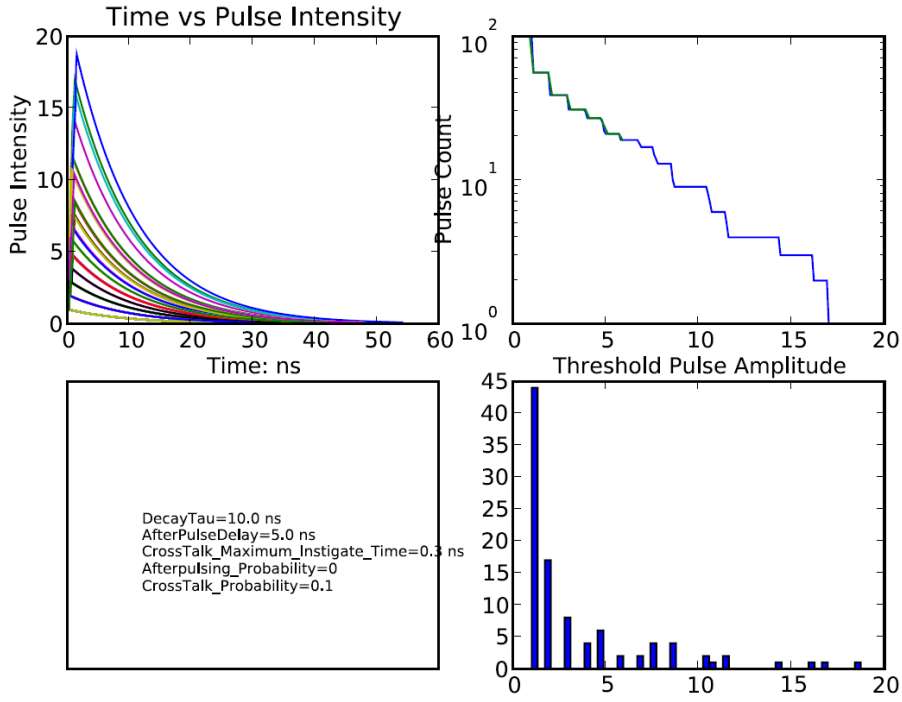

(e) crosstalk probability = 0.1

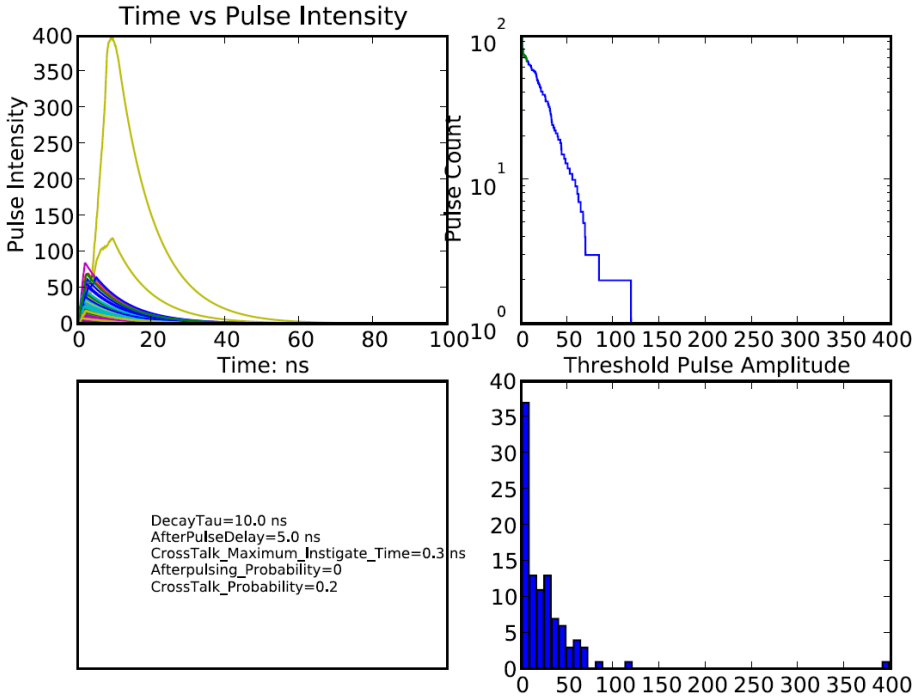

(f) crosstalk probability = 0.2

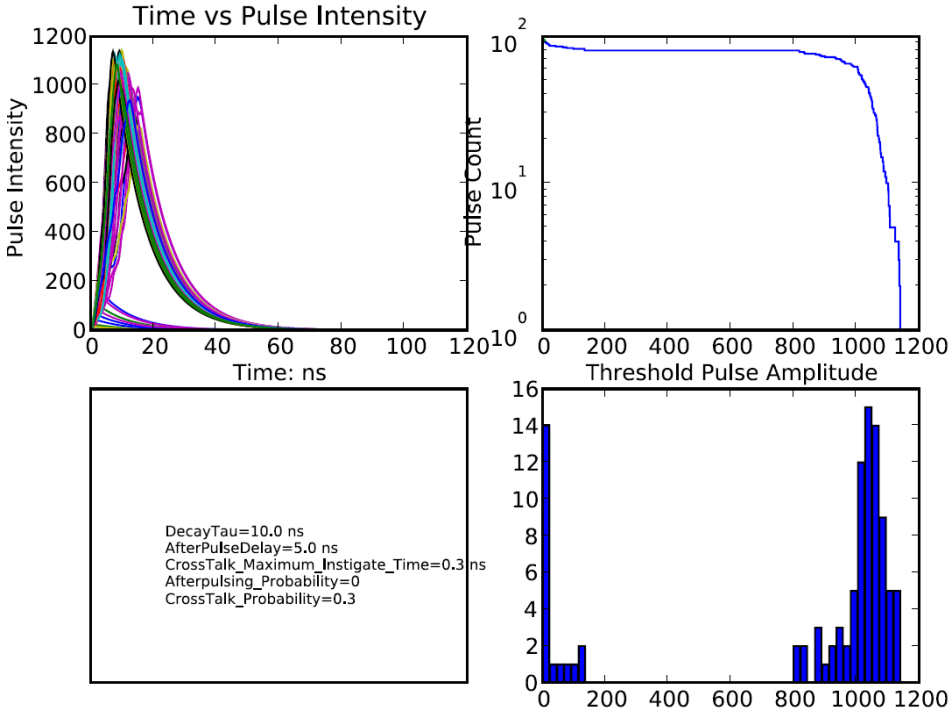

(g) crosstalk probability = 0.3

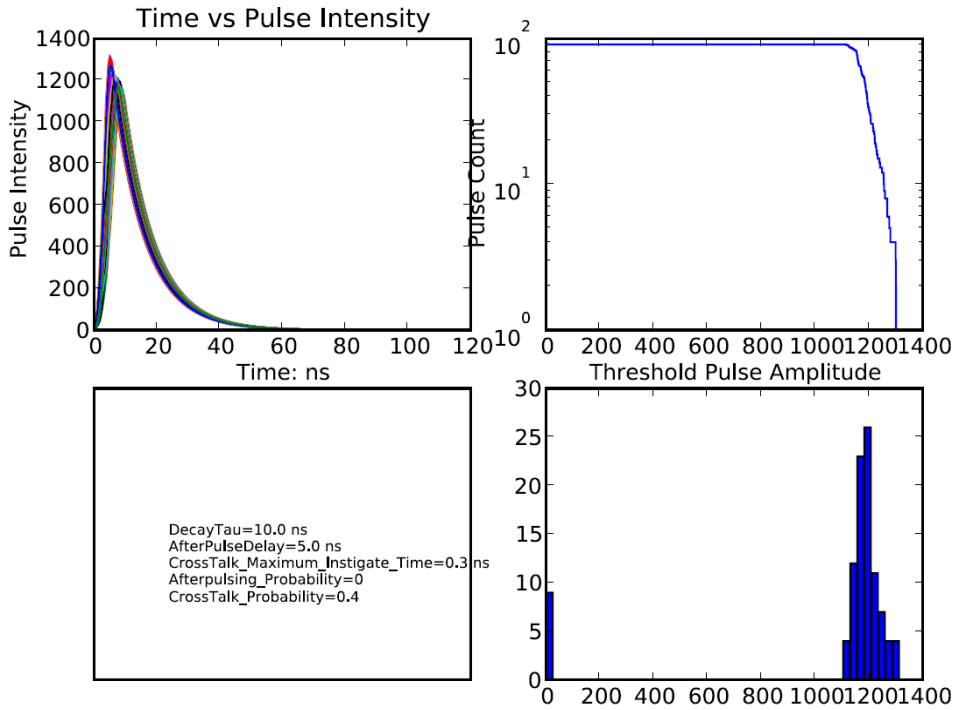

(h) crosstalk probability = 0.4

Figure 5.8 Simulation results of 1600-pixel SiPM with zero afterpulsing

There is one phenomenon worthy to be mentioned. In the Figure 5.8 all the output pulses are recovered in 40ns and the pulse width is less than 40ns. So I can conclude that crosstalk doesn't have effect on the dynamic range of photon counting system but have effect only on the amplitude of the output pulses. It is really a good sign for us.

5.4.2. Single-trial simulations of enhanced afterpulsing

In this section, the afterpulsing effect will be considered in the simulation. The afterpulse delay is set to be 5ns for all simulations. For each afterpulsing probability 0.0007, 0.007, 0.07, and 0.7 shown in Figure 5.9, Figure 5.10, Figure 5.11, and Figure 5.12 respectively, different crosstalk probabilities are simulated as follows.

In Figure 5.9 (b) with afterpulsing probability=0.0007, crosstalk probability=0.03, the steps in the curve of pulse count versus comparator threshold still can be observed. In

the later figures when the afterpulsing probability increases, the steps disappear. This means that the output pulse amplitude is not exactly 1p.e., 2p.e., 3p.e… It could be due to the crosstalk induced afterpulsing.

When the crosstalk probability is up to 0.3, the flat curve of pulse count versus comparator threshold can be observed. It means that more than 1000 pixels are fired simultaneously. You may notice that with non-zero afterpulsing probability the situation happens at a lower crosstalk probability and the pulse width could become much larger. Afterpulsing reduces the dynamic range of SiPM seriously. It is a noise source.

In the next section, how the afterpulsing and crosstalk affect the noise analysis of photon counting system will be discussed.

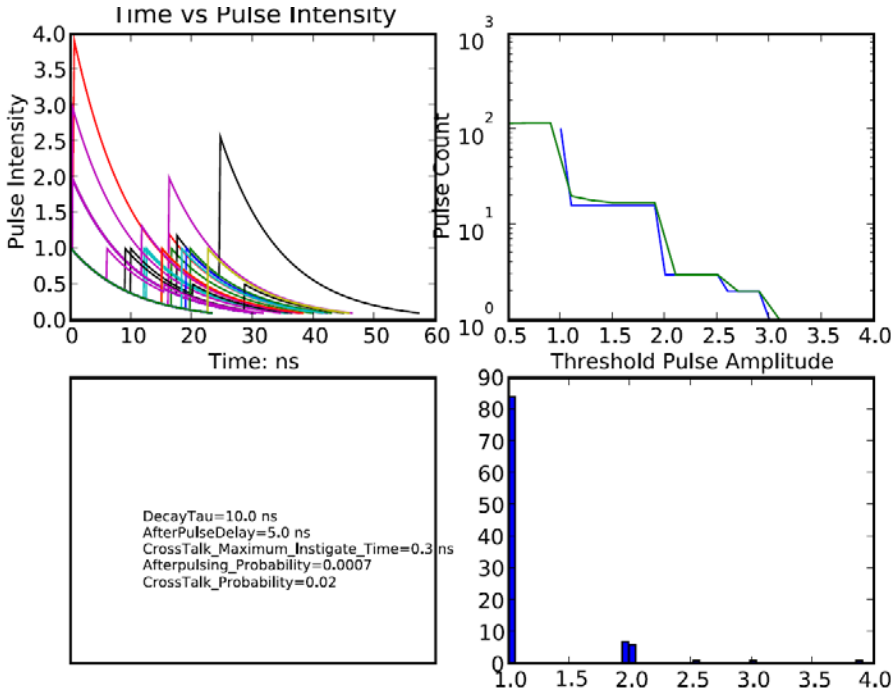

(a) crosstalk probability = 0.02

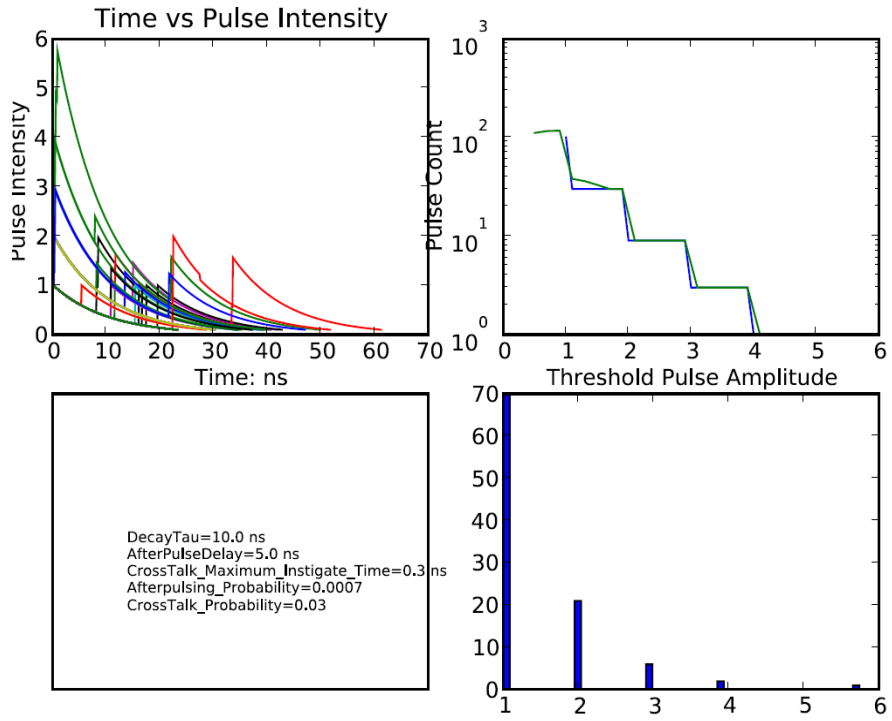

(b) crosstalk probability = 0.03

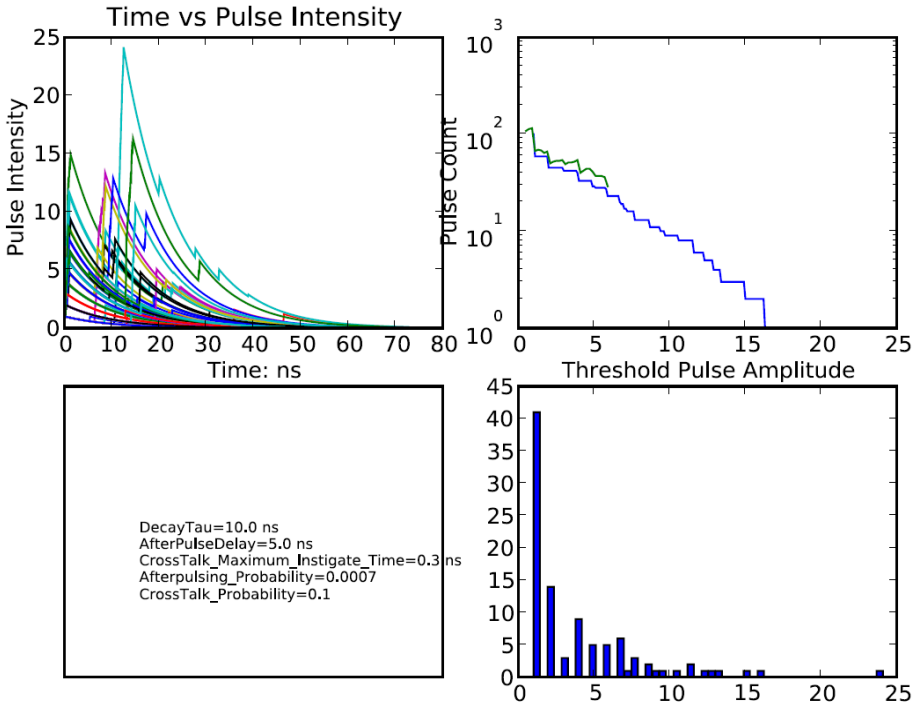

(c) crosstalk probability = 0.1

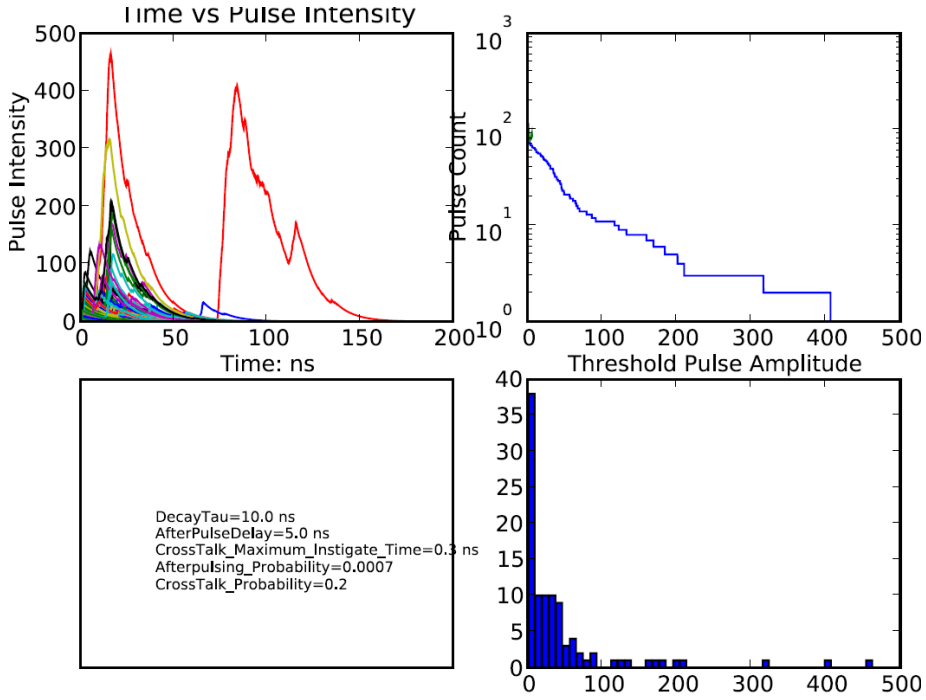

(d) crosstalk probability = 0.2

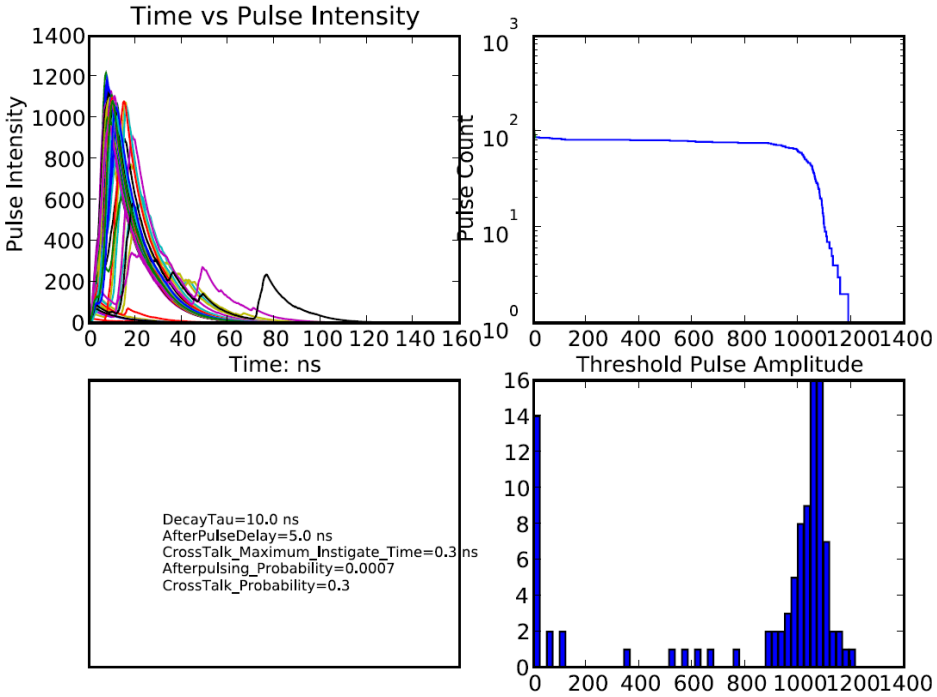

(e) crosstalk probability = 0.3

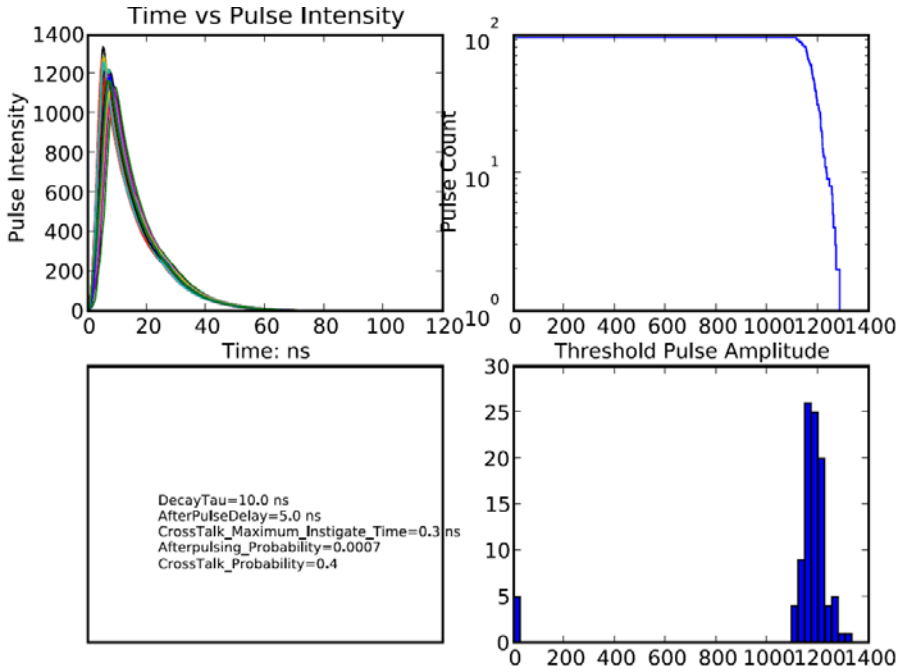

(f) crosstalk probability = 0.4

Figure 5.9 Simulation results of 1600-pixel SiPM with afterpulsing probability=0.0007

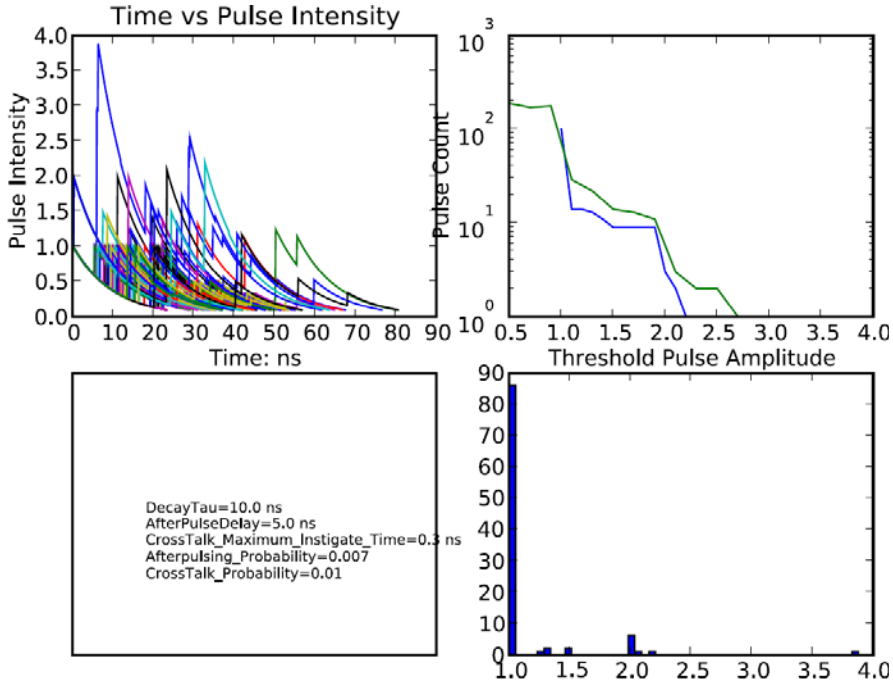

(a) crosstalk probability = 0.01

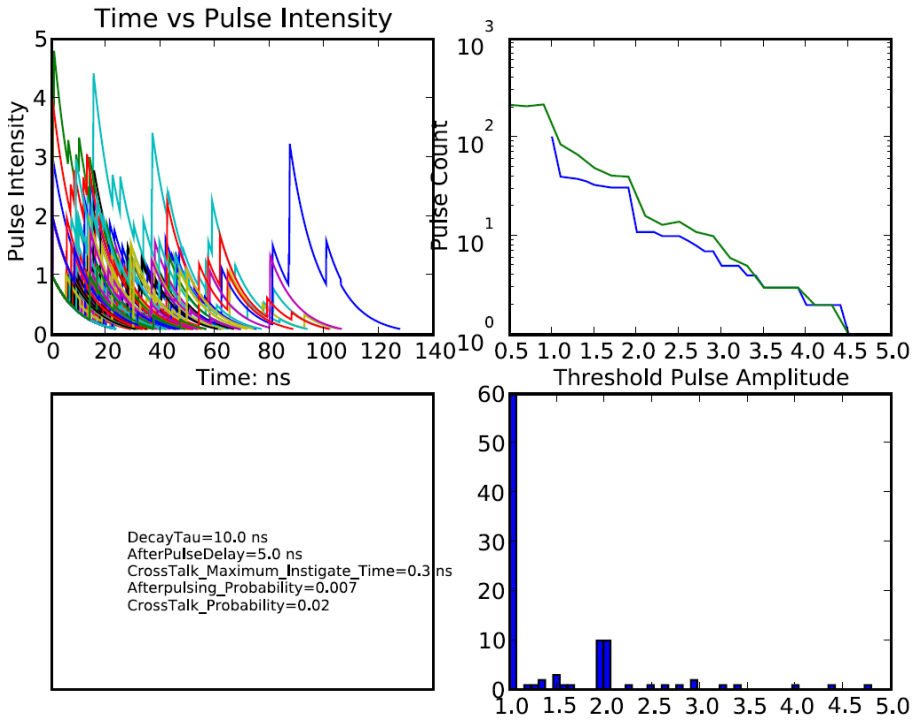

(b) crosstalk probability = 0.02

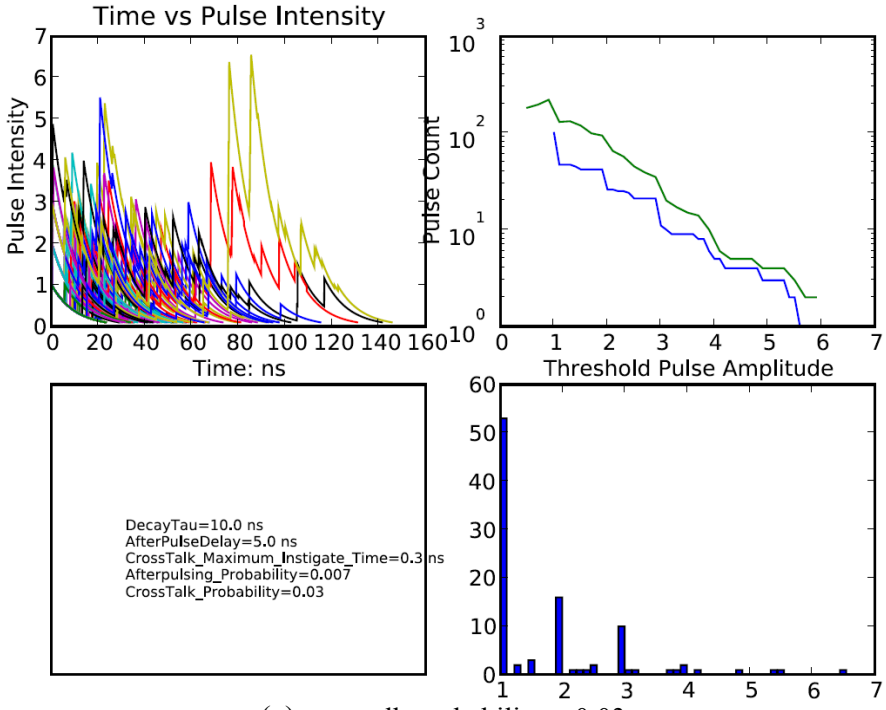

(c) crosstalk probability = 0.03

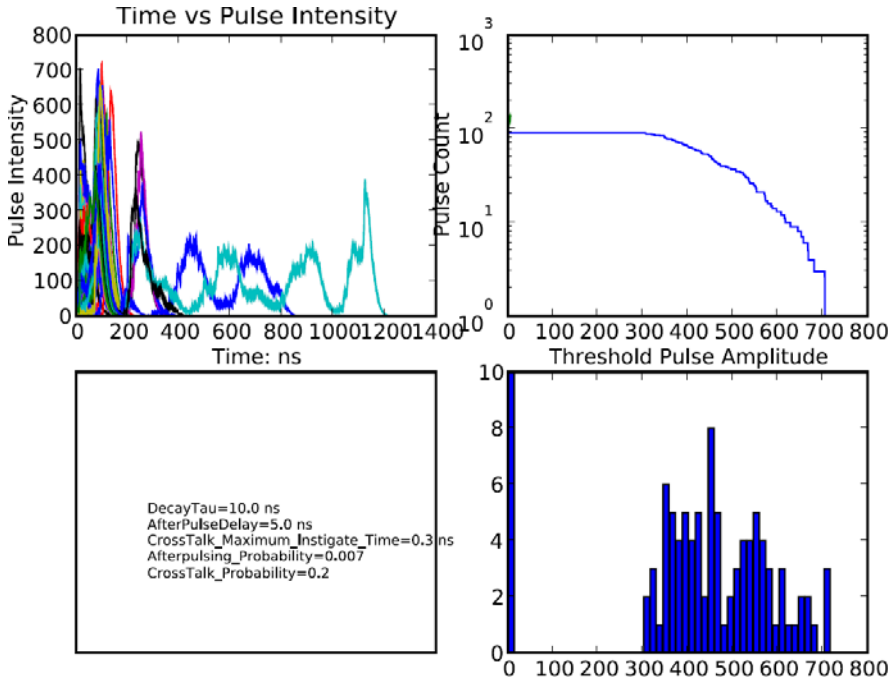

(d) crosstalk probability = 0.2

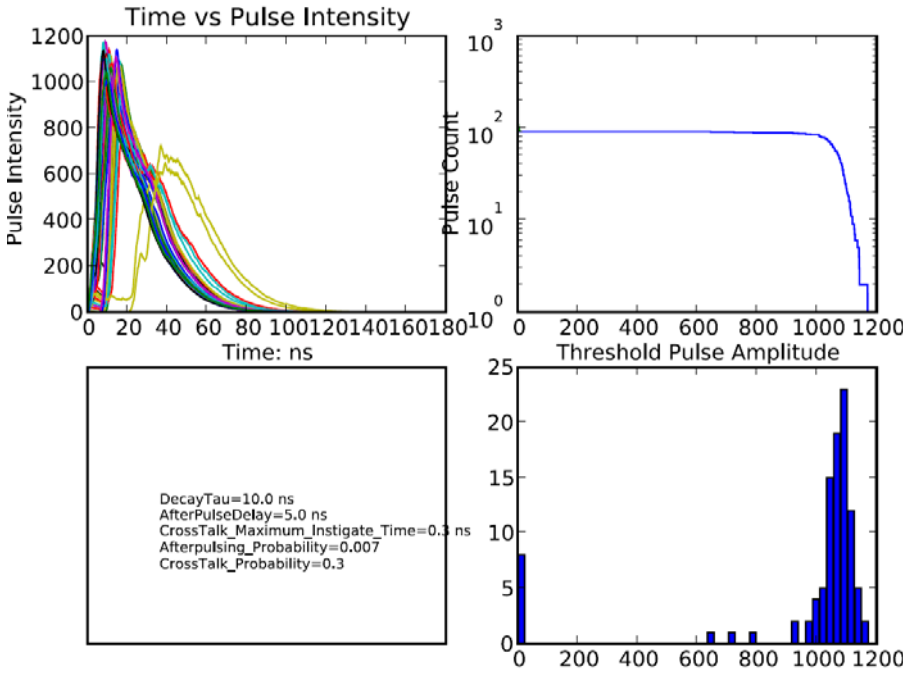

(e) crosstalk probability = 0.3

Figure 5.10 Simulation results of 1600-pixel SiPM with afterpulsing probability=0.007

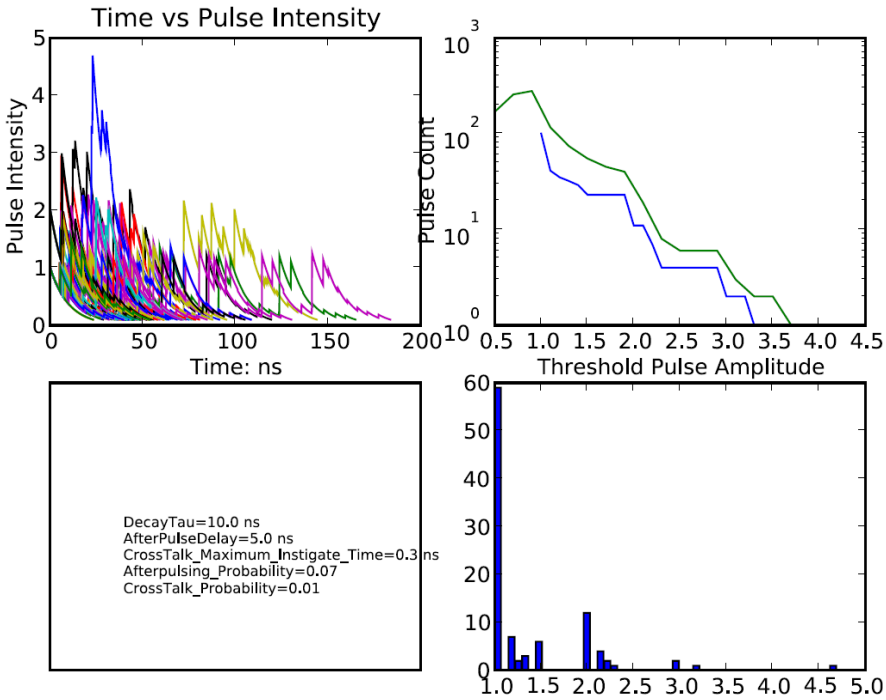

(a) crosstalk probability = 0.01

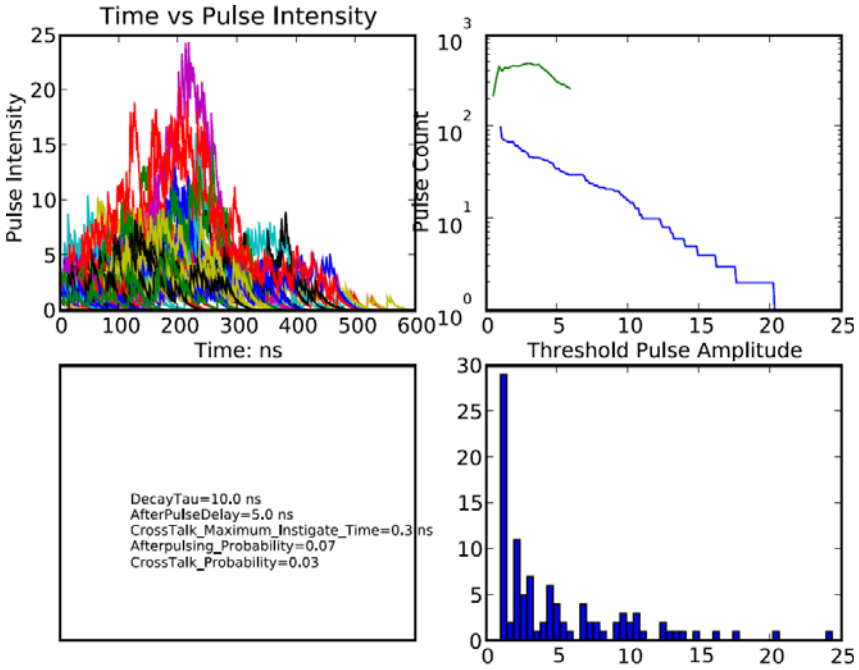

(b) crosstalk probability = 0.03

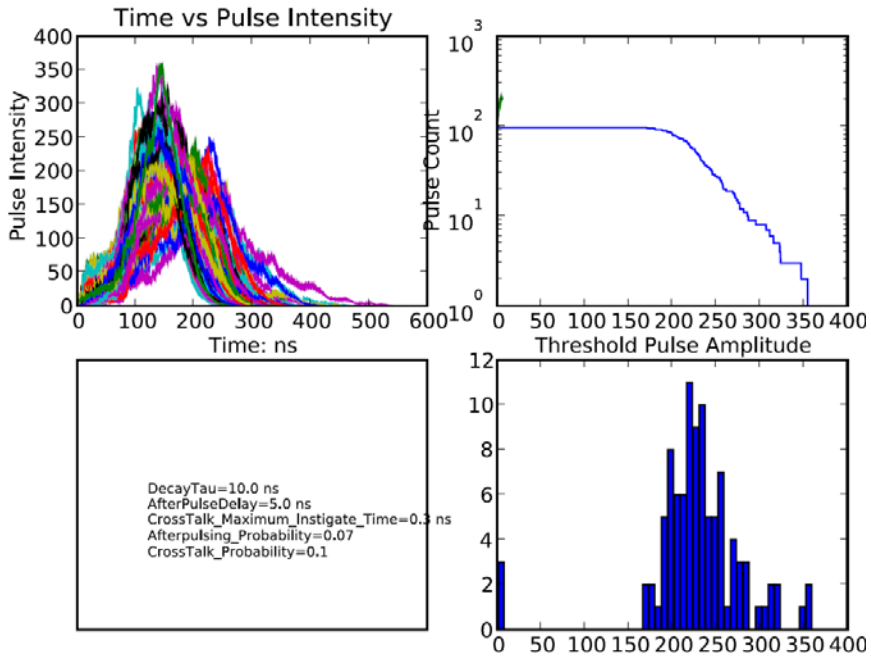

(c) crosstalk probability = 0.1

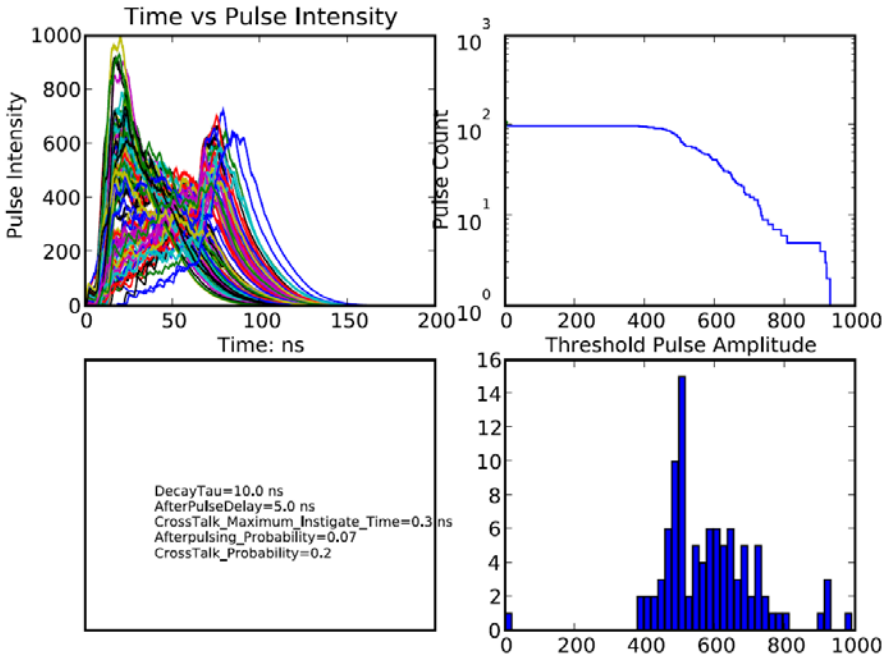

(d) crosstalk probability = 0.2

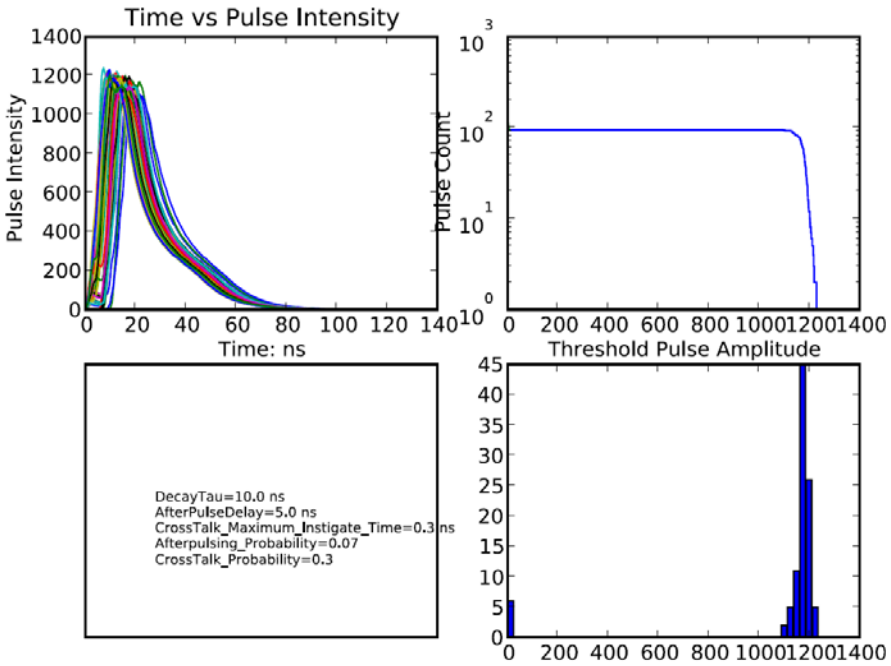

(e) crosstalk probability = 0.3

Figure 5.11 Simulation results of 1600-pixel SiPM with afterpulsing probability=0.07

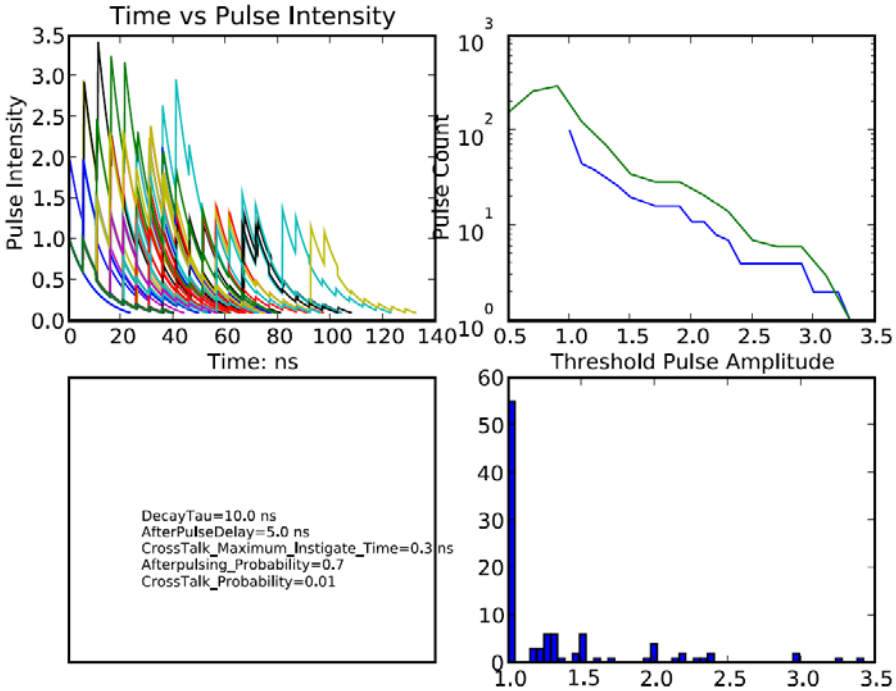

(a) crosstalk probability = 0.01

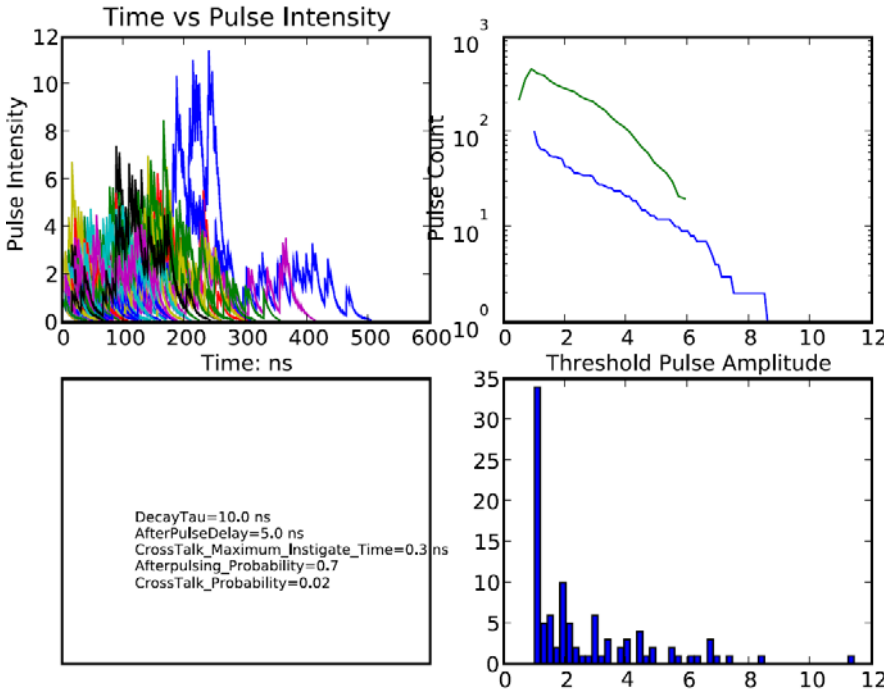

(b) crosstalk probability = 0.02

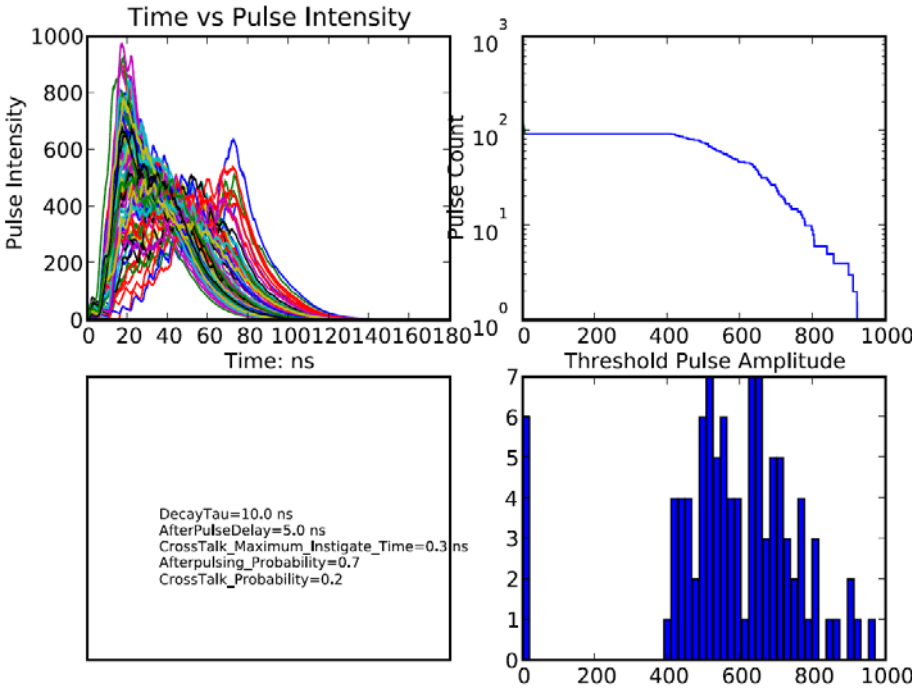

(c) crosstalk probability = 0.2

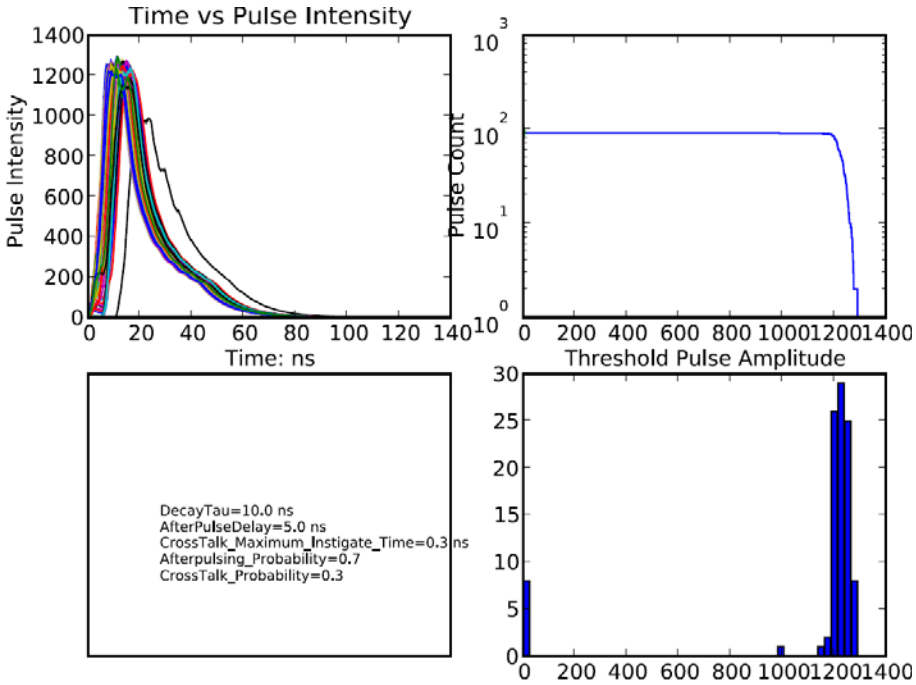

(d) crosstalk probability = 0.3

Figure 5.12 Simulation results of 1600-pixel SiPM with afterpulsing probability=0.7

5.5. Noise analysis of photon counting system

The noise is a very important parameter to evaluate the performance of a photon counting system. The minimum noise of photon detectors in the photon counting system is defined by the Poissonian noise which can be measured by the Poissonian fluctuation of the dark counts. The ideal photon counting system follows a Poisson distribution where the variance of the dark count rate is equal to its mean value. In order to characterize the noise, the dark count is recorded during thousands of integration intervals as in the Figure 5.13(a) and the distribution is calculated as in the Figure 5.13(b).

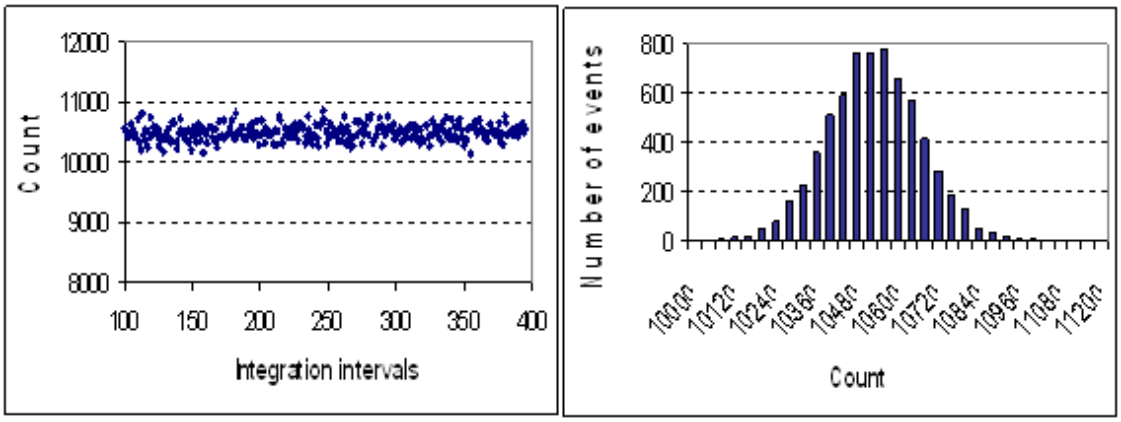

(a) (b)

Figure 5.13 (a) dark count rate recorded during integration intervals (b) dark count rate distribution

Each microcell of SiPM is working as an SPAD, so SiPM suffers from the non-linear noise of afterpulsing just as SPAD does. Due to the different nature, SPAD only suffers from afterpulsing whereas SiPM suffers from both afterpulsing and optical cross-talk.

To study the effect of cross-talk and afterpulsing on the noise analysis of photon counting system, a multi-trail simulator has been developed in our lab to simulate the dark count rate distribution of SiPM on different comparator threshold. The shell program of the multi-trial simulator is as follows:

```
import core
class settings:
   def __init__(self   ):
      pass

settings.number_of_trials=100 #The number of trial.
settings.mean_experiments_per_trial=100 #The mean number of
experiments per
#trial. A poisson distribution centered around the mean will be used.
#This computes settings.number_of_photons

settings.x_size=40
settings.y_size=40

settings.DecayTau=10.0                          #in ns
settings.AfterPulseDelay=5.0                     #in ns
settings.CrossTalk_Maximum_Instigate_Time=0.3    #in ns
```

```
settings.Afterpulsing_Probability=0.0007*0     #The afterpulsing
probability.
settings.CrossTalk_Probability=0.004
settings.Comparator_Delay=3                 # in ns
settings.Comparator_Threshold_Start = 0.5
settings.Comparator_Threshold_Step = 0.2
settings.Comparator_Threshold_Stop = 6.5

#Run the simulation
core.run(settings)
```

As you can see, the parameters in the multi-trial simulator are the same as the parameters used in the single-trial simulator which were introduced in the previous section except two parameters ***number_of_trials*** and ***mean_experiments_per_trial.*** The ***number_of_trials*** is to simulate the number of integration intervals in which the dark count rate is recorded in the experiments. The ***mean_experiments_per_trial*** actually has the same meaning of the ***number_of_photons*** mentioned in the previous section and this number is a poisson distribution centered on the mean value set by users. For each trail, the simulator does the same thing as the single-trial simulation by setting the number of photons programmedly. Then the mean and variance is calculated for all trials and plotted on different comparator threshold values. The deviation between the mean value and the variance value shows the level of noise.

5.5.1. Multi-trial simulations of enhanced crosstalk

Different from photon number resolving applications, in photon counting applications only one larger pulse is registered for each photon even if crosstalk happens. Due to the mechanics of crosstalk, theoretically it doesn't have any effect on noise analysis of photon counting system. It is very interesting topic to study.

In this section, the afterpulsing probability is set to zero for all simulations. ***number_of_trials=100*** and ***number_of_trials=1000*** have been simulated for the same conditions. It is proved that ***number_of_trials=100*** is large enough to obtain the accurate distribution and much more time saving. All the following multi-trial simulations are run and plotted on 100 trials.

The simulated result window is very like the measured curve of dark count rate versus comparator threshold. But there are two curves in each simulated window: the blue one is the mean values of photon count plotted on comparator thresholds; the green one is the variance values of photon count plotted on comparator thresholds. The ***mean_experiments_per_trial*** is set to 100 for all simulations, so the ***number_of_photons*** for each trial is calculated by the program according to Poisonian distribution. Figure 5.14 and Figure 5.15 are the simulated results of crosstalk probability = 0.02 and 0.4 respectively.

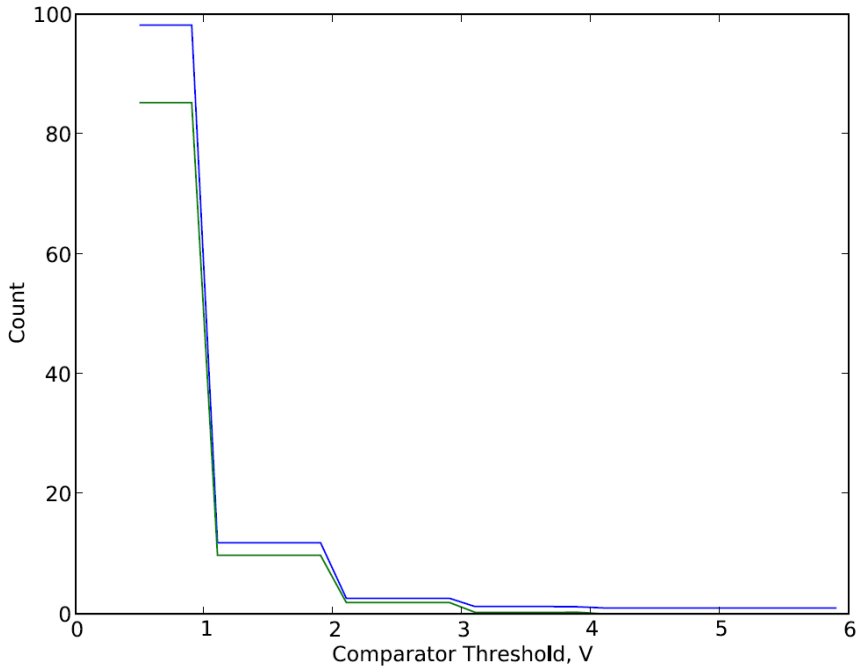

Figure 5.14 multi-trial simulation result: crosstalk probability=0.02, afterpulsing probability=0

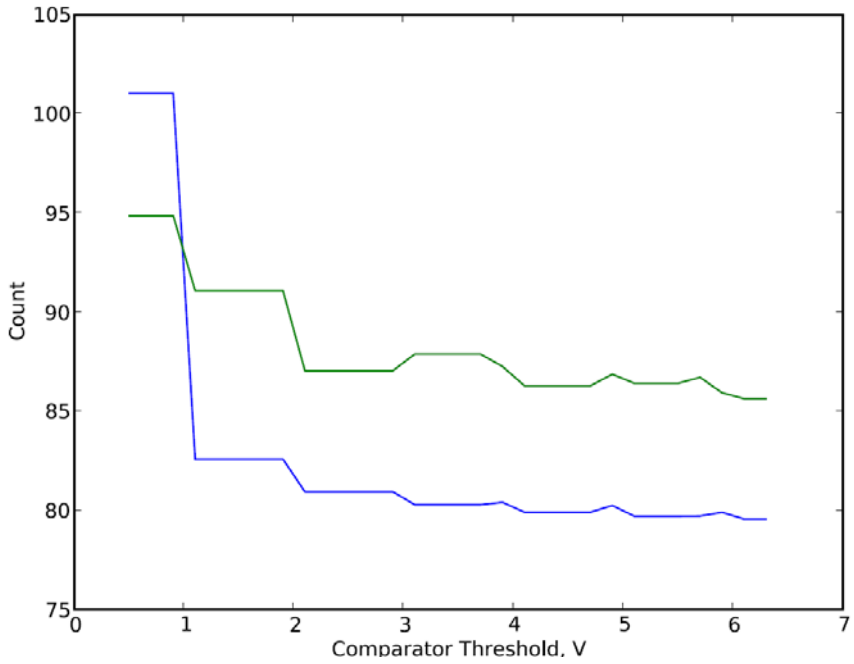

Figure 5.15 multi-trial simulation result: crosstalk probability=0.4, afterpulsing probability=0

As seen from the above figures when the crosstalk probability is small, most of the output pulses are 1p.e; there are only 3 steps can be observed. When the crosstalk is up to 0.4, all the output pulses have the same amplitude which is larger than 6p.e (comparator thresholds larger than 7p.e are not shown). This result is consistent to the single trial simulations.

With zero afterpulsing probability there is only several count deviations between the mean curve and the variance curve for both crosstalk probabilities. And with the comparator threshold increases, the deviation is becoming smaller and smaller. That mean the noise of this photon detector is very small or ignorable if afterpulsing doesn't happen at all. So I can conclude that with high enough crosstalk the SiPM will have enhanced internal gain but no noise. We know it is perfect but not real. The effect of afterpulsing has to be considered.

5.5.2. Multi-trial simulations of enhanced afterpulsing

For the moderate crosstalk probability of 0.02, afterpulsing probability of 0.0007, 0.007, and 0.07 have been simulated and the results are shown in Figure 5.16, Figure 5.17 Figure5.18 respectively. With the afterpulsing increases the steps disappear and the deviation between the mean and variance is becoming larger and larger. It means that afterpulsing is the dominating noise source of photon counting detector.

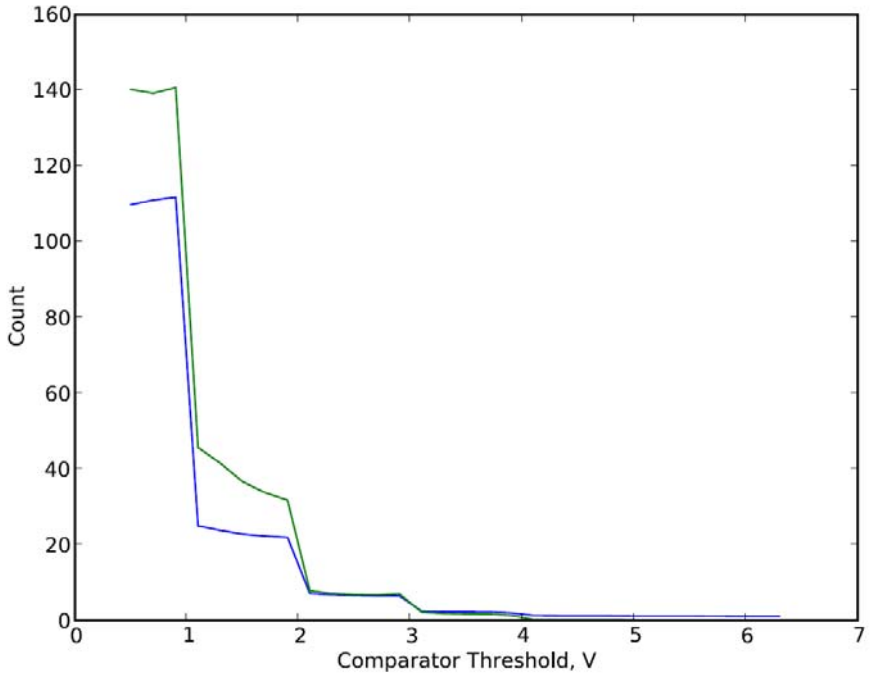

Figure 5.16 multi-trial simulation result: crosstalk probability=0.02, afterpulsing probability=0.0007

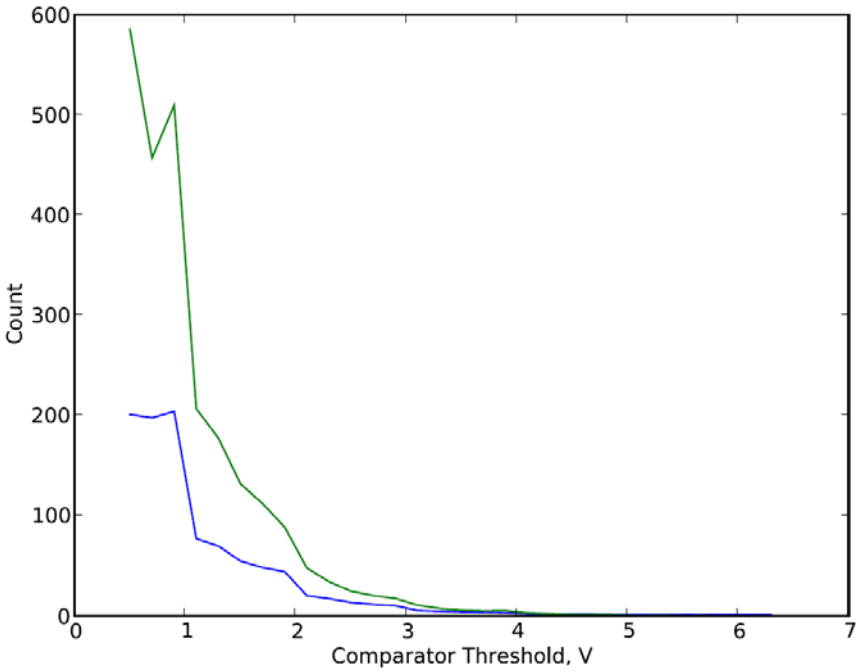

Figure 5.17 multi-trial simulation result: crosstalk probability=0.02, afterpulsing probability=0.007

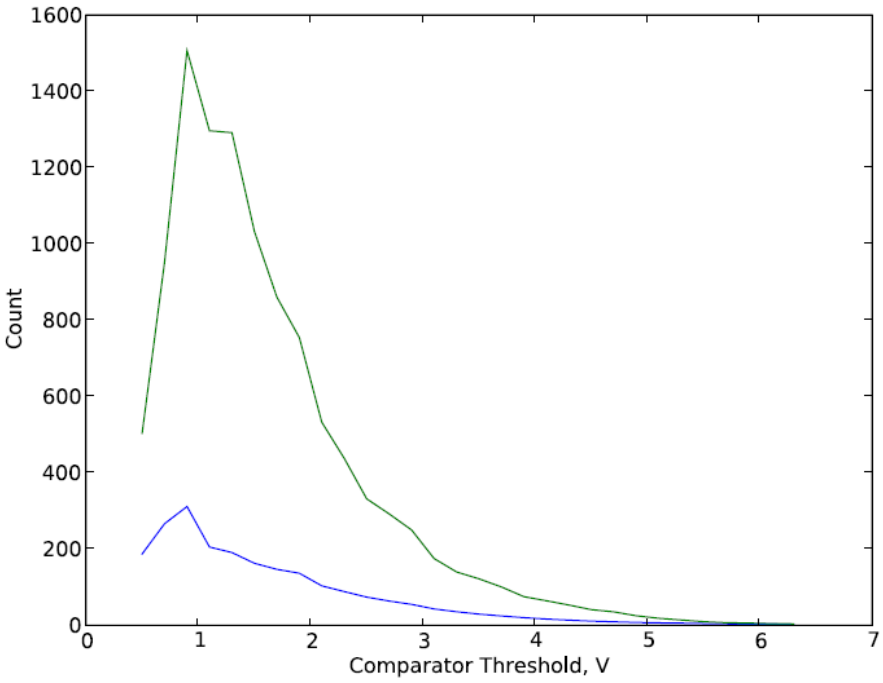

Figure 5.18 multi-trial simulation result: crosstalk probability=0.02, afterpulsing probability=0.07

6. Experiments on different types of SiPM

From the simulation results presented in the previous chapter, I am able to presume that at a properly enhanced optical crosstalk all the microcells of SiPM can be totally fired or partially fired simultaneously. Under this situation additional 100~1000 times (proportional to the number of microcells) internal gain can be obtained by SiPM itself and no external amplification is required.

However it is very hard to enhance the optical crosstalk of packaged SiPMs in the lab, the optical crosstalk can be enhanced by increasing the bias voltage of the device. With the bias voltage increasing the number of charge carriers crossing the junction increase so that the afterpulsing increases accordingly. In the experiments, we can't enhance crosstalk probability or afterpulsing separately but enhance them both at the same time.

In this chapter, experimental results of SiPMs from two manufactures have been presented and discussed. Three different pixel sizes of SiPMs called MPPC series are from Hamamatsu; the so-called Russian SiPM (diode) is from Russia.

To study the effect of enhanced optical cross-talk on the output signals, I measured the dark count rate distribution of SiPMs with not only operating voltage but over voltages (~10V above breakdown voltage), because to increase the bias voltage is the only way to increase crosstalk probability on the packaged diodes in the lab.

6.1. Hamamatsu MPPC series

The datasheet of Hamamatsu MPPC series is shown in the Figure 6.1. There are three different pixel sizes of diodes in this series, so called 100-pixel device, 400-pixel device, and 1600-pixel device. They are all 1mm*mm device. The feasibility of this series being used for DNA sequencing has been described in the chapter 5.1. Its linearity, dynamic range, and dark count rate are measured in operating voltage and results are presented in the chapter 5.

Active area 1 × 1 mm type (Typ. unless otherwise noted, Ta=25 ˚C)

S10362-11-025U /-050U/-100U

S10362-11-025C /-050C/-100C

Parameter	Symbol	S10362-11 series			Unit
		-025U, -025C	-050U, -050C	-100U, -100C	
Chip size	-	1.5 × 1.5			mm
Effective active area	-	1 × 1			mm
Number of pixels	-	1600	400	100	-
Pixel size	-	25 × 25	50 × 50	100 × 100	μm
Fill factor *1	-	30.8	61.5	78.5	%
Spectral response range	λ	270 to 900			nm
Peak sensitivity wavelength	λp	400			nm
Quantum efficiency (λ=λp)	QE	70 Min.			%
Photon detection efficiency *2 (λ=λp)	PDE	25	50	65	%
Recommended operating voltage range	-	70 ± 10 *3			V
Dark count	-	300	400	600	kcps
Dark count Max.	-	600	800	1000	kcps
Terminal capacitance	Ct	35			pF
Time resolution (FWHM)	-	200 to 300			ps
Temperature coefficient of reverse voltage	-	50			mV/˚C
Gain	M	2.75×10^5	7.5×10^5	2.4×10^6	-

Figure 6.1 Datasheet of Hamamatsu MPPC series:
-025U is 1600-pixel device, -050U is 400-pixel device, and -100U is 100-pixel device

6.1.1. Experimental set-up and measured output pulses

Output pulses (illustrated in Figure 6.5) can be observed from the oscilloscope with the setup shown in Figure 6.2. The bias connection for Hamamatsu MPPC series is seen as in the Figure 6.3. The output signals from external amplifiers are going to the Stanford

counter SR200 which is used to record the dark count number per second (see Figure 6.4).

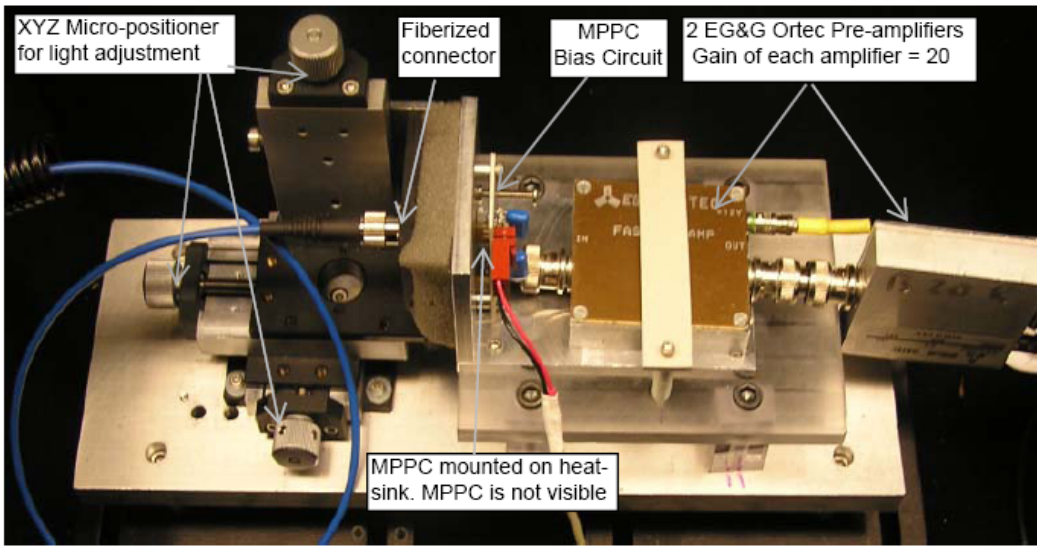

Figure 6.2 Experimental set-up for Hamamatsu MPPC series.

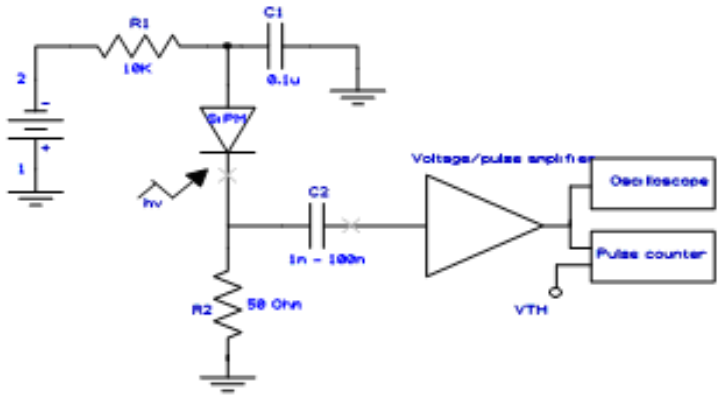

Figure 6.3 Schematic of Hamamatsu MPPC bias circuit

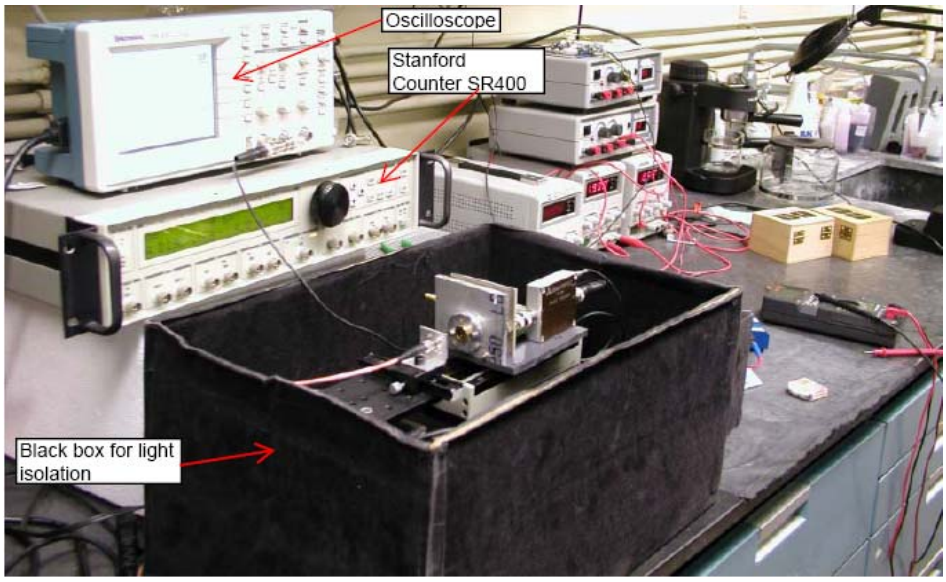

Figure 6.4 Experimental set-up used for characterizing all SiPMs

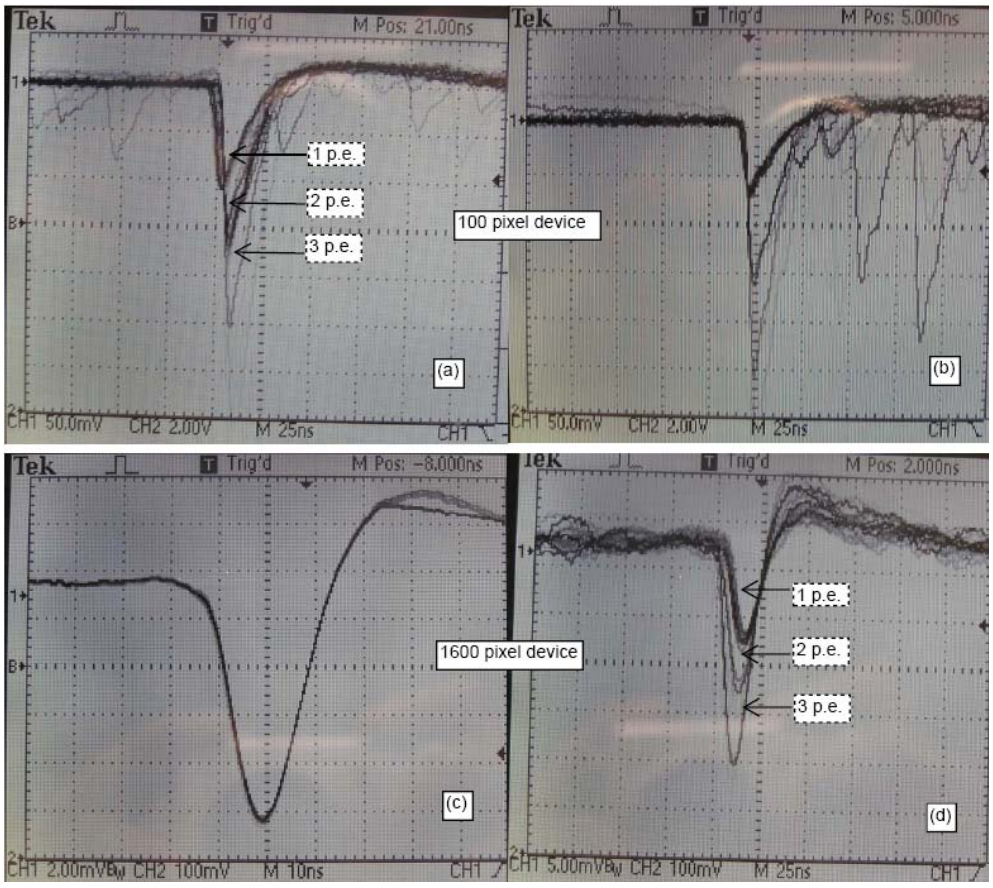

Figure 6.5 Output pulses, (a, b) 100-pixel device, (c, d) 1600-pixel device at low (left) and high (right) V_{OV}. Note: (c) was recorded in the averaging mode.

The FWHM for 100-pixel and 1600-pixel device is approximately 20ns and 18ns respectively; maximum pulse width for 100-pixel and 1600-pixel device is 35-40ns and 25-30 respectively. Pulses due to 1p.e. 2p.e. etc. are distinctly visible with these devices as shown in Figure 6.5a and 6.5d. Therefore the expected maximum achievable count rate should be in the range of 25-30 MHz for 100-pixel device and 33-40 MHz for the 1600-pixel device. The expected dynamic range of SiPMs is better than that of large area APD which is expected to be 16~20MHz, because dynamic range of SiPM is not limited to the dead time of quenching circuit.

6.1.2. DCR measurement with operating voltage

The recommended operating voltage (Vop) of Hamamatsu MPPC series is 70.89V, 69.72V, and 69.72V respectively for 1600-pixel device, 400-pixel device, and 100-pixel device. The dark count rate (DCR) has been recorded by the external Stanford counter SR400 for the three devices at Vop, Vop+0.5V, and Vop+1V respectively. At this level of bias voltage, two external amplifiers are required to register all the output pulses. The gain of each amplifier used is 20 times, so the total external amplification is 400 times.

The relationship between DCR and the comparator thresholds of the counter is demonstrated for each device in Figure 6.6, Figure 6.7, and Figure 6.8. Step like characteristics can be observed for all the devices at around operating voltage. For the step like characteristics of SiPM DCR, please see the explanation in Chapter 4.3.2. With the bias voltage increasing, the steps disappear gradually. It is hard to observe the steps when the bias voltage increases to Vop+1V.

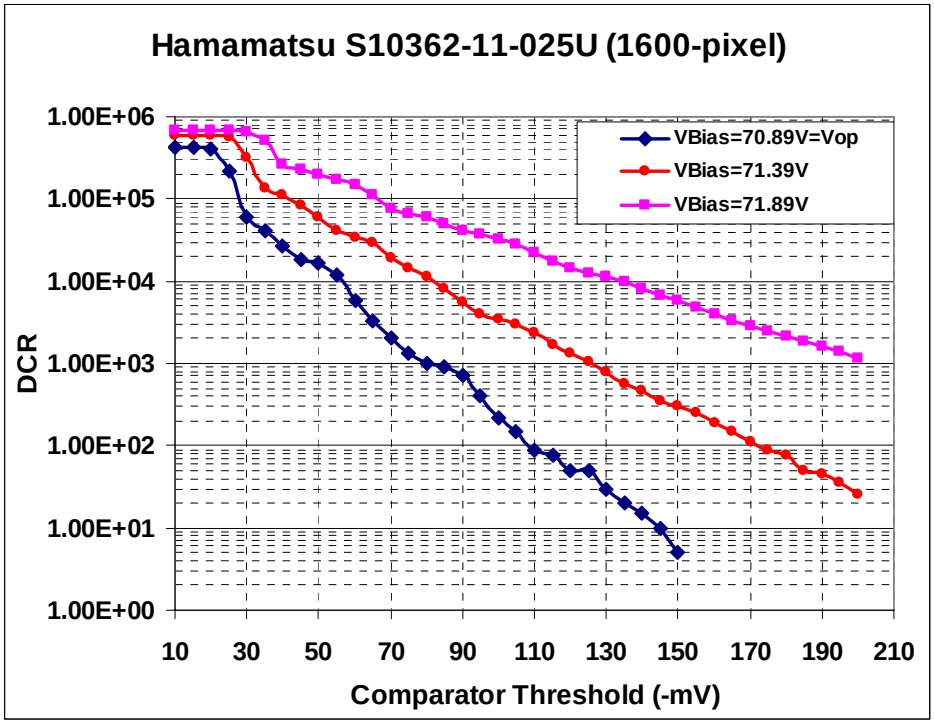

Figure 6.6 1600-pixel device: DCR vs. Comparator threshold at Vop, Vop+0.5V, and Vop+1V

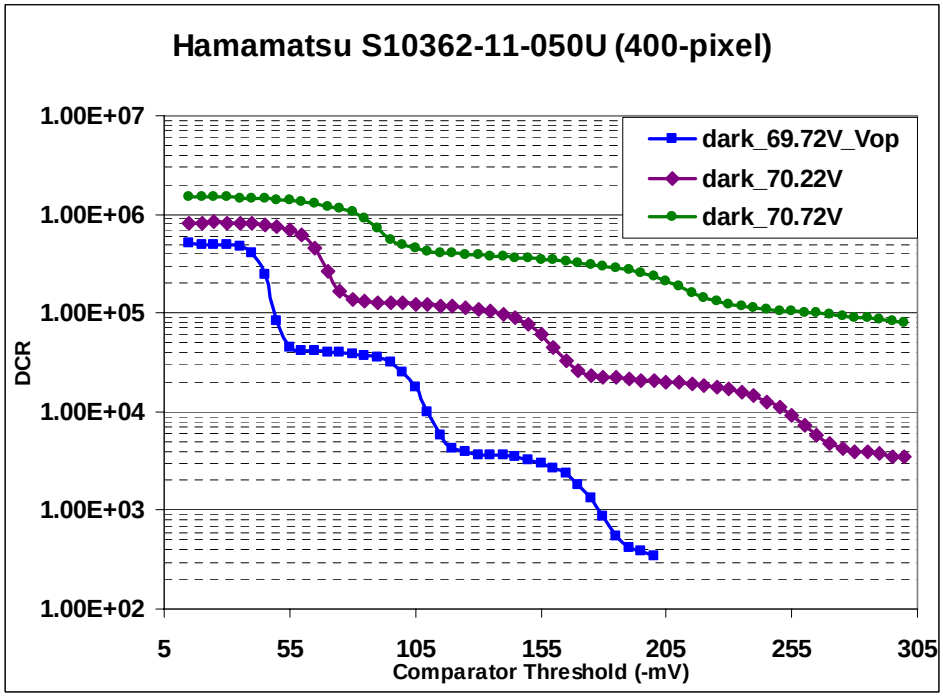

Figure 6.7 400-pixel device: DCR vs. Comparator threshold at Vop, Vop+0.5V, and Vop+1V

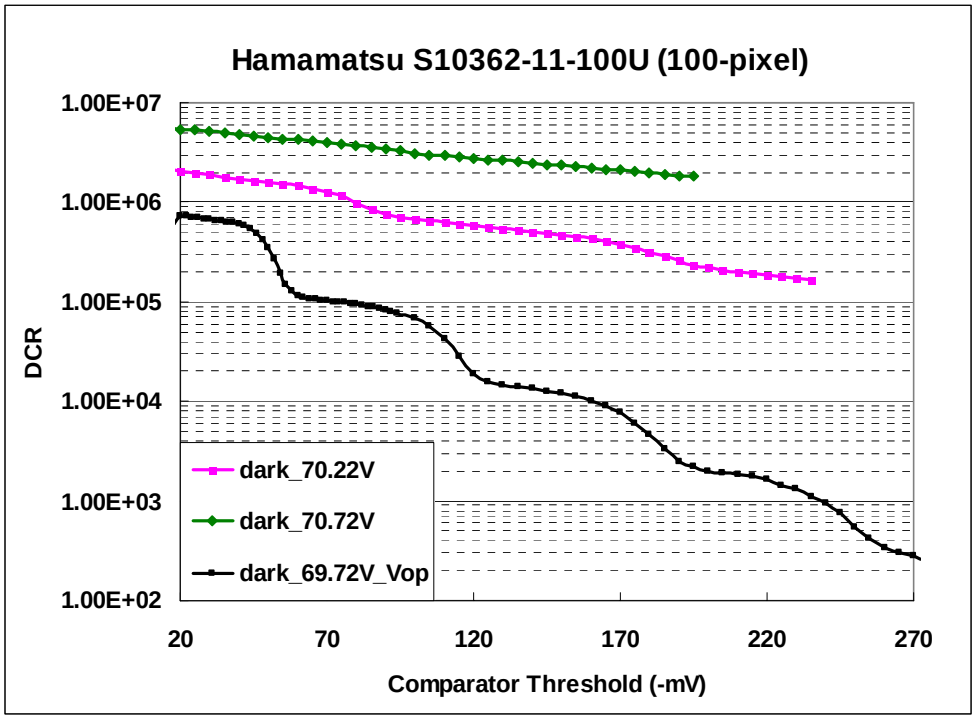

Figure 6.8 100-pixel device: DCR vs. Comparator threshold at Vop, Vop+0.5V, and Vop+1V

You can see from above figures with same external amplification, at the operating voltage the DCR and 1 p.e. pulse amplitude of 100-pixel device is largest. It means that 100-pixel device has a larger internal gain due to the largest pixel size. Using the method described in Chapter 4.3.5, the cross-talk rate can be calculated by the ratio of drop in count rate from step1 to step 2 for each device roughly. 100-pixel device has the largest cross-talk rate maybe due to its largest fill factor. Obviously the cross-talk rate and internal gain increase for all of the three devices when the bias voltage is higher than the operating voltage.

Another thing worthy to be noticed is that with the bias voltage 1V above Vop the DCR of 100-pixel device increases dramatically from ~700K to ~4M counts/sec; however the DCR of 1600-pixel device increases from ~400K to 600K. Because the gain

of 100-pixel device is 10 times larger than the gain of 1600-pixel device, the charge flowing through 100-pixel device during avalanche is larger than what 1600-pixel device does. This makes the afterpulsing probability of 100-pixel device larger and leads to dramatically increasing DCR with 1V over-voltage.

6.1.3. DCR measurement with over-voltage

With only 1V above operating voltage, we can observe the DCR change due to the change of cross-talk and afterpulsing probability. To study the effect of cross-talk and afterpulsing, measurement with higher over-voltage is meaningful. For the over-voltage measurement, only one external amplifier of 20 times gain has been used. The curves of DCR vs. comparator threshold with bias voltage from Vop to Vop+10V are illustrated in Figure 6.9 for 100-pixel device.

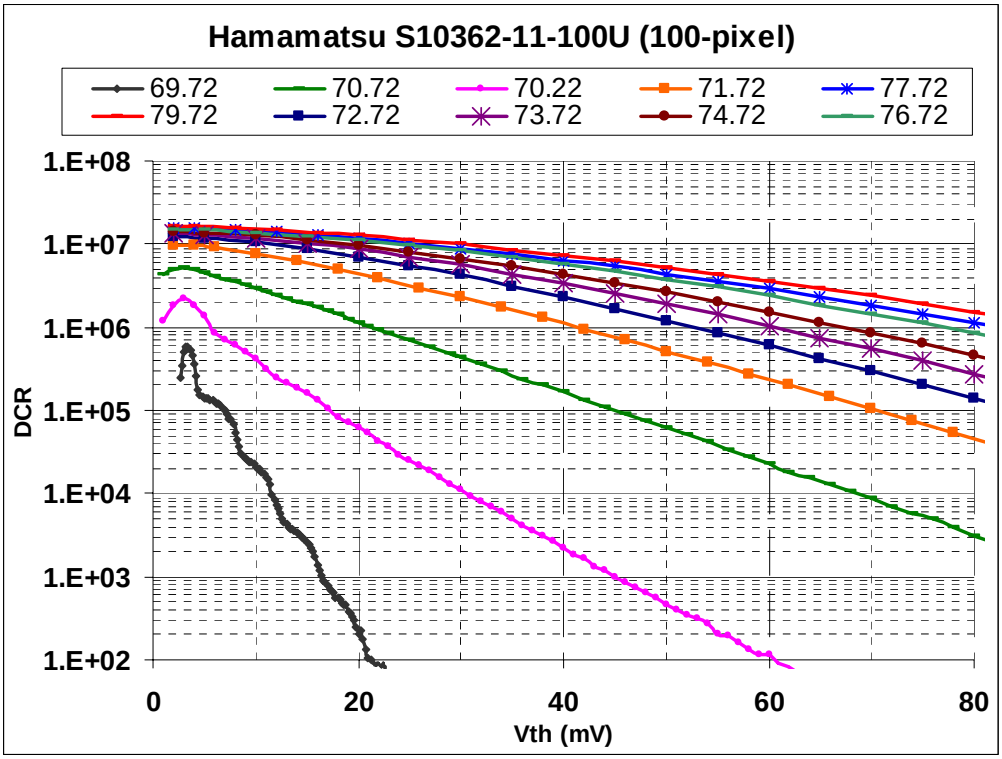

Figure 6.9 100-pixel device: DCR vs. Comparator threshold at Vop~Vop+10V

The curves of DCR vs. comparator threshold with bias voltage from Vop to Vop+6V are illustrated in figure 6.10 for 1600-pixel device.

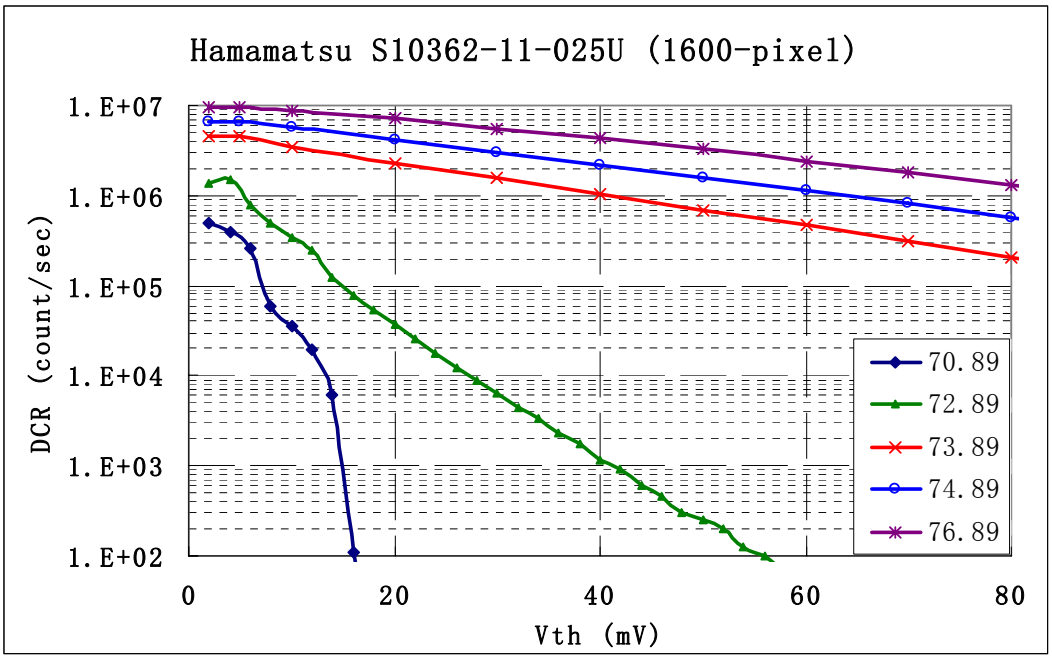

Figure 6.10 1600-pixel device: DCR vs. Comparator threshold at Vop~Vop+6V

The over-voltage measurement shows that for 100-pixel device maximum DCR increased from ~600K to ~10M counts/sec when the bias voltage changed from Vop to Vop+2V; and more than 1M counts out of the 10M pulses are larger than 80mV when the bias voltage up to Vop+8V. The pulse amplitude larger than 80mV means that the original output pulse from SiPM without any external amplification is 4mV, which is a detectable signal for many comparators and counters. For 1600-pixel device, the maximum DCR increased from ~400K to ~10M counts/sec when bias voltage changed from Vop to Vop+6V; and more than 1M counts out of 10M pulses are larger than 80mV. However at around Vop 100-pixel device seems to have high cross-talk rate, 1600-pixel has larger output pulses and lower DCR with same over-voltages. Comparable low DCR is an advantage of 1600-pixel over 100-pixel and 400-pixel device.

6.1.4. DCR measurement for noise analysis

As introduced in Chapter 5.5, the internal noise of photon detectors in the photon counting system is defined by the Poissonian fluctuation of the dark (photo) counts. The ideal photon counting system follows a Poisson distribution where the variance of the dark (photo) count rate is equal to its mean value. And the noise is calculated by the square root of the variance.

In order to characterize the noise, the dark count with different external amplification is recorded during thousands of integration intervals by the 32-channel counter and associate software developed by our group. The photo of the 32-channel counter, 32-channel amplifier and comparator, and a variable gain attenuator is shown in Figure6.11. The block diagram of the connection for noise measurement is shown in Figure 6.12.

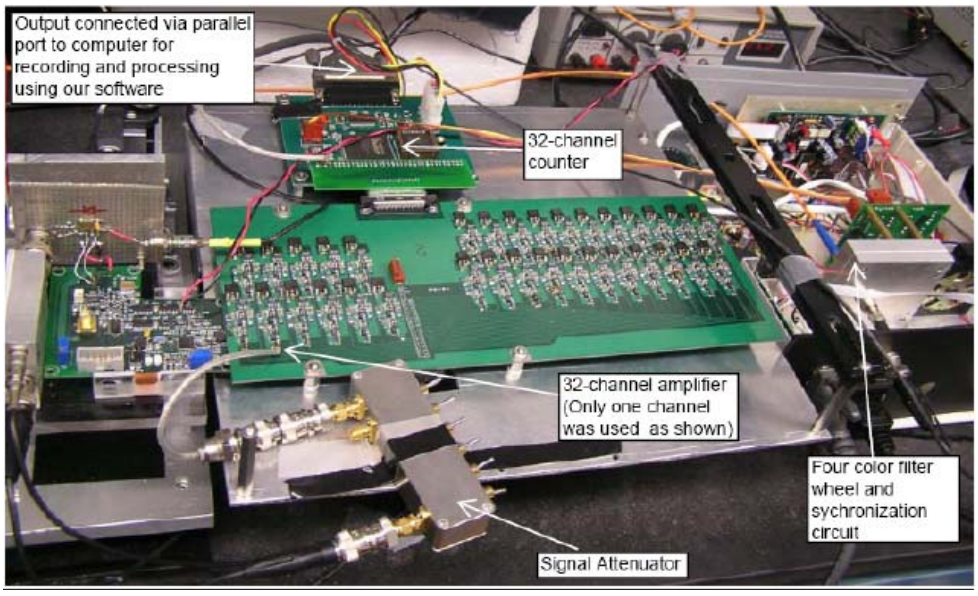

Figure 6.11 Experimental set-up of noise characterization for SiPM

The output of SiPM is connected to Ortec preamplifier with 20 times gain. Then the signal goes to a variable gain attenuator and 32-channel amplifier so that we can measure the DCR with different external amplification. The 32-channel amplifier is connected to the 32-channel counter that can be connected to the computer via the parallel port. Further, the counter circuit is synchronized with the filter wheel that determines the integration time. Because we wanted to measure the fluctuation of dark count of only one SiPM, only one channel out of the 32-channels was utilized. Figure 6.12 shows the block diagram of the set-up.

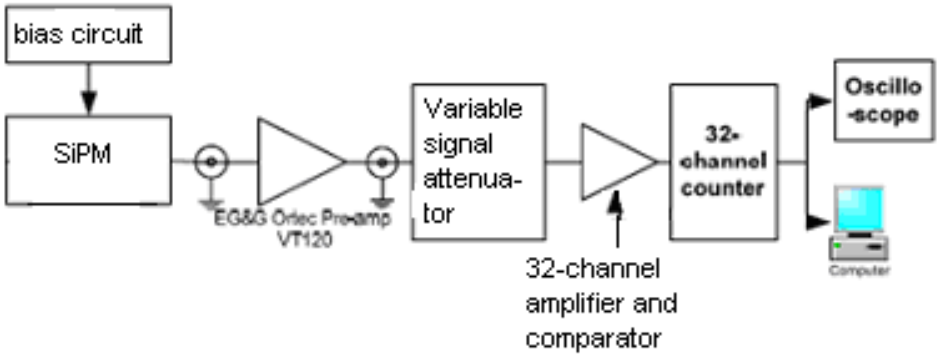

Figure 6.12 Block diagram of noise characterization set-up for SiPM

The DCR during thousands of integration intervals are recorded by the software BASE. BASE is the software developed by our group, which works with our single-lane DNA sequencer. The measured data have been imported to EXCEL and the DCR distribution has been calculated. The variations of the mean and variance of DRC to different external amplification are shown in Figure 6.13 and Figure 6.14 for 1600-pixel device and 100-pixel device respectively.

We can conclude from the experimental results: with more external amplification, the deviation between mean and variance is larger, the noise is larger; for the same amplification, the higher over-voltage, and the larger the noise.

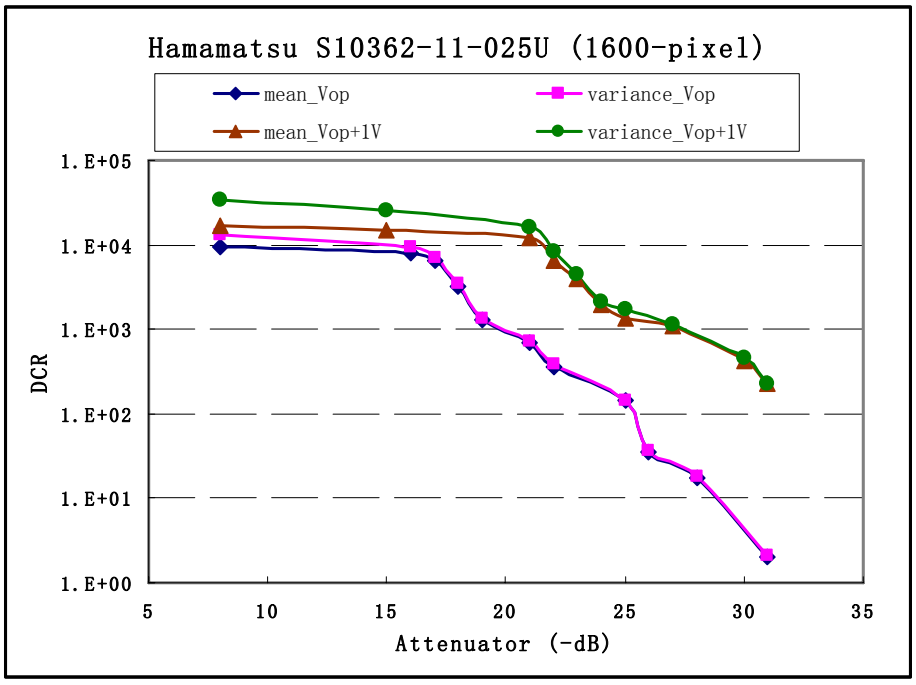

Figure 6.13 1600-pixel device: DCR distribution vs. external amplification

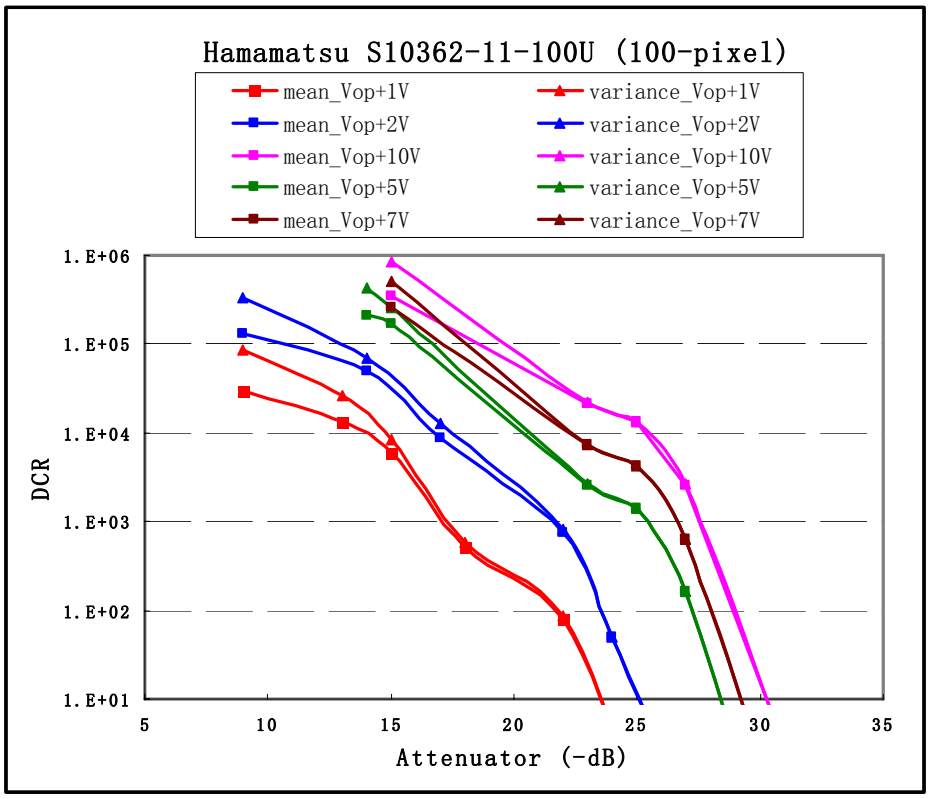

Figure 6.14 100-pixel device: DCR distribution vs. External amplification

So the higher over-voltage and the lower noise is a tradeoff. Is that possible to operate SiPM at a low over-voltage to obtain high cross-talk rate so that it can have a large internal gain without increasing noise?

6.2. Russian SiPM (diode)

A SiPM from another manufacture, called Rissian diode has been measured under the same procedure. The basic specification of Russian diode is shown in Table 6.1.

Table 6.1 Specification of Russian diode

Specification	Value
Chip Size (mm^2)	1.1
No of pixels	1024
Operating Voltage (V)	56V

The close-up photo under microscope and the photo for the whole package are shown in Figure 6.15.

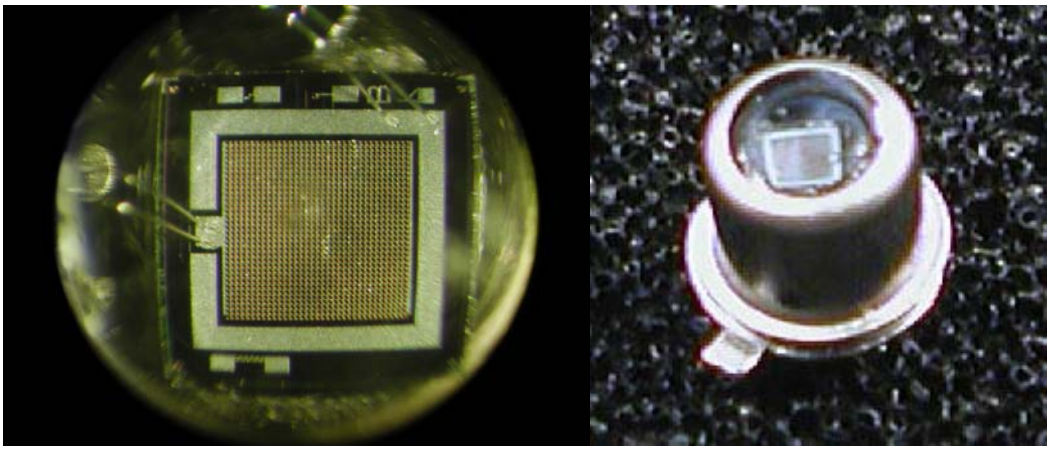

Figure 6.15 Photos of Russian diode

6.2.1. Measured output pulses

The experimental set-up for Russian diode is the same as the set-up for Hamamatsu MPPC series except only one external amplifier with 20 times gain used.

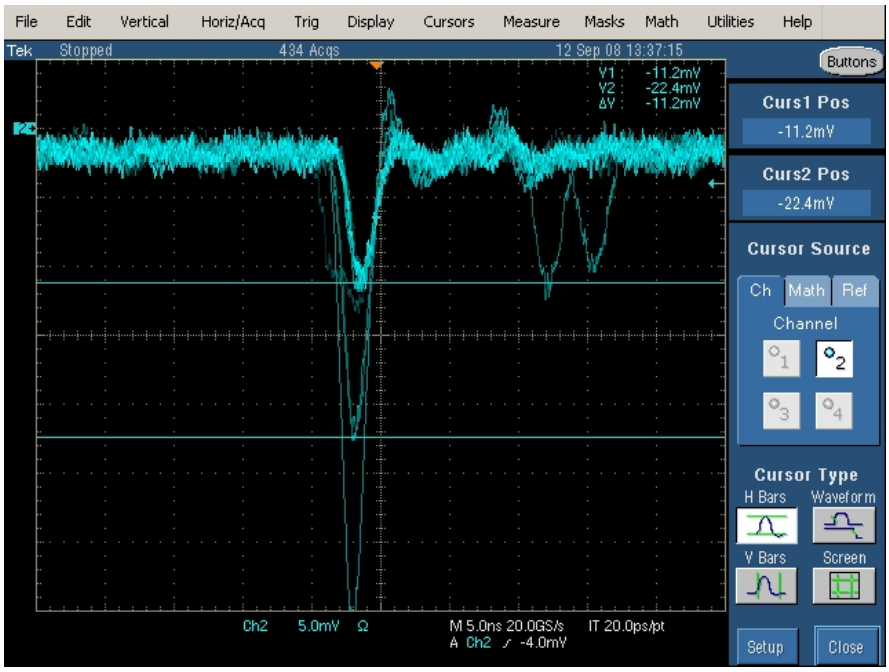

(a) Vbias = 54V

(b) Vbias = 55V

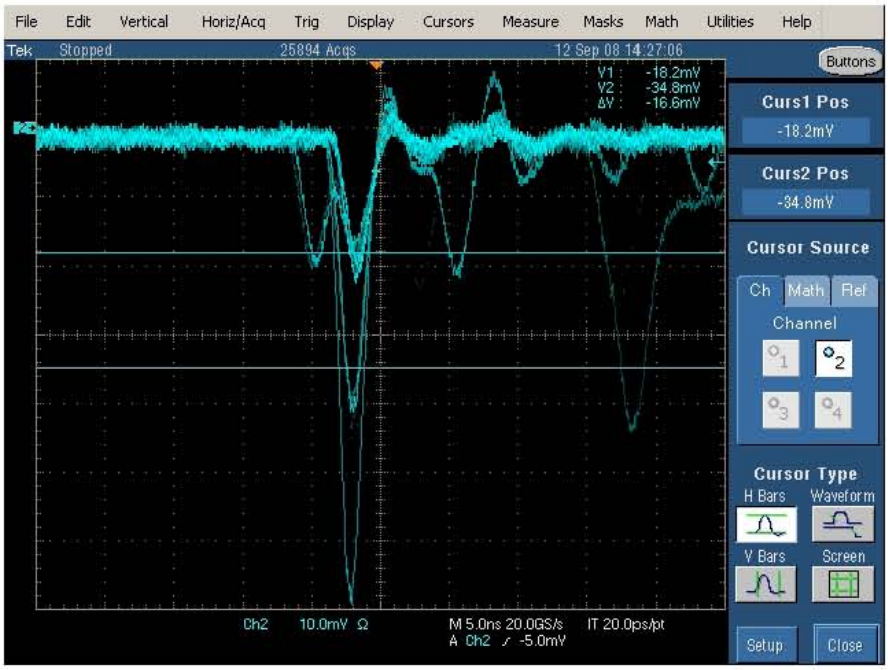

(c) Vbias = 56V

(d) Vbias = 57V

Figure 6.16 Russian diode: output pulses for different bias voltages

All of the observed output pulse width is not more than 10ns. Pulses due to 1p.e. 2p.e. etc. are distinctly visible as shown in Figure 6.16. Therefore the expected maximum

achievable count rate should be in the range of 100MHz. The expected dynamic range of Russian diode is much better than that of large area APD, even better than that of Hamamatsu MPPC series. With bias voltage increasing from 54V to 57V, the pulse width doesn't change; the number of observed afterpulsing is more.

6.2.2. DCR measurement with operating voltage

The operating voltage of Russian diode is 56V. Output pulses can be observed by oscilloscope from 54V. The dark count rate has been measured with one ORTEC VT120 preamplifier for bias voltages of 54V, 55V, 56V, and 57V.

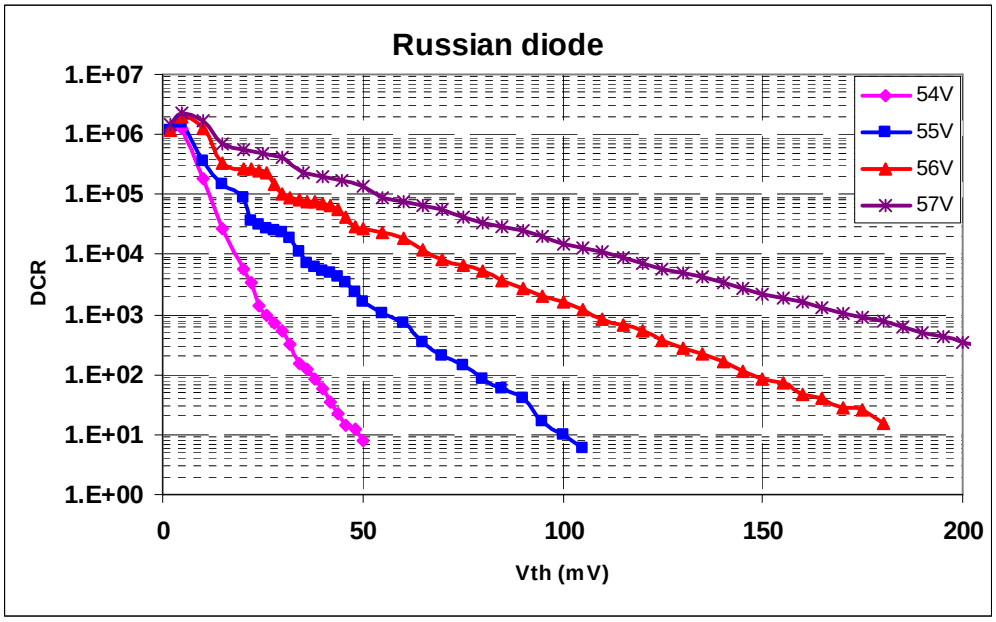

Figure 6.17 Russian diode: DCR vs. Comparator threshold at around Vop

The DCR curves for the four bias voltages start from the same level. I doubt that the first step is from noise instead of real dark count. Noise pulses with amplitude of about 4mV can be seen from the snapshot of oscilloscope.

6.2.3. DCR measurement with over-voltage

With the bias voltage increasing from 54V to 57V, the cross-talk rate is becoming larger and larger. The DCR with over-voltage up to Vop+6V has been measured on Russian diode. For the over-voltage measurement, one external amplifier of 20 times gain has been used. Due to the range limit of external counter, the maximum comparator threshold is 300mV. The curves of DCR vs. comparator threshold with bias voltage from Vop to Vop+6V are illustrated in Figure 6.18.

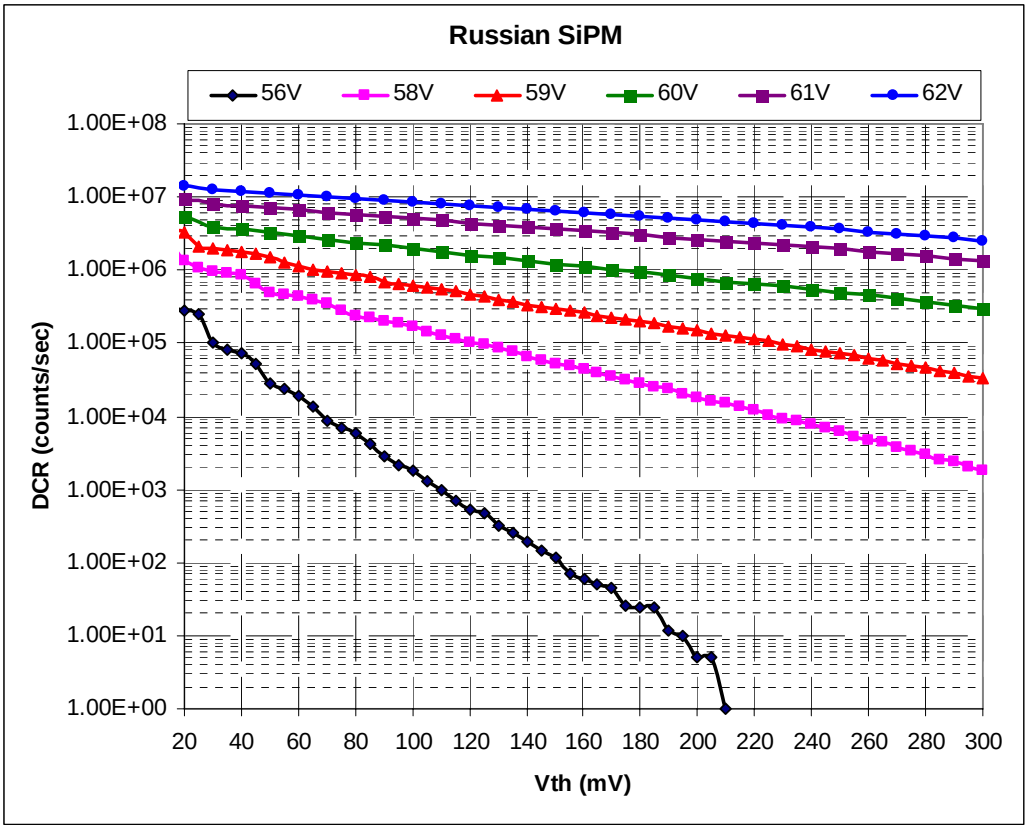

Figure 6.18 Russian diode: DCR vs. Comparator threshold at Vop~Vop+6V

You see the amplitude of more than 1M counts out of 10M pulses are larger than 300mV when the bias voltage is up to Vop+5V with 20 times external amplification. It means that 10% of original pulses from Russian diode is larger than 15mV. So far, Russian diode is known as a SiPM with fastest response time and largest output pulse.

6.3. Compare experimental results with simulations

6.3.1. Compare of output pulse

In the experiments, the optical cross-talk and afterpulsing can be enhanced by increasing the bias voltage of the device. So DCR measurement with both operating voltage and over-voltages has been done for Hamamatsu 100-pixel device and 1600-pixel device. Comparing the experimental results with the simulations in the previous chapter is very interesting. At operating voltage the step-like characteristic can be measured for both 1600-pixel device and 100-pixel device (as seen in Figure 6.19 and Figure 6.21). The situation is very similar to the simulation with a small cross-talk and afterpulsing probability, which is shown in Figure 6.20 (a) and Figure 6.22 (a).

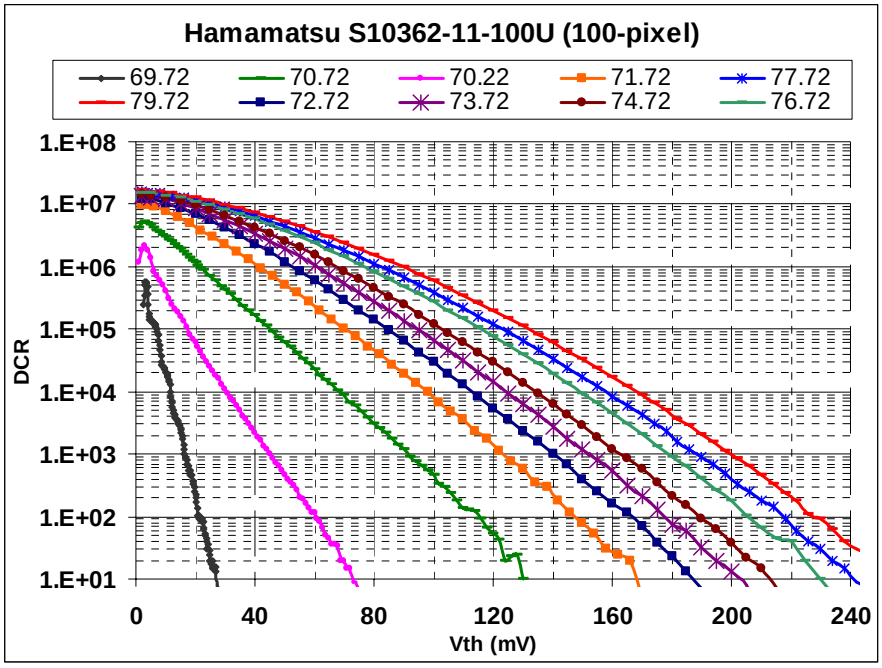

Figure 6.19 100-pixel device: measured DCR vs. comparator threshold for Vop~Vop+10V

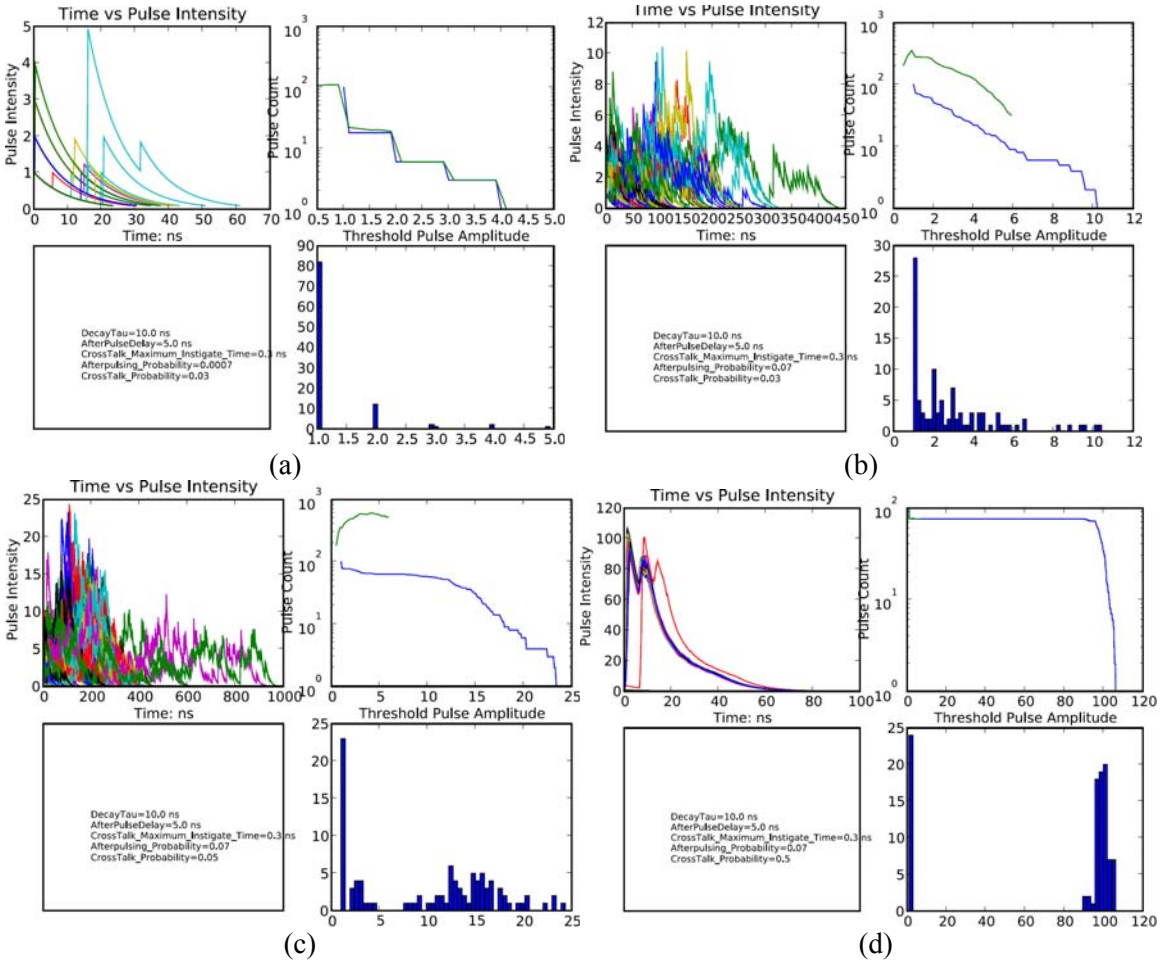

Figure 6.20 100-pixel SiPM simulation for different cross-talk and afterpulsing (a) cross-talk probability=0.03, afterpulsing probability=0.0007; (b) cross-talk probability=0.03, afterpulsing probability=0.07; (c) cross-talk probability=0.05, afterpulsing probability=0.07; (d) cross-talk probability=0.5, afterpulsing probability=0.07

The curves with bias voltage of Vop+0.5V and Vop+1V (as seen in Figure 6.19) have a similar shape to the simulated curve in Figure 6.20 (b). With bias voltage increasing, steps disappear; the curves of DCR vs. comparator threshold are becoming flatter and flatter. The measured curves shown in Figure 6.19 are more and more like the simulation in Figure 6.20 (c). However we can't obtain a measured flat curve like Figure 6.20 (d) even with a 10V over-voltage. The reason why we can't have a perfect flat DCR vs. comparator threshold curve like in the simulation could be that we are not able to have enough cross-talk probability in the experiments.

The same situation happens to 1600-pixel device, please compare Figure 6.21 with Figure 6.22. And the DCR increasing with bias voltage increasing is also a concern for our application. DCR lower than 10M counts/sec is a requirement for the single photon detector selection. So it is a tradeoff between high cross-talk probability and low DCR. Is that possible to make optical cross-talk larger without increase in DCR?

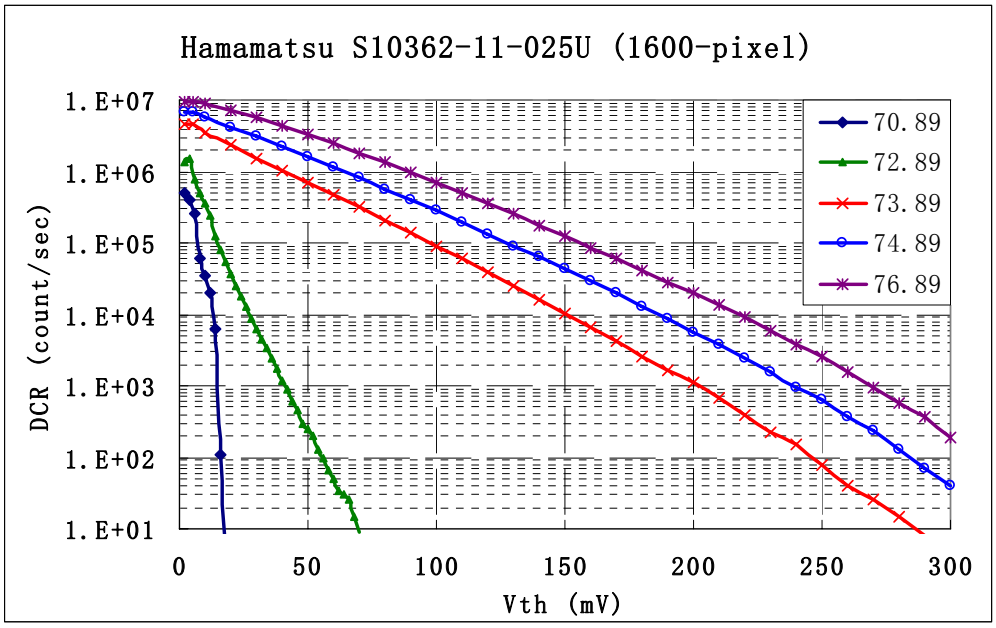

Figure 6.21 1600-pixel device: measured DCR vs. comparator threshold for Vop~vop+6V

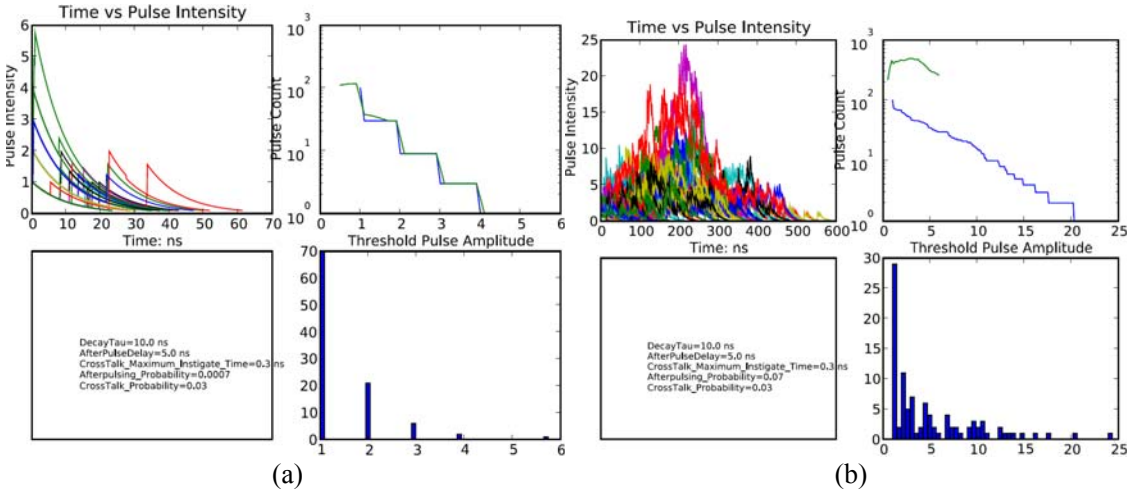

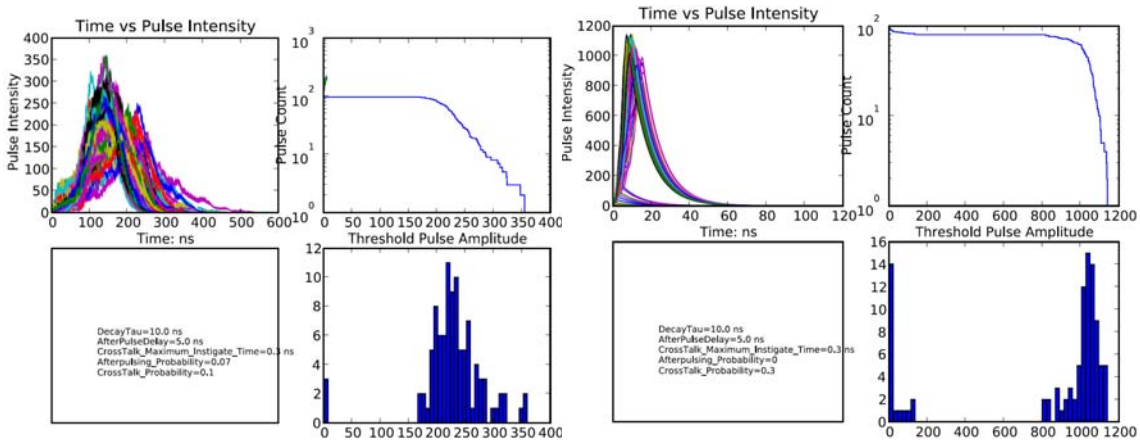

(c) (d)

Figure 6.22 1600-pixel SiPM simulation for different cross-talk and afterpulsing (a) cross-talk probability=0.03, afterpulsing probability=0.0007; (b) cross-talk probability=0.02, afterpulsing probability=0.07; (c) cross-talk probability=0.3, afterpulsing probability=0.07; (d) cross-talk probability=0.3, afterpulsing probability=0

6.3.2. Compare of noise analysis

The noise of single photon detectors has been simulated by our multi-trial simulator. The simulated mean and variance curves of photon count distribution have been demonstrated in Chapter 5.5. And the fluctuation of DCR for 100-pixel device and 1600-pixel device has been measured and recorded as presented in Chapter 6.1.4.

Compare the measured curves in Figure 6.13 and Figure 6.14 with the simulated curves in Figure 5.16, Figure 5.17, and Figure 5.18. The same relationship between the mean and variance of DCR and the comparator threshold (or external amplification) has been obtained for both simulations and measurements.

For both 100-pixel device and 1600-pixel device, it has been observed that the mean and variance converge with decreasing external amplification and decreasing over-voltage. The mean and variance become equal for some combinations of over-voltage and amplification. In the simulation, the mean and variance converge with increasing comparator threshold and decreasing cross-talk and afterpulsing probabilities.

The experiments have been done with decreasing external amplification, corresponding to the simulations with increasing comparator threshold; and the experiments done with increasing over-voltage, corresponding to the simulations with cross-talk and afterpulsing probabilities increasing.

With smaller amplification, the original pulses need to be large enough to be registered by counter, so cross-talk contributes more at these points. With large amplification, more afterpulses can be registered, because most of afterpulses are smaller than 1pe. So this measurement and simulation shows that afterpulsing adds much noise, crosstalk does not add so much noise in photon counting mode.

However in experiments DCR increases dramatically with over-voltage increasing, in simulations this situation doesn't happen. So the increasing DCR is not caused by thermally generated carriers in the junction but is due to afterpulsing which is mostly caused by the short lifetime traps. During avalanche some carriers are captured by deep levels (traps) in the junction depletion layer and subsequently released with a statistically fluctuating delay. So to cool the device is one of the methods to reduce afterpulsing.

6.4. Cool SiPM using Liquid Nitrogen

Is that possible to enhance optical cross-talk making the output pulse amplitude larger but without increasing the DCR? To operate semiconductor photodiode under low temperature is a method to reduce dark noise. In order to cool the device, it is usually mounted on a TE cooler and can be cooled lower to -80C. There are thermal resistors or

thermistors sitting on the peltier element inside the hermetically sealed cooled device. They sense the temperature on the peltier and send feedback to the temperature controller circuit that can control the operating temperature very accurately.

So far there is no commercially available cooled SiPM. And we are not able to fabricate the device with TE cooler in our lab. So the low temperature experiments have been done on two types of SiPM using liquid nitrogen. Though liquid nitrogen can cool the device very well, it is hard to control the temperature at a certain value. So these measurements are not that accurate, however we can have a roughly understanding of how SiPM work at the low temperature. Figure 6.23 and Figure 6.25 shows the relationship between DCR and temperature at a fixed bias voltage for Russian diode and 1600-pixel device respectively.

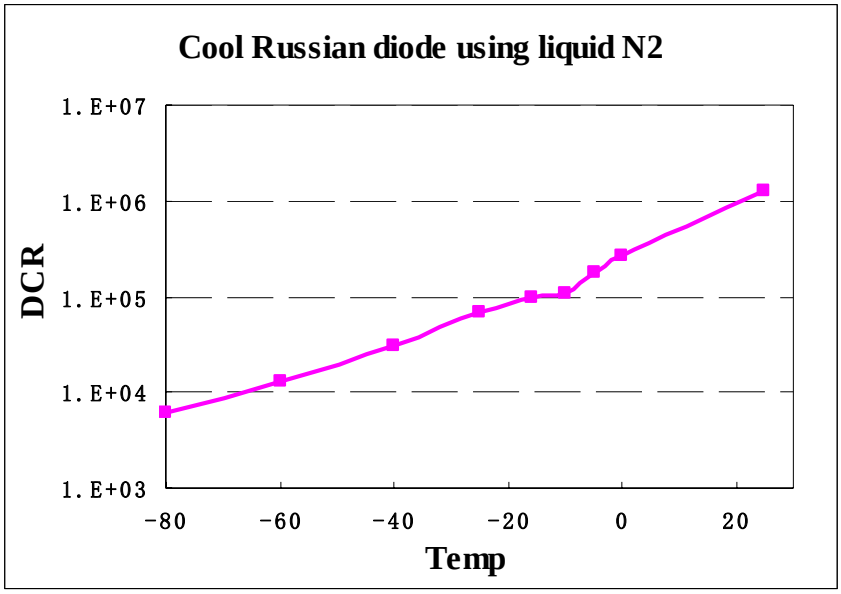

Figure 6.23 Russian diode: DCR vs. Temperature at Vbias=56V

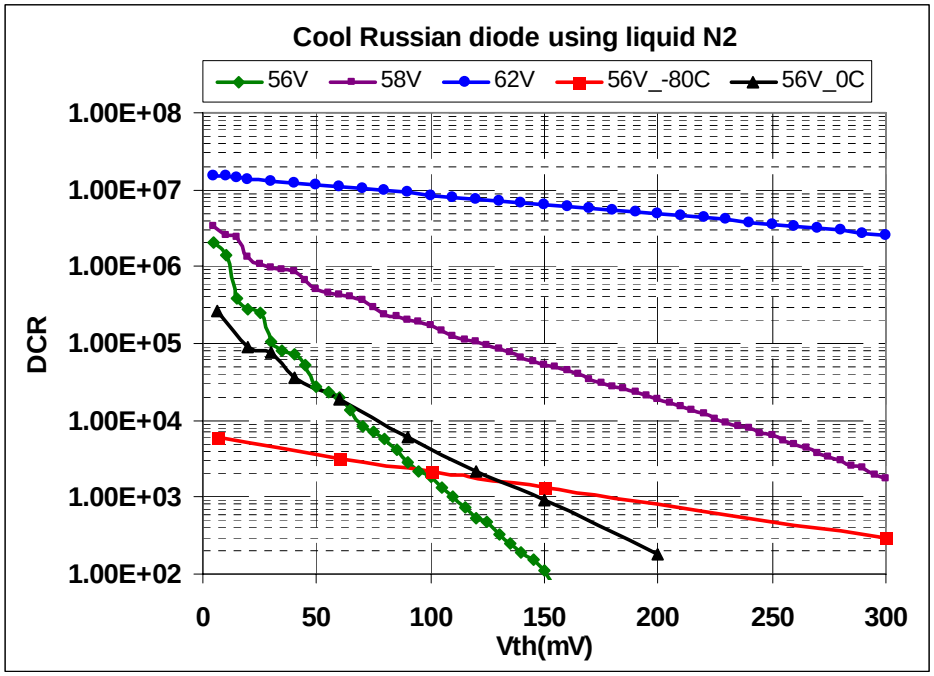

Figure 6.24 Russian diode: DCR vs. Comparator threshold at different Vbias and temperature

One thing need to be mentioned here: the breakdown voltage of SiPM depends on temperature due to the thermal effect. Breakdown voltage becomes lower with temperature becoming lower. All these low temperature measurements have been done at a fixed bias voltage, the operating voltage at room temperature. It means that with the temperature decreasing the over-voltage is increasing.

For Russian diode the relationship between DCR and temperature is kind of linear at the bias voltage of 56V. At -80C DCR is reduced more than 100 folded comparing to DCR at room temperature. The curves of DCR versus comparator threshold are measured for -80C and 0C at Vbias=56V. In Figure 6.24 these two curves compare with the curves measured with over-voltage at room temperature. When this diode is cooled to -80C and biased to only 56V, it has 1000 folded lower DCR but the same cross-talk rate comparing to the curve measured with 62V bias voltage at room temperature (in Figure 6.24 the red curve is parallel to the blue curve). This is our goal: low DCR but high cross-talk rate.

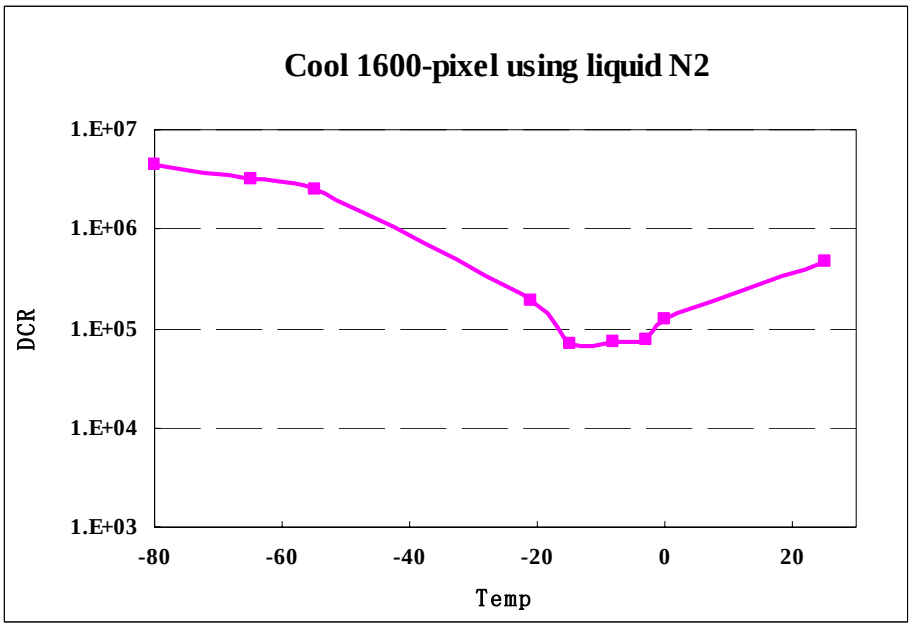

Figure 6.25 160-pixel device: DCR vs. Temperature at Vbias=70.89V

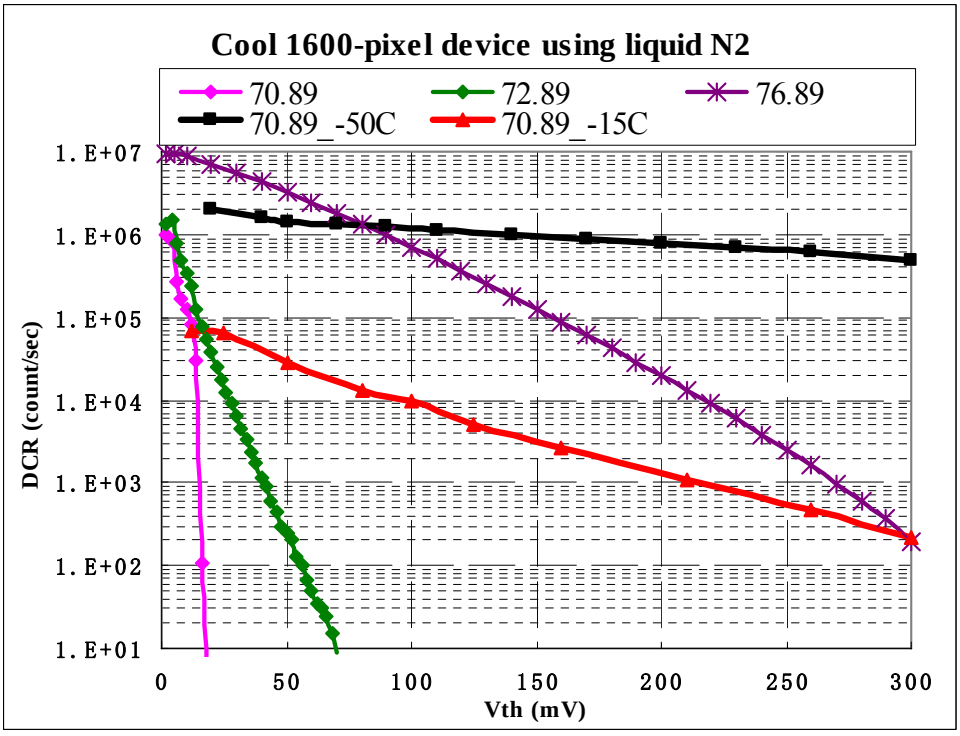

Figure 6.26 1600-pixel device: DCR vs. Comparator threshold at different Vbias and temperature

The situation of Hamamatsu 1600-pixel device is little bit different. In Figure 6.25, we can see the relationship between DCR and temperature is not linear at a fixed bias voltage. At -80C it has even higher DCR than at room temperature. It can be explained that at such a low temperature, the break down voltage of this device becomes lower so as to make the over-voltage higher. DCR of this device is caused mainly by high over-voltage instead of thermal effect. From Figure 6.26 we can see that at -15C and 70.89V bias voltage the device has 100 folded less DCR and much better cross-talk rate comparing to the DCR of 76.89V at room temperature.

6.5. Summary

The experimental set-up which integrated SiPM into our single-lane DNA sequencer and excellent DNA sequencing results show that with moderate external amplification SiPM can definitely be used as single photon detectors for sequencing the DNA and potentially other applications.

A single-trial simulator has been built up by our lab and output pulses of SiPM have been simulated for different optical cross-talk probabilities and afterpulsing probabilities. The simulations show that with a reasonable optical cross-talk all the pixels of SiPM can be fired simultaneously or partially, so 100~1000 times internal gain can be obtained. It means that SiPM can work as single photon detector without any external amplification or any quenching circuit. A multi-trial simulator is also built up for noise analysis. Multi-trial simulations show that the noise of SPD decreases with the external

amplification deceasing. And the afterpulsing effect adds more noise than optical cross-talk.

Experiments have been done to four devices from two different manufactures. Measurements at operating bias voltage and at over-voltage have been done to verify the conclusion of simulations. However SiPM working as SPD without any amplification and quenching is possible, high DCR is still a problem under this situation. Low temperature experiments have been done using liquid nitrogen. The preliminary experimental results show that cooling the device to -80C, at least 100~1000 folded reduction of DCR can be obtained. Based on our research, an optimum SPD without any additional electronics is made possible with SiPM.

7. Conclusion and Future work

7.1. Conclusion

Two types of low cost solid-state photodiodes working as single photon detectors and their applications for highly sensitive fluorescence detection systems have been studied in this work. One is the Hamamatsu Si APD S9073 which is designed for linear-mode operation initially. The other is SiPM which has been used in photon resolving mode but not in photon counting mode yet. Based on our experiments and simulations, we have positive conclusions on both devices.

APD

For the first time, Hamamatsu Si APD S9073, which is a photodiode designed for working in linear-mode has been operated in Geiger-mode and quenched by our unique quenching circuit. A detectable output pulse has been obtained from this small diode. So this low cost device is potentially can be used as a SPD (single photon detector) and be a replacement of the dedicated and expensive large area APD (C30902S-DTC model) from PerkinElmer Optoelectronics. High DCR and high frequency is observed on this APD. Being cooled to -60C, it is believed to reduce DCR by at least 100 folded. Based on our

analysis at least 8 times gain is required to detect single photon by increasing over-voltage or by adding micro-circuit for amplification. And a fast quenching is needed to work with this fast device. Then with moderate DCR and detectable output pulse, Hamamatsu Si APD S9073 will be a very good candidate for single photon detection systems.

SiPM

SiPM is a device with response time in the range of 10ns. This advantage makes SiPM have the potential to replace large area SPAD as high-speed photon detectors without the need of quenching circuits. A novel design is proposed in this work, which utilizes the unique feature of SiPM, optical cross-talk, to make the output pulse from SiPM detectable without any external amplification. Neither external amplification nor quenching circuit being necessary is a perfect situation for single photon detection development. Based on our simulations and measurements, single photon to fire total or partial pixels of SiPM simultaneously without adding noise is feasible so that 100~1000 internal gain can be obtained depending on the number of pixels. For the current available SiPMs, optical cross-talk needs to be enhanced and DCR needs to be kept at the reasonable level at the same time. Some future work is recommended for this purpose.

7.2. Recommended future work

To reduce DCR

Low DCR can be achieved for semiconductor single photon detectors at room temperature with the use of purer silicon. To remove the impurities and crystal defects will reduce the afterpulsing induced DCR dramatically. DCR will further decrease as the technology progresses.

To cool semiconductor photodetectors to a lower temperature, for example, -80C, at least 1000 folded less DCR will be obtained based on our preliminary low temperature experiments. The research on cooled device mounted on the TE cooler and controlled by temperature controller is meaningful to many photon counting applications.

To enhance optical cross-talk

Optical cross-talk is usually not welcome. Many efforts have been taken to avoid it, such as grooving between each pixel for optical isolation between pixels. We would remove these grooving to enhance cross-talk in order to obtain partial cross-talk enhancement or 100% cross-talk rate.

Very high optical cross-talk rate has been reported by Nepomuk Otte who is from Max-Planck-Institute for the backside illuminated SiPM. Though they are trying to reduce the high cross-talk, we can utilize the special structure to get 100% optical cross-talk rate without increasing over-voltage so as to keep the afterpulsing induced DCR at a reasonable level but to have a detectable output pulse without using any external amplifications.

Bibliography

[1] S.M. Sze, Physics of semiconductor devices, Willey, New York

[2] R. H. Haitz, “Model for the electrical behavior of a microplasma,” *J. Appl. Phys.*, vol. 35, no. 5, pp. 1370–1376, May 1964.

[3] WEBB, P. P., and MCINTYRE, R. J., 1970, Bull. *Am. Phys. SOC.,* Ser. Ii - 15, 813.

[4] C.Piemonte, “Characterization of the First Prototypes of Silicon Photomultiplier Fabricated at ITC-irst” IEEE TRANSACTIONS ON NUCLEAR SCIENCE, VOL. 54, NO. 1, FEBRUARY 2007.

[5] P. Buzhan, B. Dolgoshein, A. Ilyin, V. Kantserov, V. Kaplin, and A.Karakash *et al.*, “An advanced study of silicon photomultiplier,” *ICFA Instrumentation Bulletin*, vol. 23, p.28, 2001.

[6] SPCM-AOR Single-Photon Counting Module Data Sheet, Perkinelmer Optoelectronics, http://opto.Perkinelmer.Com.

[7] S. Cova, M. Ghioni, A. Lotito, I. Rech, and F. Zappa, “Evolution and prospects for single-photon avalanche diodes and quenching circuits,”*J. Mod. Opt.*, vol. 51, pp. 1267–1288, 2004

[8] Vinit Dhulla et al., "Single Photon Detection Module for multi-channel detection of weak fluorescence signals", conference on smart medical and biomedical sensor technology III, Proc.of SPIE Vol.6007 600719-1,pp. 1-9, Boston, Massachusetts, USA, Oct 23-26, 2005

[9] S. Cova, M. Ghioni, A. Lacaita, C. Samori, and F.Zappa, “Avalanche photodiodes and quenching circuits for single-photon detection,” Appl. Opt. 35, pp.1956-1963 (1996)

[10] P. P. Webb, R. J. McIntyre, and J. Conradi, "Properties of avalanche photodiodes," RCA Rev. 35, 235-278 (1974)

[11] LACAITA, A. L., GHIONI, M., and COVA, S., 1989, *Electron. Lett.,* 25, 841.

[12] Brian F. Aull, Andrew H. Loomis, Douglas J. Young, Richard M. Heinrichs, Bradley J. Felton, Peter J. Daniels, and Deborah J. Landers “Geiger-Mode Avalanche

Photodiodes for Three-Dimensional Imaging" VOLUME 13, NUMBER 2, 2002, LINCOLN LABORATORY JOURNAL

[13] S. Cova, A. Longoni, and G. Ripamonti, ''Active-quenching and gating circuits for single-photon avalanche diodes (SPADs),'' IEEE Trans. Nucl. Sci. NS-29, 599–601 (1982); presented at the IEEE 1981 Nuclear Science Symposium, SanFrancisco, Calif., 21–23 October 1981.

[14] ANTOGNETTI, P., COVA, S., and LONGONI, A., 1975, *Proceedings* Of *2nd IEEE Ispra Nuclear Electronics SYMPOSIUM,* Stresa, 20-23 May 1975, Euratom Publication EUR 537e, p. 453.

[15] R. J. McIntyre and P. Webb, "Low-noise, reach-through avalanche photodiodes," U.S. Patent 5 583 352, 1996

[16] .W. Lightstone and R. J. McIntyre, ''Photon counting silicon avalanche photodiodes for photon correlation spectroscopy,'' in Photon Correlation Techniques and Applications, Vol.1 of OSA Proceedings Series (Optical Society of America, Washington, D.C., 1988), pp. 183–191

[17] T. O. Regan, H. C. Fenker, J. Thomas, and J. Oliver, ''A method to quench and recharge avalanche photodiodes for use in high rate situations,'' Nucl. Instrum. Methods A 326**,** 570–573 119932; H. C. Fenker, T. O. Regan, J. Thomas, and M. Wright, ''Higher efficiency active quenching circuit for avalanche photodiodes,'' ICFA Instrumentation Bulletin No. 10 1Fermilab, Batvaia, Ill., December (993), pp. 12–14

[18] Trottier et al. "Active quench circuit and reset circuit for avalanche photo diode", U.S. patent 5532474 (2nd August 1999)

[19] Dautet et al. "Active quench circuit for an avalanche current device", U.S. patent 5933042 (2nd July 1996)

[20] W. J. Kindt and K. J. de Langen, "Integrated readout electronics for geiger mode avalanche photodiodes," in Proc. Eur. Solid-State Circuits Conf., Sept. 1998, pp. 216–219

[21] S. Cova, ''Active quenching circuit for avalanche photodiodes,'' U.S. patent 4,963,727 (20 October 1990) (Italian patent 22367A/88); licensed for industrial production to Silena SpA, Milano, Italy

[22] H. Dautet, P. Deschamps, B. Dion, A. D. MacGregor, D. MacSween, R. J. McIntyre, C. Trottier, and P. P. Webb, ''Photon counting techniques with silicon avalanche photodiodes,''Appl. Opt. 32**,** 3894–3900 (1993); SPCM-AQ Single Photon Counting Module Data Sheet (EG&G Optoelectronics Canada, Ltd., Vaudreuil, Quebec, Canada, 1994)

[23] M. Ghioni, S. Cova, F. Zappa, and C. Samori, “Compact active quenching circuit for fast photon counting with avalanche photodiodes,” Rev. Sci. Instrum., vol. 67, pp. 3440–3448, 1996.

[24] Si APD datasheet, Hmamatsu, http://sales.hamamatsu.com/assets/pdf/parts_S/S5343_etc.pdf

[25] N. S. Nightingale, ‘‘A new silicon avalanche photodiode photon counting detector module for astronomy,’’ Exp. Astron.1**,** 407–422 (1991)

[26] P. D. Townsend, J. G. Rarity, and P. R. Tapster, ‘‘Single photon interference in 10 km long optical fiber interferometer,’’Electron. Lett. 29, 634–635 (1993)

[27] L-Q. Li and L. M. Davis, ‘‘Single photon avalanche diode for single molecule detection,’’ Rev. Sci. Instrum. 64, 1524–1529 (1993)

[28] S. A. Soper, Q. L. Mattingly, and P. Vegunta, ‘‘Photon burst detection of single near-infrared fluorescent molecules,’’ Anal.Chem. 65, 740–747 (1993)

[29] B. F. Levine and C. G. Bethea, ‘‘Room-temperature optical time domain reflectometer using a photon counting InGaAs/InP avalanche detector,’’ Appl. Phys. Lett. 46**,** 333–335 (1985)

[30] G. Ripamonti and S. Cova, ‘‘Optical time-domain reflectometry with centimeter resolution at 10215 W sensitivity,’’ Electron.Lett. 22, 818–819 (1986)

[31] A. Lacaita, P. A. Francese, S. Cova, and G. Ripamonti, ‘‘Single-photon optical time-domain reflectometer at 1.3μm with 5-cm resolution and high sensitivity,’’ Opt. Lett. 18**,** 1110–1112 (1993)

[32] G. Ripamonti and A. Lacaita, ‘‘Single-photon semiconductor photodiodes for distributed optical fiber sensors: state of the art and perspectives,’’ in Distributed and Multiplexed Fiber Optic Sensors II, J. P. Dakin and A. D. Kersey, eds., Proc. SPIE 1797, 38–49 (1993)

[33] M. Hoebel and J. Ricka, ‘‘Dead-time and afterpulsing correction in multiphoton timing with non-ideal detectors,’’ Rev. Sci. Instrum. 65, 2326–2336 (1994)

[34] I. Prochazka, K. Hamal, and B. Sopko, ‘‘Photodiode based detector package for centimeter satellite laser ranging,’’ in Proceedings of the Seventh International Workshop on Laser Ranging Instrumentation, C. Veillet, ed. 1OCA-CERGA, Grasse, France, (1990), pp. 219–221

[35] F. Zappa, G. Ripamonti, A. Lacaita, S. Cova, and C. Samori,‘‘Tracking capabilities of SPADs for laser ranging,’’ in Proceedings of the Eighth International Workshop on

Laser Ranging Instrumentation, J. J. Degnan, ed., NASA Conf. Publ. 3214 1NASA, Greenbelt, Md., (992), pp. 5, 25–30

[36] F. Stellari, F. Zappa, S. Cova, and L. Vendrame, “Tools for Non-Invasive Optical Characterization of CMOS Circuits," Proceedings of International Electron Device Meeting IEDM '99, 5-8 December 1999, Washington D.C. USA

[37] V. Saveliev, V. Golovin, “Silicon avalanche photodiodes on the base of metal-resistor-semiconductor (MRS) structures” Nuclear Instruments and Methods in Physics Research A 442 (2000) 223}229

[38] Antich, P.; Parkey, R.; Tsyganov, E.; Zinchenko, A. “Conductor-resistor-semiconductor avalanche diodes for scintillation light detection: medical applications” Nuclear Science Symposium, 1998. Conference Record. 1998 IEEE Volume 1, Issue, 1998 Page(s):389~396 vol.1 Digital Object Identifier 10.1109/NSSMIC.1998.775168

[39] A. Andreev, et al., Nucl. Instr. and Meth. A 540 (2005) 368.

[40] A. Lacaita, et al., IEEE TED (1993).

[41] P. Buzhan, B. Dolgoshein, L. Filatov, A. Ilyin, V. Kantzerov, V. Kaplin, A. Karakash, F. Kayumov, S. Klemin, E. Popova, S. Smirnov "Silicon photomultiplier and its possible applications” Nuclear Instruments and Methods in Physics Research A 504 (2003) 48–52

[42] Deborah J. Herbert, Valeri Saveliev, Nicola Belcari, Nicola D’Ascenzo, Alberto Del Guerra, and Alexei Golovin "First Results of Scintillator Readout With Silicon Photomultiplier” IEEE TRANSACTIONS ON NUCLEAR SCIENCE, VOL. 53, NO. 1, FEBRUARY 2006 389

[43] V.D. Kovaltchouka, G.J. Lolosa,_, Z. Papandreoua, K. Wolbaumb “Comparison of a silicon photomultiplier to a traditional vacuum photomultiplier” Nuclear Instruments and Methods in Physics Research A 538 (2005) 408–415

[44] I. Britvitch, Y. Musienko, D. Renker, “Investigation of a photon counting avalanche photodiode from Hamamatsu photonics” Nuclear Instruments and Methods in Physics Research A 567 (2006) 276–280

[45] D. Beznosko, G. Blazey, D. Chakraborty, A. Dyshkant, K. Francis, D. Kubik, J.G. Lima, V. Rykalin_, V. Zutshi “Investigation of a solid-state photodetector” Nuclear Instruments and Methods in Physics Research A 545 (2005) 727–737

[46] P. Buzhan, B. Dolgoshein_, A. Ilyin, V. Kantserov, V. Kaplin, A. Karakash, A. Pleshko, E. Popova, S. Smirnov, Yu. Volkov L. Filatov and S. Klemin F. Kayumov “AN ADVANCED STUDY OF SILICON PHOTOMULTIPLIER” ICFA Instrumentation

Bulletin

[47] I. Britvitch,_, I. Johnson, D. Renker, A. Stoykov, E. Lorenz “Characterisation of Geiger-mode avalanche photodiodes for medical imaging applications” Nuclear Instruments and Methods in Physics Research A 571 (2007) 308–311

[48] Makoto Taguchi Master's thesis “Development of Multi-Pixel Photon Counters and readout electronics”

[49] Claudio Piemonte,Roberto Battiston, Maurizio Boscardin, Gian-Franco Dalla Betta, Alberto Del Guerra,Nicoleta Dinu, Alberto Pozza, and Nicola Zorzi “Characterization of the First Prototypes of Silicon Photomultiplier Fabricated at ITC-irst” IEEE TRANSACTIONS ON NUCLEAR SCIENCE, VOL. 54, NO. 1, FEBRUARY 2007

[50] Cristiano Niclass, Alexis Rochas, Pierre-Andr´e Besse, Radivoje Popovic, Edoardo Charbon “A 4ns integration time imager based on CMOS single photon avalanche diode technology” Sensors and Actuators A 130–131 (2006) 273–281

[51] Multi pixel photon counter catalogue, Hamamatsu Photonics, Japan, [Online]. Available: http://jp.hamamatsu.com/resources/products/ssd/pdf/mppc_kapd0002e02.pdf

[52] Uriel Feige, David Peleg, Prabhakar Raghavan and Eli Upfal “Randomized broadcast in networks” Lecture Notes in Computer Science Volume 450/1990

[53] L. Alaverdian, S. Alaverdian, O. Bilenko, I. Bogdanov, E. Filippova, D. Gavrilov, B. Gorbovitski, M. Gouzman, G. Gudkov, S. Domratchev, O. Kosobokova, N. Lifshitz, S. Luryi, V. Ruskovoloshin, A. Stepukhovich, M. Tcherevishnick, G. Tyshko, V. Gorfinkel, “A family of novel DNA sequencing instruments based on single photon detection” Electrophoresis 23, pp. 2804-2817, 2002.

[54] Dovichi, N. J., Martin, J. C., Jett, J. H., Trkula, M., Keller, R. A., *Anal. Chem.* 1984, *56*, 348–354.

[55] Chen, D. Y., Dovichi, N. J., *Anal. Chem.* 1996, *68*, 690–696.

[56] Soper, S. A., Davis, L. M., Shera, E. B., *J. Opt. Soc. Am. B* 1992, *9*, 1761–1769.

[57] Soper, S. A., Mattingly, Q. L., Vegunta, P., *Anal. Chem.* 1993, *6*, 740–747.

[58] Goodwin, P. M., Affleck, R. J., Ambros, W. P., Demos, J. N., Jett, J. H., Martin, J. C., Reha-Krantz, L. J., Semin, D. J., Schecker, J. A., Wu, M., Keller, R. A., *Exp. Techn. Phys.* 1995, *41*, 294–297.